THE MOLECULAR MECHANISMS OF IRON AND FERRITIN METABOLISM IN NORMAL AND NEOPLASTIC CELLS

XIANGCONG XU

A thesis submitted in fulfilment of the requirements

for the Degree of Doctor of Philosophy

Faculty of Medicine University of Sydney

Thanks to the “LORD OF THE RINGS”, both the books and movies,

to give me strength and passion to finish my thesis.

Now I have finally reached Mount Doom, to forge a new ring for myself.

DECLARATION

This thesis is submitted in accordance with the regulations for the Degree of Doctor of Philosophy at The University of Sydney. I declare that, to the best of my knowledge, this thesis does not contain any material previously published except as acknowledged in the text. It has not been submitted, in whole or in part, for a degree at this or any other university.

Xiangcong Xu

TABLE OF CONTENTS

ACKNOWLEDGEMENTS

I wish to extend my gratitude to the following people, whose help and support have made this thesis possible.

First and foremost, I must extend my most sincere thanks to my supervisor, Professor Des Richardson. His guidance, enthusiasm and encouragement have been invaluable, especially during the “hard times” of the project. I would also like thank Des with regards to the hard work and patience involved in helping with the preparation of manuscripts. None of this would have been possible without his support, dedication and craziness.

I would like to extent my gratitude to numerous people who have shared their expertise and knowledge with me over the past few years. Thanks to Dr. Juliana Kwok and Dr. Cynthia Wong for guiding me in the beginning of my PhD, helping me with many experimental procedures and giving me passion to finish my degree. I would like to thank my colleague Dr. Robert Sutak and Prof. Daniel Vyoral (Institute of Hematology and Blood Transfusion, Prague) for their enormous help with FPLC and two dimensional gel electrophoresis techniques. Without them, I could never finish my studies successfully.

The excellent technical assistance provided by the following individuals during the course of this work is much appreciated. My gratitude to Dr. Mark Raftery (Bioanalytical Mass Spectrometry Facility, University of New South Wales, Australia) for performing the LC-MS analyses of my FPLC samples and Mr. Kashem Abul Mohammad for analysing the MS data from the 2D-electrophoresis experiments.

I would also like to acknowledge the various members of the Richardson laboratory for their technical assistance and expertise. Many thanks to Ms Megan Whitnall for breeding the MCK mice for my experiments. I must also extend my gratitude to Dr. David Lovejoy and Dr. Ralph Watts for their endless supply of ^{59}Fe-transferrin. Uncle Dr. H. Lennart Persson (Faculty of Health Sciences, University of Linköping, Linköping, Sweden) is thanked for sharing his knowledge in fluorescence studies and the preparation of manuscripts.

Many thanks to the friendship and support of my colleagues, past and present, who have made this journey a very interesting and colourful one. I'd like to thank my fellow PhD students, Mr Yohan Suryo Rahmanto and Ms Danuta Kalinowski. Also, Dr Robert Sutak (bobo), Dr. Dong Fu (7.5 inch Donga), Dr. Erika Becker (pretty lady), Dr. Neil Davis (my swim mate), Dr. Theinga Ga Tut (master), Dr. Egaritster Noul (Thai friend), Dr. Louise Dunn (lulu), Dr. Patric Jansson (999th tennis player), Dr. Eric Sekyere, Dr. Jonathan Howard, Dr. Jenny Park, Ms Min Kim (oppa), Mr Michael Huang, Mr Edwin Lim and Ms Zaklina Kovacevic are thanked for the much needed laughs and amusement. Their great personalities helped me to endure many days of hard work and sleepless nights.

Finally, I'd like to thank the never-tiring and never-failing support from my family, especially my parents, auntie and grandparents, for their support and understanding. I also feel grateful that my cousin stays with me and provids me great support. I am always indebted to you and I thank you for always being a pillar of strength which I could rely on. This thesis is dedicated to you.

CONTRIBUTIONS TO THE THESIS:

Chapter 3: The work reported in this chapter was performed solely by the candidate, with the exception of the FPLC and native gel electrophoresis (Section 3.3.6). These were performed with the assistance of Dr. Robert Sutak.

Chapter 4: The work reported in the chapter was performed solely by the candidate, with the exception of the animal breeding, size exclusion FPLC and the LC-MS analyses. The animal breeding was performed by Ms Megan Whitnall (Section 4.2.1.1). The size exclusion FPLC was performed with the assistance of Dr. Robert Sutak (Sections 4.3.2 and 4.3.3). The LC-MS analysis was performed by Dr. Mark Raftery (Section 4.3).

Chapter 5: The work reported in the chapter was performed by the candidate, with the exception of the animal breeding and 2D electrophoresis. The animal breeding was performed by Ms Megan Whitnall (Section 5.2.1). The 2D electrophoresis was performed with the assistance of Dr. Robert Sutak (Section 5.3.1).

ABSTRACT

Iron (Fe) is essential for cell growth and replication as many Fe-containing proteins catalyse key reactions involved in energy metabolism (cytochromes, mitochondrial aconitase and Fe-S proteins of the electron transport chain), respiration (hemoglobin and myoglobin) and DNA synthesis (ribonucleotide reductase). If not appropriately shielded, Fe could participate in one-electron transfer reactions that lead to the production of extremely toxic free radicals. The Fe storage protein, ferritin, is essential to protect cells against Fe-mediated oxidative stress by accommodating excess Fe into its protein shell (Xu et al., 2005). However, despite intensive research over the last few decades, many questions relating to intracellular Fe metabolism, *e.g.* Fe release from ferritin remain unanswered. Therefore, it is important to elucidate the molecular mechanisms of Fe trafficking in cells.

At the beginning of my candidature, little was understood regarding the effect of anti-cancer agents, anthracyclines on the Fe-regulated genes, including *transferrin receptor-1* (*TfR1*), *N-myc downstream-regulated gene-1* (*Ndrg1*) and *ferritin*. Furthermore, the mechanisms of ferritin-Fe release and anthracycline-mediated ferritin-Fe accumulation are unclear. The work presented in Chapters 3 and 4 has addressed these issues. Apart from the studies examining the molecular interactions of anthracyclines with Fe, a mouse model with perturbed Fe metabolism was used and the marked alterations of protein expression in the heart of this knockout mouse model was discussed in Chapter 5.

Chapter 3

Anthracyclines are effective anti-cancer agents. However, their use is limited by cardiotoxicity, an effect linked to their ability to chelate iron (Fe) and perturb Fe metabolism (Xu et al., 2005). These effects on Fe-trafficking remain poorly understood, but are important to decipher as treatment for anthracycline cardiotoxicity utilises the chelator, dexrazoxane. Incubation of cells with doxorubicin (DOX) up-regulated mRNA levels of the Fe-regulated genes, *transferrin receptor-1* (*TfR1)* and *N-myc downstream-regulated gene-1* (*Ndrg1*). This effect was mediated by Fe-depletion, as it was reversed by adding Fe and was prevented by saturating the anthracycline metal-binding site with Fe. However, DOX did not act like a typical chelator, as it did not induce cellular Fe mobilisation. In the presence of DOX and ^{59}Fe-transferrin, Fe-trafficking studies demonstrated ferritin-^{59}Fe accumulation and decreased cytosolic-^{59}Fe incorporation. This could induce cytosolic Fe-deficiency and increase *TfR1* and *Ndrg1* mRNA. Up-regulation of *TfR1* and *Ndrg1* by DOX was independent of anthracycline-mediated radical generation and occurred *via* HIF-1α-independent mechanisms. Despite increased *TfR1* and *Ndrg1* mRNA after DOX treatment, this agent decreased TfR1 and Ndrg1 protein expression. Hence, the effects of DOX on Fe metabolism were complex due to its multiple effector mechanisms.

Chapter 4

The Fe storage protein, ferritin, can accommodate up to 4500 atoms of Fe in its protein shell (Harrison and Arosio, 1996). However, the underlying mechanism of ferritin-Fe release remains unknown. Previous studies demonstrated that anti-cancer agents, anthracyclines, led to ferritin-^{59}Fe accumulation (Kwok and Richardson, 2003). The increase in ferritin-^{59}Fe was shown to be due to a decrease in the release of Fe from

this protein. It could be speculated that DOX may impair the Fe release pathway by preventing the synthesis of essential ferritin partner proteins that induce Fe release. In this study, a native protein purification technique has been utilised to isolate ferritin-associated partners by combining ultra-centrifugation, anion-exchange chromatography, size exclusion chromatography and native gel electrophoresis. In addition to cells in culture (namely, SK-Mel-28 melanoma cells), liver taken from the mouse was used as a physiological *in vivo* model, as this organ is a major source of ferritin. Four potential partner proteins were identified along with ferritin, *e.g.* aldehyde dehydrogenase 1 family, member L1 (ALDH1L1). Future studies are required to clarify the relationship of these proteins with cellular Fe metabolism and ferritin-Fe release.

Chapter 5

A frequent cause of death in Friedreich's ataxia patients is cardiomyopathy, but the molecular alterations underlying this condition are unknown. We performed two dimensional electrophoresis to characterise the changes in protein expression of hearts using the muscle creatine kinase frataxin conditional knockout (KO) mouse. Pronounced changes in the protein expression profile were observed in 9-week-old KO mice with severe cardiomyopathy. In contrast, only a few proteins showed altered expression in asymptomatic 4-week-old KO mice. In hearts from frataxin KO mice, components of the iron-dependent complex-I and -II of the mitochondrial electron transport chain and enzymes involved in ATP homeostasis (creatine kinase, adenylate kinase) displayed decreased expression. Interestingly, the KO hearts exhibited increased expression of enzymes involved in the citric acid cycle, catabolism of branched-chain amino acids, ketone body utilisation and pyruvate decarboxylation. This constitutes evidence of metabolic compensation due to decreased expression of

electron transport proteins. There was also pronounced up-regulation of proteins involved in stress protection, such as a variety of chaperones, as well as altered expression of proteins involved in cellular structure, motility and general metabolism. This is the first report of the molecular changes at the protein level which could be involved in the cardiomyopathy of the frataxin KO mouse.

LIST OF PUBLICATIONS

1. **Xu X.**, Persson H.L., Richardson D.R. (2005) Molecular pharmacology of the interaction of anthracyclines with iron. *Mol. Pharmacol.* 68:261-71. (Impact factor 4.6)

2. **Xu X.,** Sutak R., Richardson D.R. (2008) Iron chelation by clinically relevant anthracyclines: alteration in expression of iron-regulated genes and atypical changes in intracellular iron distribution and trafficking. *Mol. Pharmacol.* 73:833-44. (Impact factor 4.6)

3. Sutak R., **Xu X.,** Whitnall M., Abul1 K., Vyoral D., Richardson D.R. (2008) Proteomic analysis of hearts from frataxin knockout mice: marked rearrangement of energy metabolism, a response to cellular stress and altered expression of proteins involved in cell structure, motility and metabolism. *Proteomics.* 8:1731-41. (Impact factor 5.8)

4. Whitnall M., Suryo Rahmanto Y., Sutak R., **Xu X.,** Becker E., Richardson D.R., Ponka P. (2008) The MCK Mouse Heart Model of Friedreich's Ataxia: Alterations in Iron-Regulated Proteins and Iron Chelation Limits Cardiac Hypertrophy. *PNAS* (In press, Impact factor 9.6)

LIST OF INVITED CONFERENCE PRESENTATIONS

1. **Xu X.** and Richardson D.R. Iron chelation by clinically relevant anthracyclines: alteration in expression of iron-regulated genes and atypical changes in intracellular iron distribution and trafficking. 4th Joint Meeting of the Society for Free Radical Research of Australasia & Japan, Kyoto, Japan, 2007.

2. Sutak R., **Xu X.,** Megan W., Vyoral D., Kashem A., Helen P., Richardson D.R. Proteomic analysis of hearts from frataxin knock mice. The Australian Health and Medical Research Congress, Hobart, Australia, 2007.

3. **Xu X.** and Richardson D.R. Transferrin receptor-dependent iron uptake is decreased by anthracyclines due to reduced transferrin receptor 1 expression. Health@Sydney, Health Research Conference 2006 "From Cell to Society", Leura, Australia, 2006.

4. **Xu X.** and Richardson D.R. Anthracyclines up-regulate transferrin receptor 1 (TfR1) at the mRNA level, but down-regulate TfR1 protein at the translational level. The Australian Health and Medical Research Congress, Melbourne, Australia, 2006.

5. **Xu X.** and Richardson D.R. Anthracycline-mediated ferritin-Fe accumulation is not protective against cytotoxicity induced by iron-loading. 15th International Conference on Oral Chelation in the Treatment of Thalassaemia and Other Diseases, Taichung, Taiwan, 2005.

6. **Xu X.** and Richardson D.R. Generation of free radicals are partially involved in anthracyclines-mediated ferritin-Fe accumulation. 3rd Joint Meeting of the Society for Free Radical Research of Australasia & Japan, Gold Coast, Australia, 2005.

7. **Xu X.** and Richardson D.R. Anthracycline-mediated ferritin-iron accumulation is not a protective response against these cytotoxic agents. The Australian Society for Medical Research NSW Scientific Meeting, Sydney, Australia, 2005.

8. **Xu X.** and Richardson D.R. Anthracycline-mediated ferritin-Fe accumulation is not protective against cytotoxicity induced by iron-loading. 13th Annual Conference of the Society of Free Radical Research Australasia, Christchurch, New Zealand, 2004.

ABBREVIATIONS

ALDH1L1	aldehyde dehydrogenase 1 (member L1)
ARD	aci-reductone dioxygenase
DAU	daunorubicin
5-i-DAU	5-imino-daunorubicin
DFO	desferrioxamine
DMT1	divalent metal transporter 1
DMSO	dimethyl sulphoxide
DOX	doxorubicin
DXR	dexrazoxane
EPI	epirubicin
FA	Friedreich's ataxia
FAC	ferric ammonium citrate
FCS	foetal calf serum
Fe	iron
^{59}Fe-Tf	$^{59}Fe_2$-transferrin
ferritin-H	ferritin heavy chain
ferritin-L	ferritin light chain
FPLC	fast pressure liquid chromatography
HFE	human gene for hemochromatosis
HIF-1α	hypoxia inducible factor-1α
HRE	hypoxia response element
Hsp	heat shock protein
ICL-670A	4-[3,5-bis-(hydroxyphenyl)-1,2,4-triazol-1-yl]- benzoic acid
IRE	iron-responsive element

IRP	iron regulatory protein
ISC	iron-sulfur cluster
KO	knockout
LC-MS	liquid chromatography mass spectrometry
MCK	muscle creatine kinase
MEFs	murine embryo fibroblasts
MnTBAP	Mn(III) tetrakis (4-benzoic acid)-porphyrin
Ndrg1	N-myc downstream-regulated gene-1
PAGE	polyacrylamide gel electrophoresis
PBS	phosphate buffered saline
PCIH	2-pyridylcarboxaldehyde isonicotinoyl hydrazone
PCTH	2-pyridylcarboxaldehyde 2-thiophenecarboxyl hydrazone
PIH	pyridoxal isonicotinoyl hydrazone
ROS	reactive oxygen species
RR	ribonucleotide reductase
RS	radical scavengers
SDHA	succinate dehydrogenase complex
SIH	salicylaldehyde isonicotinoyl hydrazone
SOD	superoxide dismutase
Tf	transferrin
TfR1	transferrin receptor 1
TfR2	transferrin receptor 2
VEGF1	vascular endothelial growth factor-1
WT	wild type
311	2-hydroxy-1-naphthylaldehyde isonicotinoyl hydrozone

LIST OF FIGURES

CHAPTER 1: INTRODUCTION

CHAPTER 3: IRON CHELATION BY CLINICALLY RELEVANT ANTHRACYCLINES: ALTERATIONS IN EXPRESSION OF IRON REGULATED GENES AND ATYPICAL CHANGES IN INTRACELLULAR IRON DISTRIBUTION AND TRAFFICKING

LIST OF TABLES

CHAPTER 1 :

INTRODUCTION

This work has been published in:

Xu, X., Persson, H. L. and Richardson, D. R. (2005) Molecular pharmacology of the interaction of anthracyclines with iron. *Mol Pharmacol*. 68(2):261-71.

1.1 GENERAL INTRODUCTION

Anthracyclines are potent anti-neoplastic agents used extensively to treat a range of cancers, including leukemias, lymphomas, sarcomas, and carcinomas (for review, see Gewirtz, 1999). Doxorubicin, daunorubicin and epirubicin are clinically used anthracyclines (Figure 1.1). The intricate and complex cellular responses to anthracyclines hinder efforts to unveil the mechanisms involved in their cytostatic and cytotoxic actions. However, anthracyclines are proposed to disrupt macromolecular biosynthesis by various mechanisms, including DNA intercalation and the inhibition of DNA polymerase and topoisomerase II (Tewey et al., 1984a; Tewey et al., 1984b). Anthracyclines can also induce DNA damage by the generation of free radicals that react with a variety of macromolecules, thus inhibiting cellular proliferation or causing apoptosis (Gewirtz, 1999). Generally, the anti-tumour effect of anthracyclines are mainly attributed to their DNA-binding and damaging abilities. Indeed, the pharmacological aspects of these drugs have been extensively reviewed (Minotti et al., 2004a; Myers, 1998), and will not be discussed in depth in this chapter.

A major problem with the clinical use of anthracyclines is their cardiotoxicity, which limits administration exceeding an accumulated dose of approximately 550 mg/m^2 (Singal et al., 1997). The toxic effects of anthracyclines to cardiomyocytes are not due to inhibition of DNA synthesis, since these cells do not replicate (Myers, 1998). While the reasons for the cardiotoxicity of these drugs are not fully understood, a number of observations suggest that the interactions of anthracyclines with iron are of great importance (Minotti et al., 1998; Kotamraju et al., 2002; Kwok and Richardson, 2002, 2003). The redox state of iron can be converted between the iron(II) and iron(III) states by interaction with anthracyclines, generating toxic reactive oxygen species (ROS)

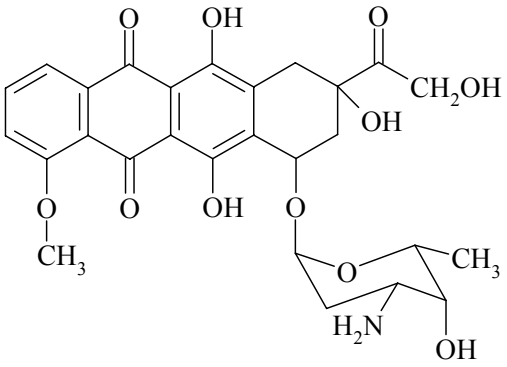

Doxorubicin (DOX)

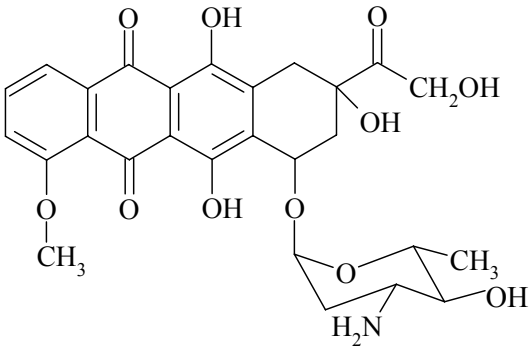

Epirubicin (EPI)

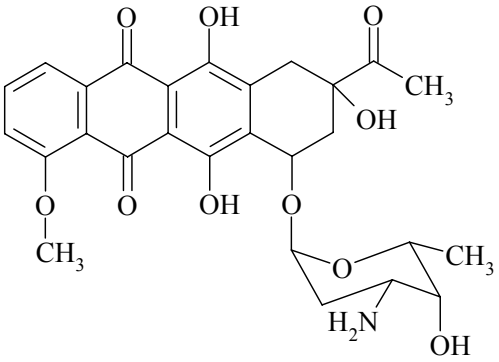

Daunorubicin (DAU)

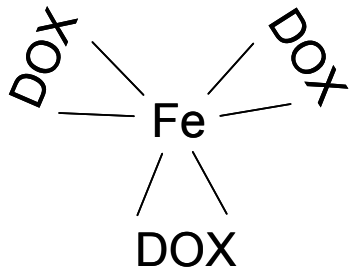

Fe complex of DOX

Figure 1.1 Illustration of the structures of doxorubicin (DOX), daunorubicin (DAU), epirubicin (EPI), and the iron complex of doxorubicin.

(Minotti et al., 2004a; Mizutani et al., 2005; Myers, 1998). Before beginning a description of the reactions of anthracyclines with iron, we will first briefly detail the molecular mechanisms involved in the processing and trafficking of intracellular iron.

1.2 CELLULAR AND MOLECULAR PHYSIOLOGY OF IRON METABOLISM

1.2.1 The Transferrin – Transferrin Receptor Mechanism of Iron Uptake

Iron is a crucial element for living cells and is found in two functional forms of macromolecules, *i.e.* haem and non-haem iron-containing proteins (for review, see Richardson and Ponka, 1997). Briefly, ferric iron [iron(III)], is transported through the body in a soluble form bound to transferrin (M_r = 80 kDa), a protein mainly synthesized by the liver and also sanctuary sites such as the brain and testis. Transferrin donates iron to cells through binding to the dimeric transferrin receptor 1 (TfR1) on the cell membrane, which is subsequently endocytosed (Figure 1.2). Within late endosomes at acidic pH, iron is liberated from transferrin, and in the ferrous form [iron(II)] is then transported into the cytosol by the divalent metal transporter 1 (DMT1; for review see Napier et al., 2005; Morgan, 1981). The transferrin-TfR1 complex, on the other hand, is returned to the cell surface, where apotransferrin is released from its receptor into the extracellular space (Figure 1.2). The binding of transferrin to the TfR1 and the subsequent uptake of iron is regulated by a number of factors, including: (1) TfR1 expression, which is modulated by intracellular iron levels (see Section 1.2.2.2); (2) the competitive binding of transferrin to the TfR1 by the product of the *hemochromatosis* (*HFE*) gene (Feder et al., 1996; Lebron et al., 1999; Pietrangelo, 2002); and (3) the saturation of transferrin with iron, since apotransferrin has a very low affinity for the TfR1 in contrast to diferric transferrin.

The description of the detailed structure of the iron-transferrin-TfR1 complex has unveiled important insights into the iron uptake process (Cheng et al., 2004). This latter investigation revealed that HFE and transferrin compete for the same binding site on each of the TfR1 monomers which is in agreement with the findings of a previous study (Lebron et al., 1999). Interestingly, the apical part of the receptor within the transferrin-TfR1 complex remains free and potentially accessible to interaction with other molecules. It is possible that DMT1 and/or the postulated ferrireductase, which reduces iron(III) to iron(II) within transferrin, could associate with the TfR1 at this site (Cheng et al., 2004).

A recently identified second transferrin receptor (TfR2; Kawabata et al., 1999) probably plays an important role in iron homeostasis, since mutations of this molecule can lead to hemochromatosis (Camaschella et al., 2000). Even though TfR2, like TfR1, is a type II membrane protein with a large C-terminal ectodomain and a small N-terminal cytoplasmic domain, the affinity of TfR2 for transferrin is approximately 25-times less than TfR1 (Kawabata et al., 1999). On the other hand, TfR1 binds to HFE with nanomolar affinity (Lebron et al., 1999), while HFE binding to the TfR2 is not detectable (West et al., 2000). In contrast to the iron-dependent, post-transcriptional regulation of TfR1, the expression of TfR2 is regulated, at least in part, by the erythroid transcription factor, GATA-1 (Kawabata et al., 2001; Vogt et al., 2003). Presently, it is unclear whether there is direct interaction between TfR1 and TfR2. However, Vogt et al. (2003) have suggested that these molecules form heterodimers due to their similar internalization and co-localization patterns.

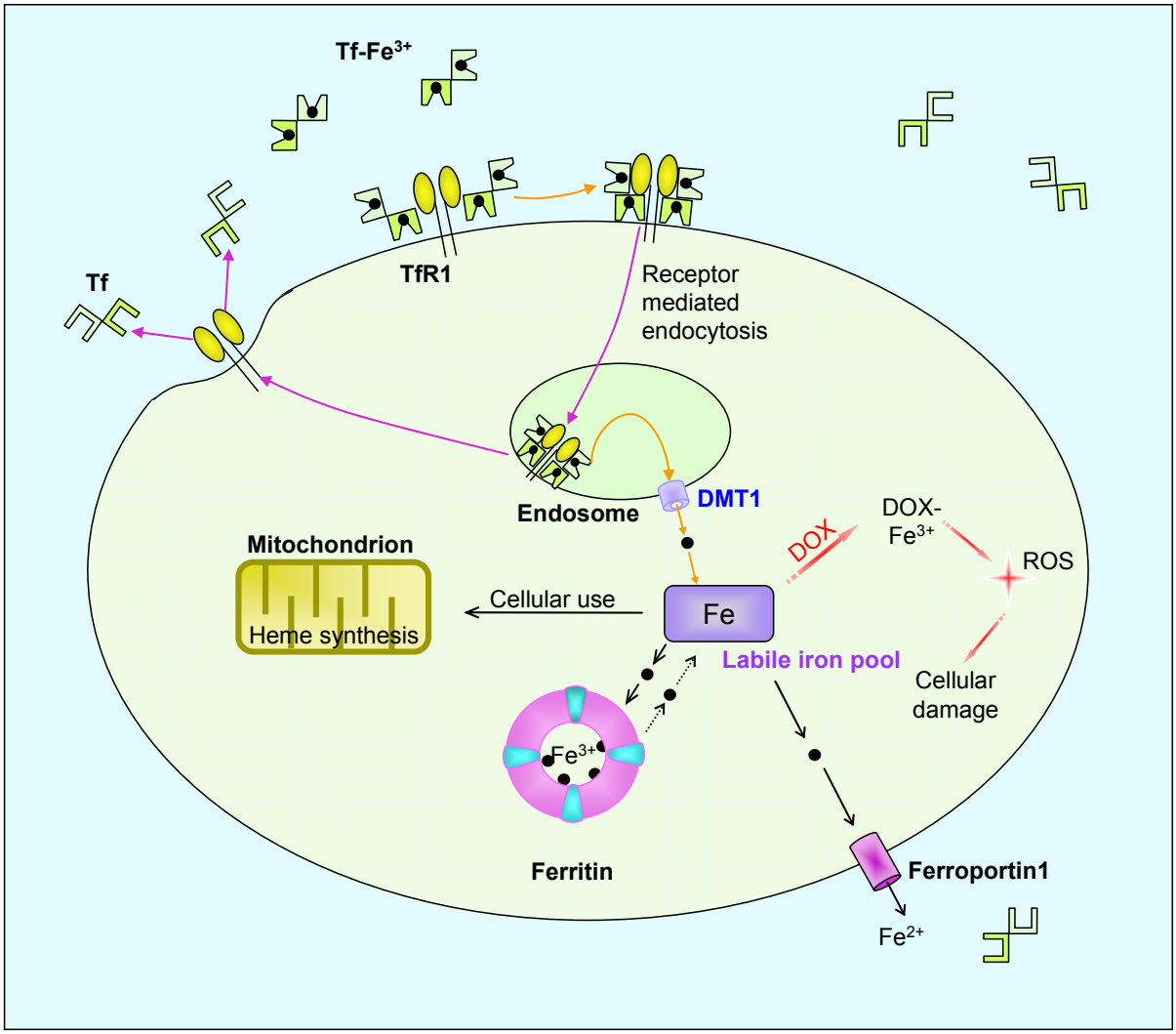

Figure 1.2 Schematic illustration of iron metabolism in human cells. Diferric transferrin in the serum avidly binds to TfR1 on the cell membrane. The transferrin-TfR1 complex is then internalized into an endosome by receptor-mediated endocytosis. The iron is released from transferrin by a decrease in endosomal pH that is mediated by a proton pump in the endosome membrane. Once iron is released from transferrin, it is believed to be reduced by a ferrireductase and is then transported through the endosomal membrane by DMT1. Upon leaving the endosome, the iron becomes part of a poorly characterised compartment known as the intracellular labile iron pool. Iron can be redistributed from the labile iron pool for cellular use, stored in ferritin, or potentially pumped out of the cell by ferroportin1. Doxorubicin and other anthracyclines bind iron to form drug-iron(III) complex, which is known to generate ROS and to lead to cellular damage and apoptosis.

1.2.2 Intracellular Iron Metabolism

1.2.2.1 Hephaestin, Ferroportin and Hepcidin

Apart from transferrin, TfR1 and TfR2, more recently several other proteins have been implicated in the trafficking and release of intracellular iron, including: hephaestin (Vulpe et al., 1999), ferroportin1 (Donovan et al., 2000) and hepcidin (for review see Ganz, 2003). The hephaestin molecule is a trans-membrane ceruloplasmin homologue that is markedly expressed in the intestine and was first identified in the *sla* mouse (Vulpe et al., 1999). The mutation in this animal leads to reduced iron release into the circulation, resulting in iron accumulation within enterocytes (Vulpe et al., 1999). Therefore, hephaestin may play a role in facilitating iron release in cooperation with the iron transporter, ferroportin1, which is believed to be responsible for iron release from enterocytes into the bloodstream (Donovan et al., 2000).

Studies over the last 3 years have shown that hepcidin, a peptide hormone secreted by the liver, is critical in iron homeostasis by acting as a iron regulatory hormone (Ganz, 2003). Under conditions of iron overload, hepcidin is highly expressed in the liver (Pigeon et al., 2001). It is thought that hepcidin negatively regulates intestinal iron absorption, maternal-fetal iron transport across the placenta and iron release from hepatic stores and macrophages (Ganz, 2003). Once in the circulation, hepcidin may bind to ferroportin1 on the cell membrane leading to its internalization and degradation (Nemeth et al., 2004). This results in reduced iron efflux from enterocytes and completes a homeostatic loop, whereby iron regulates hepcidin secretion that then affects ferroportin 1 expression (Nemeth et al., 2004). In addition to these molecules, the serum protein, ceruloplasmin, is also involved *in vivo* in mediating iron efflux from cells (Richardson and Ponka, 1997).

1.2.2.2 The Regulation of Iron Homeostasis by Iron-Regulatory Proteins

The iron-regulatory proteins 1 and 2 (IRP1 and IRP2; M_r 90-95 kDa) are mRNA-binding molecules involved in the control of normal iron homeostasis (Figure 1.3; for review see Hentze and Kuhn, 1996). The IRP1 contains an [4Fe-4S] cluster and is identical to cytoplasmic aconitase. Iron-responsive elements (IREs) are present in the 5' or 3'-untranslated regions of mRNAs of a variety of molecules that play a role in iron metabolism, including the TfR1 and ferritin. Within ferritin mRNA, the IRE is found in the 5'-untranslated region and its binding with either IRP inhibits translation, thereby decreasing iron storage (Hentze and Kuhn, 1996). However, in the case of *TfR1* mRNA, the IRE is in the 3'-untranslated region and IRP-IRE binding leads to increased translation by stabilization of the mRNA against degradation, in turn causing enhanced iron uptake via the TfR1. The mRNA-binding activity of IRP1 is determined by the presence of the [4Fe-4S] cluster within the protein (Kuhn and Hentze, 1992; Theil and Eisenstein, 2000). In cells that are iron-deplete, the [4Fe-4S] cluster is absent (apo-IRP1) and allows IRP1-IRE binding (Figure 1.3). Conversely, when intracellular iron levels are high, the [4Fe-4S] cluster forms within the protein (holo-IRP1) and prevents IRP1-IRE binding (Kwok and Richardson, 2002). To date, two forms of IRP1 have been well characterised; a high-affinity binding type which spontaneously binds mRNA and a low affinity form unable to bind IREs (Figure 1.3). In cellular assays, the low affinity form can be converted to the high affinity IRP-RNA-binding molecule by the addition of β-mercaptoethanol. This allows an estimate of the total IRP-RNA binding activity, thus representing the total IRP present in the cell (Kwok and Richardson, 2002).

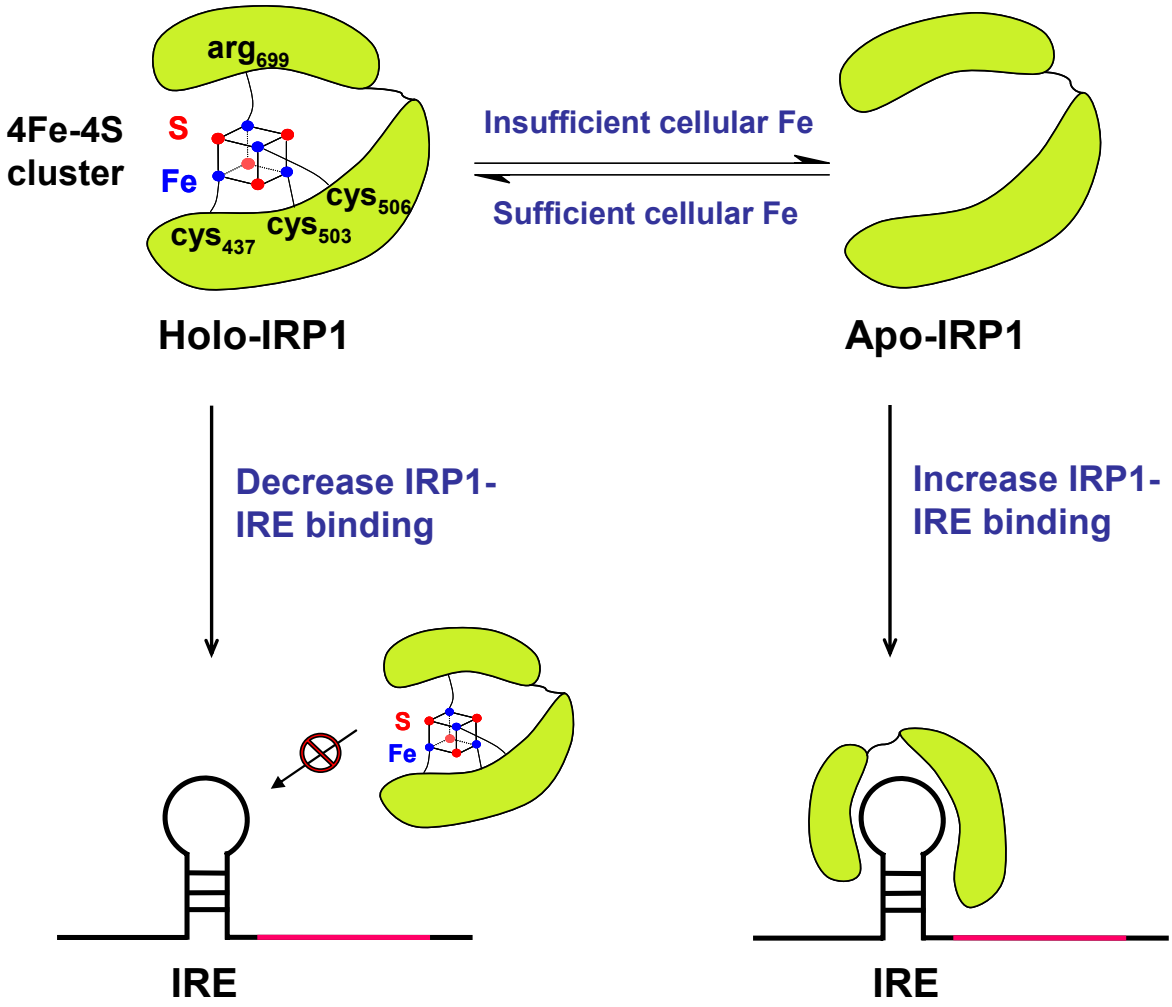

Figure 1.3 The mRNA binding activity of IRP1 is regulated by the presence of an [4Fe-4S] cluster within the protein. When cellular iron levels are high, the [4Fe-4S] cluster is present in the IRP1, which abrogates mRNA binding and is known as holo-IRP1 or cytoplasmic aconitase. On the other hand, when cells are iron-depleted, the [4Fe-4S] cluster is absent, and the protein has mRNA binding activity and is known as apo-IRP1.

It is noteworthy that IRP1 and IRP2 share extensive sequence homology apart from a 73 amino acid sequence unique to IRP2 that mediates its degradation (Theil and Eisenstein, 2000). The IRP2 molecule contains no [4Fe-4S] cluster and in iron-replete cells, IRP2 is degraded by a proteasome-dependent mechanism (Guo et al., 1995). Although both IRPs are ubiquitously expressed, IRP1 is more abundant in most tissues (Kim et al., 1995; Kwok and Richardson, 2002; Rouault TA et al., 1990). However, it should be noted that IRP2 is not a null protein. In fact, IRP2(-/-) mice develop neurodegeneration and movement-disorder symptoms due to significant iron accumulation in white matter tracts and nuclei of the brain (LaVaute et al., 2001). In contrast, IRP1(-/-) mice demonstrate normal serum chemistry and all major tissues are without histological abnormalities (Meyron-Holtz et al., 2004). Consequently, it has been argued that IRP2 is highly expressed in many tissues, and in comparison to IRP1, appears to dominate the regulation of iron metabolism (Meyron-Holtz et al., 2004).

1.2.2.3 The Intracellular Labile Iron Pool

After iron(II) is transported out of the endosome, it enters the intracellular iron pool or labile iron pool (Figure 1.2). This entity is not well understood, although it is classically thought to be composed of chelatable iron [iron(II) and iron(III)], associated with low M_r ligands, such as citrate or ATP (Richardson and Ponka, 1997). More recent work has failed to demonstrate the presence of low M_r intermediates in the iron uptake process and the possible involvement of high M_r iron-binding chaperone molecules have been suggested (Petrak and Vyoral, 2001). Alternatively, or in combination with iron-binding chaperone proteins, interactions between organelles such as the endosome and mitochondrion might be involved in intracellular iron trafficking (Zhang et al., 2005). Irrespective of its character, the labile iron pool donates iron to a variety of iron-

containing molecules required for cellular metabolism and also for iron storage in ferritin.

The labile iron pool is generally referred to as being cytosolic and represents < 5% of total cellular iron (for review see Esposito et al., 2002). A transit pool of chelatable iron is also required in the mitochondrion during haem synthesis, and chelatable redox-active iron may exist within other organelles (Esposito et al., 2002; Gurgueira and Meneghini, 1996; Napier et al., 2005; Ponka, 1997). However, the size and molecular nature of these different subcellular iron pools remains to be investigated. A growing body of evidence suggests that a significant amount of iron, mainly in a redox-active form, is located within the lysosome (Persson et al., 2001). The concentration and distribution of chelatable iron in different intracellular compartments in rat hepatocytes has been determined via quantitative laser scanning microscopy using the fluorescent chelator, Phen Green (Petrat et al., 2001). The highest concentrations of iron (15.8 ± 4.1 μM) was in a subgroup of endosomes and/or lysosomes that may be responsible for degrading iron-containing proteins and mitochondria (Petrat et al., 2001). In comparison, all other cellular compartments demonstrated significantly lower concentrations of chelatable iron, for instance the mitochondria and nucleus had 3-fold lower iron levels.

1.2.2.4 Iron Storage in Ferritin and Lysosomal Iron Recycling

Iron which is not immediately required for cell function or synthesis of hemoproteins is deposited in the iron-storage protein, ferritin (Figure 1.2). Ferritin is composed of 24 subunits categorized into two subtypes: a heavy subunit (H-Ft; M_r = 21 kDa) and a light subunit (L-Ft; M_r = 19 kDa) that polymerize into a high M_r polymer (M_r = 430-

450 kDa; Arosio et al., 1978; Richardson and Ponka, 1997). The H- and L-ferritin subunits display about 55% amino acid sequence identity, and have a similar three-dimensional structure. The ferritin molecule is able to accommodate approximately 4,500 iron atoms in its protein shell. Ferritin stores iron(II) by forming a solid oxo-mineral in its core (Theil, 2003). It is suggested that the ferritin H-subunit subunits induce a rapid oxidation of iron(II) to iron(III) through a ferroxidase site composed of seven conserved residues. The L-ferritin subunit on the other hand, has a nucleation site, which is involved in the formation of the iron core (Levi et al., 1992; Wade et al., 1991).

Present knowledge favours the lysosomal pathway as being a significant route for ferritin degradation and re-utilisation of iron (Persson et al., 2001; Radisky and Kaplan, 1998; Roberts and Bomford, 1988; Sibille et al., 1989). Lysosomes degrade various macromolecules, including metalloproteins such as ferritin, and damaged cell organelles. Due to lysosomal autophagy, lysosomes become particularly rich in iron (Persson et al., 2001; Petrat et al., 2001). Solubilized lysosomal iron is either transported to the cytosol by an unknown mechanism or is stored within lysosomes as iron(III) in hemosiderin, *i.e.*, partially degraded ferritin (Persson et al., 2001).

1.3 IRON-RELATED MECHANISMS FOR ANTHRACYCLINE-INDUCED CARDIOTOXICITY

The cardiotoxic effects of anthracyclines have been suggested to be a result of a number of different mechanisms. These are discussed below with emphasis on the role of iron.

1.3.1 Cardiotoxicity Mediated by Iron-Anthracycline Complexes and Free Radical Generation

Anthracyclines bind avidly to iron, forming a 1:1, 2:1 or 3:1 drug-to-metal complex (Figure 1.1) with an overall association constant of 10^{18} (Gianni and Myers, 1992). Doxorubicin can directly bind iron and in the presence of oxygen it can cycle between the iron(II) and iron(III) states (Figure 1.4). The doxorubicin-iron(III) complex can be reduced to the doxorubicin-iron(II) complex in the presence of reducing agents such as NADPH cytochrome P450 reductase, glutathione and cysteine. These reactions are accompanied by the formation of $O_2^{\bullet-}$, and the conversion of anthracycline quinone moieties to semiquinone free radicals (Figure 1.4). The quinone structure of anthracyclines has the potential to act as an electron acceptor from enzymes such as flavin reductases, NADH dehydrogenase and cytochrome P450 reductase (Doroshow, 1983; Gianni and Myers, 1992; Graham et al., 1987). Through the iron-catalysed Haber-Weiss reaction, H_2O_2 and extremely reactive hydroxyl radicals are generated. The semiquinone radical may transform to an aglycane C7-centered radical, which is a potent alkylating agent (Figure 1.4; Jung and Reszka, 2001). It is well-known that such reactive oxygen species (ROS) generation by anthracyclines causes DNA damage and apoptosis (Minotti et al., 2004a).

Although neither H_2O_2 nor $O_2^{\bullet-}$ are particularly reactive, in the presence of redox-active iron even low quantities of ROS are cytotoxic. Since all cells contain small amounts of redox-active iron, formation of hydroxyl radicals, or similarly reactive iron-centered (ferryl and perferryl) radicals, can be promoted under appropriate conditions. These highly reactive species can attack almost all cellular constituents and a number of organelles, and create chain reactions that lead to cell death (Myers, 1998).

The increased activity of the anti-oxidant pathways, such as catalase, glutathione peroxidase, and glutathione transferase, in anthracycline-exposed cardiomyocytes further support the great importance of ROS formation in cardiac injury secondary to anthracycline treatment (Jung and Reszka, 2001). However, cardiac tissue is generally recognised to be quite vulnerable to free radical damage due to the low activity of anti-oxidant enzyme systems (Gianni and Myers, 1992). Finally, it should also be noted that there is evidence that the cytotoxic mechanisms of anthracyclines can be independent of ROS generation (Keizer et al., 1990; Wu and Hasinoff, 2005)

1.3.2 Anthracyclines Mediate Dysregulation of Iron Homeostasis

A number of studies have provided evidence for mechanisms that could be involved in anthracycline mediated cardiotoxicity that are both independent and dependent on iron. Below, we focus upon the iron-dependent mechanisms of anthracycline-mediated cardiotoxicity.

1.3.2.1 Effect of Doxorubicin on Major Regulators of Iron Homeostasis: IRP1 and IRP2

1.3.2.1.1 The Role of Doxorubicinol in Decreasing IRP-RNA-Binding Activity

The effect of doxorubicin on cellular iron homeostasis, including IRP levels, has been suggested to be a factor contributing to its cardiotoxicity (Minotti et al., 1995, 1998). The mechanisms involved in the effect of doxorubicin on IRP1 remain controversial, as a number of research groups have shown different results. Initially, doxorubicinol, a secondary alcohol metabolite of doxorubicin, was described to interact with the [4Fe-4S] cluster of IRP1, resulting in the release of iron(II), and a decrease in cytoplasmic

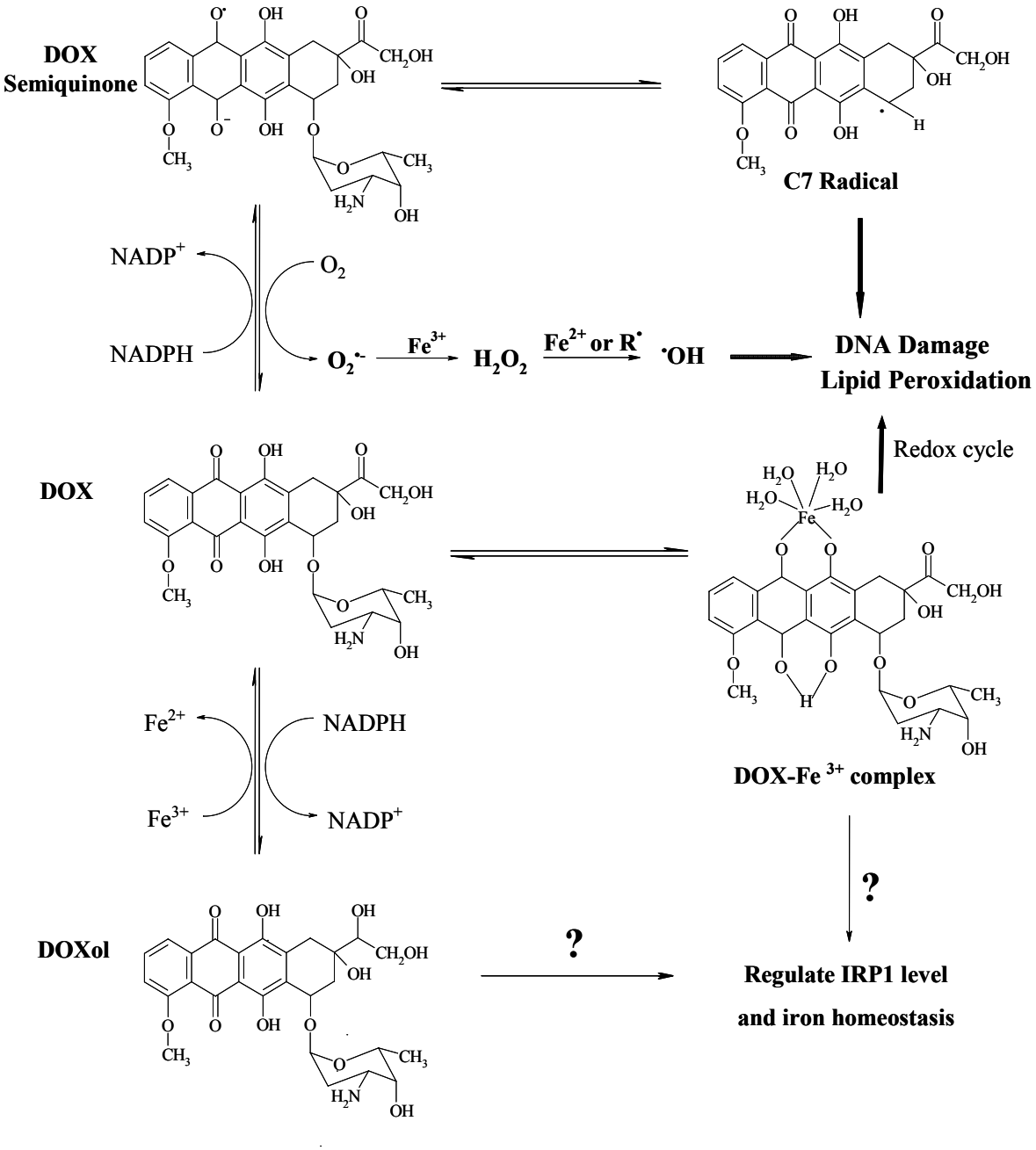

Figure 1.4 Illustration of doxorubicin-mediated redox cycling. Doxorubicin can bind to iron by forming doxorubicin-iron(III) complexes, which may lead to ROS formation and cellular damage. One electron reduction of doxorubicin generates the doxorubicin-semiquinone that induces DNA damage and lipid peroxidation by ROS formation. The semiquinone radical can be transformed to a C7 radical that can also mediate cellular damage. The reduction of doxorubicin by 2 electrons generates a secondary alcohol metabolite, doxorubicinol. Although it is clear that doxorubicin affects cellular iron regulatory protein 1 (IRP1) RNA-binding activity and iron homeostasis, it is debatable whether it is doxorubicinol, the doxorubicin-iron(III) complex, or both that are the active molecular effectors.

aconitase activity (Brazzolotto et al., 2003; Minotti et al., 1995; Minotti et al., 1998). Considering classical IRP theory, decreased cytoplasmic aconitase levels may result in increased IRP-RNA-binding (Hentze and Kuhn, 1996). In contrast, doxorubicinol led to a decrease in IRP-RNA-binding and this could not be reversed by the reducing agent, β-mercaptoethanol (Minotti et al., 1998). It was suggested that doxorubicinol in the presence of the aconitase substrate, *cis*-aconitate, directly removed iron(II) from the [Fe-S] cluster from IRP1 by a mechanism independent of free radical generation (Cairo et al., 2002; Minotti et al., 1998; Figure 1.5; Scheme 1). Moreover, a generalized model was proposed indicating that the interaction of doxorubicinol with IRP1 resulted in iron(II) release from the [4Fe-4S] cluster and the reoxidation of doxorubicinol to doxorubicin. The iron(II) released then formed a complex with doxorubicin that irreversibly inactivated IRP1 (Minotti et al., 1998).

In the investigation of Minotti et al. (1998) described above, lysates from homogenized hearts incubated with iron salts and cysteine were implemented to reconstitute the [4Fe-4S] cluster of IRP-1. Clearly, this system is undefined and the exact molecular site of the iron mobilisation observed in the lysates was not identified. Indeed, it was not clear if the iron release in the lysates after incubation with anthracyclines was due to mobilisation of iron from IRP1 or other molecules (Minotti et al., 1998). Later studies by the same authors showed that incubation of a cardiomyocyte cell line with doxorubicin increased active IRP-RNA-binding but decreased aconitase activity (Figure 1.5; Scheme 2; Minotti et al., 2001). These authors suggested that the sequential action of doxorubicinol and ROS on IRP1 leads to the generation of the null protein. However, it was not clear from this latter article why an increase in IRP1-RNA-binding was observed, which was in contrast to the decrease previously observed

in heart lysates (Minotti et al., 1998).

Further studies by other investigators assessed the effect of doxorubicin in GLC_4 small cell lung carcinoma cells resistant (GLC_4^R) and sensitive (GLC_4^S) to this agent (Brazzolotto et al., 2003). These authors showed that incubating doxorubicin with the sensitive cell type resulted in a decrease in IRP-IRE-binding activity, while it had no effect on the resistant clone (Brazzolotto et al., 2003). When recombinant human IRP1 was incubated with very high concentrations of doxorubicin or doxorubicinol (120 μM), aconitase activity was significantly reduced only after doxorubicinol treatment in the presence of oxygen. These concentrations of anthracyclines are well above those encountered within human patients administered doxorubicin, where serum concentrations reach micromolar levels. In contrast, there was no effect of doxorubicin on purified recombinant IRP2, suggesting that doxorubicin targeted IRP1 (Brazzolotto et al. 2003). This latter result was not consistent with previous studies which showed that incubation of cardiomyocyte cell lines or primary cultures with doxorubicin reduced IRP2-RNA-binding activity (Minotti et al., 2001; Kwok and Richardson, 2002).

1.3.2.1.2 The Role of the Doxorubicin-Iron Complex in Decreasing IRP-RNA-Binding Activity

In subsequent studies by others, three anthracyclines, namely doxorubicin, daunorubicin and epirubicin, had a complex effect on IRP-RNA-binding activity when incubated with cells in culture (Kwok and Richardson 2002). In these experiments, active IRP-RNA-binding activity decreased over a 6 h incubation with anthracyclines and then subsequently increased, while total IRP-RNA-binding decreased as a function

of time. In contrast to a previous investigation by Minotti and co-workers (1998), experiments using cell lysates demonstrated that doxorubicinol in the presence or absence of *cis*-aconitate had no effect on IRP-RNA-binding (Kwok and Richardson, 2002). In contrast, anthracycline-iron and -Cu complexes reduced active IRP-RNA-binding and this was reversible upon the addition of β-mercaptoethanol (Kwok and Richardson, 2002). These latter results differed to those of Minotti and associates (1998) using tissue homogenates, which suggested that the doxorubicin-iron complex irreversibly inactivated IRP-RNA-binding. This inhibitory effect could be due to the ability of the doxorubicin-iron complex to oxidize critical sulfhydryl groups involved in IRP-mRNA-binding activity (Philpott et al., 1993; Figure 1.5; Scheme 3). In this way, the doxorubicin-iron complex would act similarly to other agents that react with sulfhydryl groups, such as diamide (Philpott et al., 1993). Considering this, it is well known that the doxorubicin-iron complex catalyses a range of redox reactions. For instance, it reacts with reductants including glutathione to yield oxidized thiols and oxygen radicals (Gianni and Myers, 1992).

Using primary cultures of cardiomyocytes, Kwok and Richardson (2002) also reported that doxorubicin reduced IRP2-RNA-binding binding activity. These studies are similar to those reported using the H9c2 cardiomyocyte cell line, where doxorubicin irreversibly decreased IRP2-RNA-binding activity (Minotti et al., 2001). Since IRP2 does not possess an [Fe-S] cluster, it can be speculated that the effects of doxorubicin may also be mediated by its ability to oxidize sulphydryl groups involved in mRNA-binding activity. Indeed, anthracycline-mediated free radical production may be involved in this process since 5-iminodaunorubicin that generates far lower levels of free radicals does not affect IRP2-RNA-binding activity (Minotti et al., 2001).

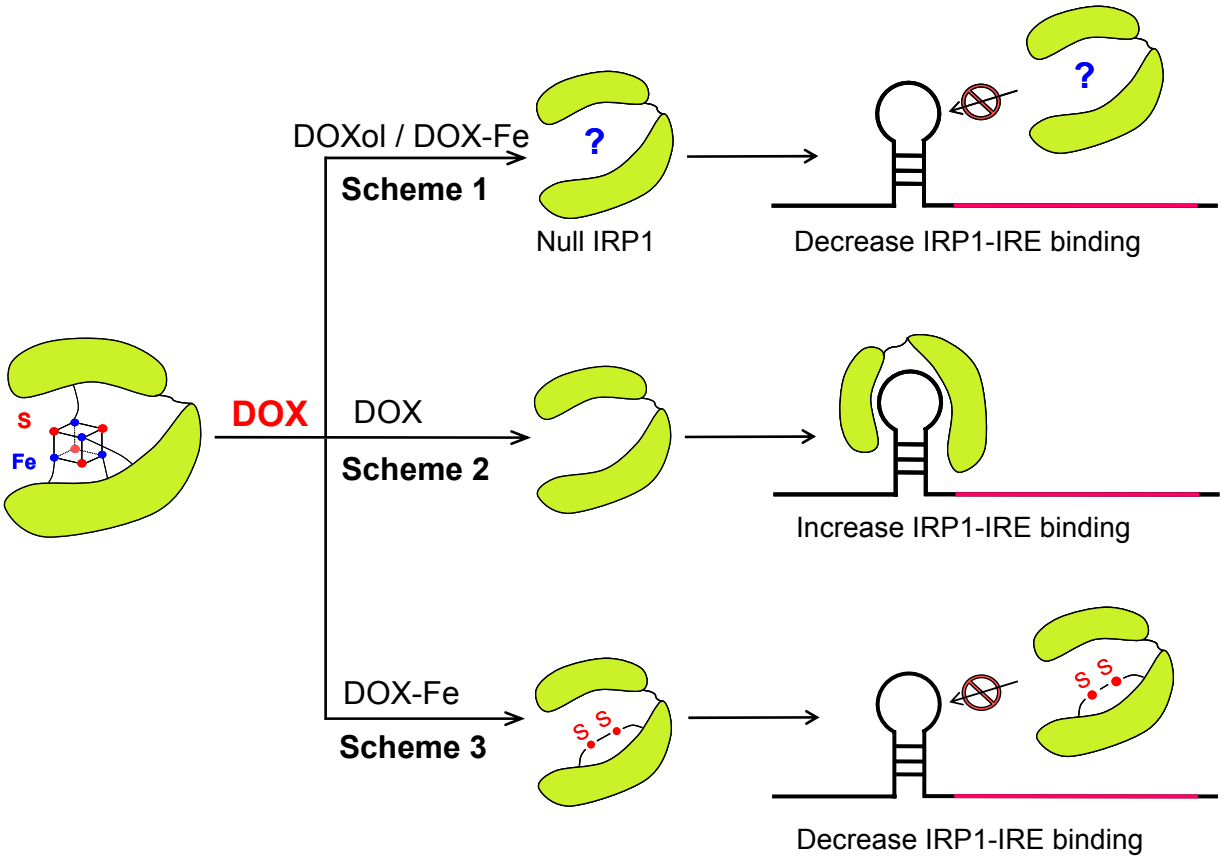

Figure 1.5 Proposed mechanisms of action of doxorubicin on IRP1-RNA-binding activity. There are three main hypotheses of how doxorubicin regulates cellular IRP1 levels: Scheme 1, doxorubicinol, a secondary alcohol metabolite of doxorubicin, together with *cis*-aconitate may act to remove iron from the [4Fe-4S] cluster of holo-IRP1. The removal of iron from the cluster results in the oxidation of doxorubicinol to doxorubicin and generation of the doxorubicin-iron complex which irreversibly converts IRP1 to a null protein (Minotti et al., 1998); Scheme 2, doxorubicin removes the [4Fe-4S] cluster of holo-IRP1 and increases IRP-IRE binding (Minotti et al., 2001; Kotamraju et al., 2002); Scheme 3, The doxorubicin-iron complex catalyses disulfide bridge formation between crucial IRP1 thiol groups inhibiting IRP-IRE binding (Kwok and Richardson, 2002).

1.3.2.1.3 Doxorubicin Increases IRP-RNA-Binding Activity in Endothelial Cells

Studies using endothelial cells have shown different effects of doxorubicin on IRP-RNA-binding activity than those described above. In fact, in an investigation by Kotamraju and colleagues (2002), doxorubicin increased IRP-RNA-binding activity within 8 h and there was also increased iron uptake and TfR1 expression. These experiments suggested that doxorubicin-induced iron uptake occurred via increased IRP-RNA-binding activity and the subsequent elevation of TfR1 levels (Kotamraju et al., 2002). The authors proposed that oxidative stress generated by doxorubicin activated IRP-RNA-binding, as anti-oxidants such as ebselen and Mn(III) tetrakis (4-benzoic acid) porphyrin complex (MnTBAP) inhibited the effect of doxorubicin on TfR1 levels and iron uptake. These results were clearly different to those using lysates from the homogenized heart (Minotti et al., 1998) or neoplastic cell lines, where doxorubicin decreased IRP-RNA-binding and may indicate a cell type-specific response.

In conclusion, the results above demonstrate that the effects of doxorubicin on IRP-RNA-binding activity are complex. In general, in most cell types, doxorubicin decreased active IRP-RNA-binding activity and this will probably result in important downstream effects on cellular iron metabolism. Further studies to clarify the precise molecular mechanisms involved need to be performed.

1.3.2.2 Effect of Doxorubicin on Iron Trafficking Pathways: Doxorubicin Induces Iron Accumulation in Ferritin

Initial studies assessing the effects of doxorubicin on cellular iron metabolism reported that doxorubicin released iron from ferritin (Thomas and Aust, 1986). However, these

experiments were performed *in vitro* using the purified ferritin protein and their physiological significance remained unclear. More recent investigations showed that a 24 h incubation of a range of neoplastic and normal cells with diferric transferrin and doxorubicin (1-10 μM) lead to 3- to 8-fold higher ferritin-iron levels compared to control cells incubated with diferric transferrin alone (Kwok and Richardson, 2003). This accumulation of ferritin-iron was due to the fact that incubation of cells with anthracyclines prevented iron release from this molecule (Figure 1.6). Moreover, the slight increase in ferritin protein levels observed after incubation with doxorubicin (to 130% of the control at 5 μM doxorubicin) could not account for the 3 to 8-fold increase in ferritin-iron accumulation (Kwok and Richardson, 2003).

Considering the mechanism of ferritin-iron accumulation after incubation with doxorubicin, the general process of iron mobilisation from this protein is poorly understood. However, catabolism of ferritin by lysosomes has been suggested to be a likely mechanism (Radisky and Kaplan, 1998; Persson et al., 2001). In addition, anthracyclines are known to accumulate in lysosomes (Hurwitz et al., 1997), and this organelle may be a target for these drugs (Figure 1.6). Recent studies have shown that ferritin iron mobilisation is an energy-dependent process that also requires protein synthesis (Kwok and Richardson, 2004). This latter observation was based on studies inhibiting protein synthesis using cycloheximide, which prevented ferritin iron release (Kwok and Richardson, 2004). It can be speculated that this effect could be due to the requirement for translation of a protein that is involved in ferritin iron mobilisation.

Additional evidence for the involvement of the lysosome in the doxorubicin-mediated inhibition of ferritin iron mobilisation was provided by implementing a number of

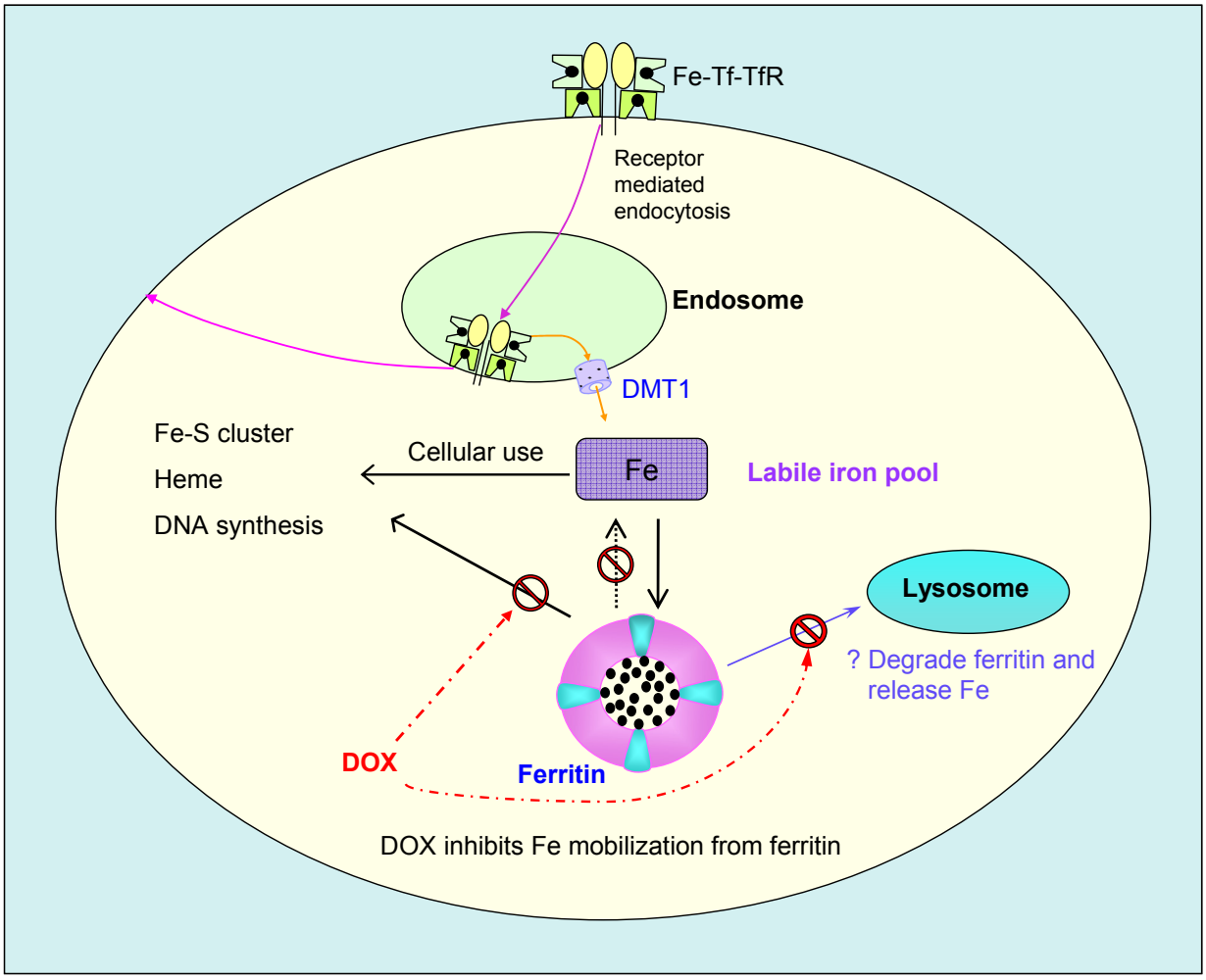

Figure 1.6 Schematic illustration of the effect of doxorubicin on cellular iron metabolism. Doxorubicin leads to iron accumulation in ferritin due to inhibition of iron mobilisation from this protein. There is no change in the total amount of iron in the cell, rather only the intracellular distribution is markedly affected. The mechanism of how doxorubicin inhibits iron release from ferritin is not known, but may, at least in part, involve disturbance to lysosomal function. Indeed, the lysosome has been reported to be involved in ferritin degradation and the release of iron from this protein. The inability of ferritin to release iron after exposure to doxorubicin may lead to cytotoxic effects due to the requirement of essential metabolic processes for iron *e.g.*, DNA synthesis. Clearly, this potential growth inhibitory mechanism is not the only one mediated by anthracyclines.

lysosomal protease inhibitors (Kwok and Richardson, 2004). Depression of lysosomal protease activity using pepstatin A, E64d, or leupeptin, demonstrated that pepstatin A had no effect, while E64d and leupeptin increased ferritin iron-loading to a level similar to doxorubicin. Considering this, since pepstatin A is an aspartic protease inhibitor, while E64d and leupeptin are cysteine or cysteine and serine protease inhibitors, respectively, it can be suggested that aspartic proteases are not involved in ferritin-iron mobilisation (Kwok and Richardson, 2004). Further support for the role of the lysosomes and/or proteosome in ferritin-iron mobilisation was achieved through the use of the lysosomotropic agents, NH_4Cl, chloroquine and methylamine, and the proteasomal inhibitors, MG-132 and lactacystin, that also prevented ferritin-iron mobilisation (Kwok and Richardson, 2004). Thus, the lysosome/proteasome pathway may be an anthracycline target, inhibiting ferritin iron release that is vital for iron-requiring processes, *e.g.*, DNA synthesis (Kwok and Richardson, 2004).

In view of the effect of anthracyclines at inhibiting iron mobilisation from ferritin, it must be noted that this is only one of the many effects of these drugs that contributes to their cytotoxicity. At present, compared to the other cytotoxic effector mechanisms of anthracyclines, the extent to which the inhibition of ferritin iron mobilisation contributes to cardiotoxicity is not clear. Furthermore, it must be noted that the potential cytotoxicity induced by inhibiting ferritin iron mobilisation is at odds with the ability of iron chelators to prevent anthracycline-mediated cardiotoxicity (see Section 1.4 below). In terms of trying to understand this apparent dichotomy, the complexity of the mechanisms of action of anthracyclines must be considered (Minotti et al., 2004a). In fact, the iron pool or other molecular sites that are targeted by chelators to prevent anthracycline-mediated cardiotoxicity are not known and it is of interest that the

chelator, dexrazoxane, does not completely prevent this problem (Swain et al., 1997a). Additional studies investigating the mechanisms of how chelators inhibit anthracycline-mediated cardiotoxicity are required.

Interestingly, similarly to anthracyclines, a number of free-radical generating agents (*i.e.*, menadione and paraquat) have also been shown to be effective at increasing ferritin iron accumulation, an effect that can be at least partially reversed by free radical scavengers (Kwok and Richardson, 2003). It has been proposed that the ability of free radical generators to induce ferritin iron accumulation may be mediated via the effects of these agents on lysosomal function (Kwok and Richardson, 2004). Further evidence for a role of free radical generation in inducing the alterations in ferritin-iron metabolism was obtained by Corna and associates (2004) comparing doxorubicin and the redox active anthracycline analogues, mitoxantrone and 5-iminodaunorubicin. These ROS-generating compounds were found to significantly induce ferritin protein expression, especially the H-ferritin subunit, suggesting that doxorubicin regulates ferritin levels via ROS formation (Corna et al., 2004). Further experiments revealed that enhanced ROS production and ferritin accumulation after doxorubicin treatment can be prevented by the ROS scavenger, *N*-acetylcysteine. Therefore, it was suggested that doxorubicin-mediated ROS production was involved in ferritin induction in the H9c2 cardiomyocyte cell line (Corna et al., 2004). Concomitant experiments showed that preincubation of doxorubicin or mitoxantrone could paradoxically protect H9c2 cells from cytotoxicity induced by iron loading with ferric ammonium citrate, while incubation with 5-iminodaunorubicin did not protect the cell. Considering that 5-iminodaunorubicin reportedly produces less ROS than either doxorubicin or Mitox, these studies suggested that the protective effect of these compounds to iron-loading

seemed to correlate with their ability to act as ROS generators (Corna et al., 2004).

Apart from the effect of doxorubicin on ferritin iron-loading, further evidence that interactions between doxorubicin and iron metabolism are involved in the cytotoxic effects of these drugs has been provided by studies examining HFE knockout mice (Miranda et al., 2003). After doxorubicin treatment, HFE knockout mice accumulate more iron in the serum and several organs compared to their wild-type counterparts, suggesting that HFE deficiency may increase susceptibility to doxorubicin-induced toxicity (Miranda et al., 2003). Doxorubicin treated HFE-deficient mice also have higher mortality rates and a greater degree of mitochondrial damage compared with the control (Miranda et al., 2003).

1.4 AGENTS THAT PREVENT DOXORUBICIN-MEDIATED CARDIOTOXICITY BY INTERACTING WITH IRON

The evidence presented above indicates that anthracyclines markedly disturb intracellular iron metabolism and a variety of studies have clearly shown that iron plays an important role in the cardiotoxicity mediated by this drug. Apart from this, it is well known that the iron chelator, dexrazoxane (also known as ICRF-187), is an effective cardioprotective agent against the effects of doxorubicin. Below, we discuss the potential of iron chelators as agents to prevent anthracycline-mediated cardiotoxicity.

1.4.1 Dexrazoxane

The only clinically approved chelator that is currently used to alleviate doxorubicin-induced cardiotoxicity is dexrazoxane (Figure 1.7; Swain et al., 1997a,b; Minotti et al.,

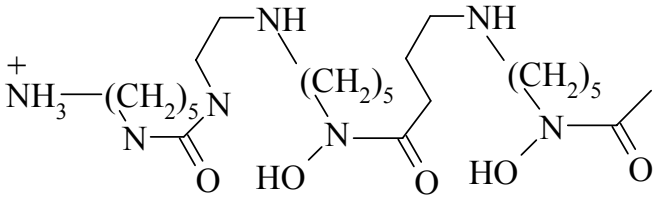

Desferrioxamine (DFO)

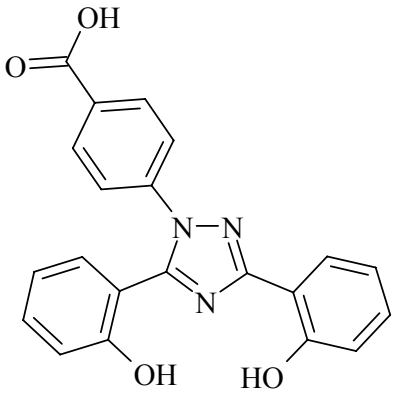

4-[3,5-bis-(hydroxyphenyl)-1,2,4-triazol-1-yl]- benzoic acid (ICL-670A)

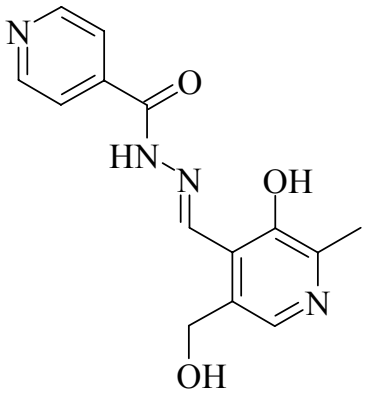

Pyridoxal isonicotinoyl hydrazone (PIH)

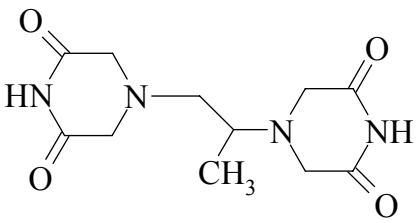

Dexrazoxane (DXR)

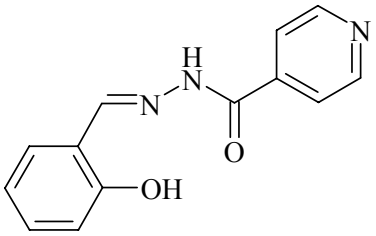

Salicylaldehyde isonicotinoyl hydrazone (SIH)

Figure 1.7 Illustration of the chemical structures of the iron chelators: desferrioxamine, dexrazoxane, pyridoxal isonicotinoyl hydrazone (PIH), 4-[3,5-bis-(hydroxyphenyl)-1,2,4-triazol-1-yl]- benzoic acid (ICL670A) and salicylaldehyde isonicotinoyl hydrazone (SIH).

2004). It is suggested that *in vivo,* dexrazoxane permeates the cell membrane and can be rapidly hydrolysed to its metal ion-binding metabolite, ADR925, thus decreasing anthracycline-iron binding and ROS formation (Hasinoff, 1998). ADR-925 quickly displaces iron(III) and copper(II) from their complexes with anthracyclines, indicating that ADR925 chelates iron(III) more strongly than doxorubicin (Hasinoff, 1998). Interestingly, metal ions, including the anthracycline-iron(III) complex, promote formation of ADR-925 and potentiate its metal chelating effect (Hasinoff, 1998).

Dexrazoxane has shown significant protection against cardiotoxicity caused by doxorubicin in numerous animal models, for example, mouse, rat, hamster, rabbit and dog (Herman and Ferrans, 1990; Herman et al., 1992; Herman et al., 1988; Imondi et al., 1996; Minotti et al., 2004a). In addition, clinical trials showed that dexrazoxane protects patients with advanced breast cancer from doxorubicin-induced cardiotoxicity (Swain et al., 1997b). With dexrazoxane therapy, patients treated with dexrazoxane-doxorubicin (ratio 10:1) were only 38% as likely to develop cardiac complications compared to treatment with doxorubicin alone (Swain et al., 1997b). Dexrazoxane also shows short-term cardioprotection against doxorubicin in childhood cancers (Wexler, 1998). Because the outcomes of long-term cardioprotection are not clear, dexrazoxane is only recommended for adult patients who have received an accumulated dosage of doxorubicin $\geq$ 300 mg/m^2 (Hensley et al., 1999). However, this agent does not confer absolute cardioprotection (Swain et al., 1997b) and causes myelosuppression (Curran et al., 1991). Considering this, other regimens of chelation therapy using a variety of ligands have been investigated and these are discussed below.

1.4.2 Desferrioxamine

Desferrioxamine (Figure 1.7) is a hexadentate iron chelator widely used for iron overload disease such as β-thalassemia major (Lombardo et al., 1996). Desferrioxamine significantly reduces iron storage and ferritin levels and has been used for many years to control the iron-loading observed in transfusion-dependent anemias (Richardson and Ponka, 1998). However, in comparison, there has been relatively few investigations assessing its protective effects against anthracycline-mediated cardiotoxicity. An early study found that after incubating isolated mice atria with doxorubicin (30 μM), desferrioxamine (200 μM) was more effective than dexrazoxane (200 μM) at preventing the doxorubicin-induced decrease in contractile force (Voest et al., 1994). In addition, Saad et al. (2001) found that desferrioxamine was highly effective at protecting against doxorubicin-induced acute cardiotoxicity when used at a dose that was 10-fold greater than doxorubicin. Treatment with desferrioxamine either prior to or after doxorubicin administration reduced the doxorubicin-mediated elevation of cardiac isoenzymes such as creatine kinase isoenzyme and lactate dehydrogenase, which are indicators of myocardial damage and compromised cellular integrity, respectively (Saad et al., 2001). However, desferrioxamine is limited to subcutaneous or intravenous infusion because of its poor absorption from the gastrointestinal tract and its short plasma half-life (Aouad et al., 2002). Moreover, considering that chelator permeability is critical to the ability of these compounds to inhibit anthracycline-mediated cardiotoxicity (Voest et al., 1994), the limited membrane permeability of desferrioxamine probably explains the need for high levels of this chelator to inhibit the effects of doxorubicin (Saad et al., 2001). These disadvantages have encouraged the design of orally active chelators with high lipophilicity and membrane permeability that can access intracellular iron pools to

inhibit anthracycline-mediated cardiotoxicity.

1.4.3 Other Iron Chelators with Potential Cardio-Protective Activity

Pyridoxal isonicotinoyl hydrazone (PIH; Figure 1.7) is a relatively lipophilic orally effective tridentate iron chelator that has high membrane permeability and possesses marked iron chelation efficacy (for review see Richardson and Ponka, 1998). In fact, PIH is able to remove iron from a variety of rodent models via the biliary route (Hershko et al., 1981; Hoy et al., 1979; Ponka et al., 1979a; Ponka et al., 1979b; Richardson and Ponka, 1998). Moreover, low doses of PIH (30 mg/kg/day) given to human patients increased iron excretion from iron-loaded patients (Brittenham, 1990). In a recent *in vivo* study, PIH pre-treatment protected rabbits from daunorubicin-mediated toxicity, although its efficacy was not as great as dexrazoxane (Simunek et al., 2005). This study showed that repeated administration of daunorubicin to rabbits (3 mg/kg, i.v. once a week for 10 weeks) led to 4 deaths, while all animals survived when PIH was administered 60 min prior to daunorubicin. Salicylaldehyde isonicotinoyl hydrazone (SIH; Figure 1.7), a PIH analogue, also showed cardioprotective potential by restoring a loss in cytochrome P450 activity after daunorubicin treatment (Schroterova et al., 2004). Hence, this class of chelators show promise as potential cardioprotective agents and require further investigation.

Other chelators with possible potential in the treatment of anthracycline-mediated cardiotoxicity include the new orally active chelator, ICL670A (4-[3,5-bis-(hydroxyphenyl)-1,2,4-triazol-1-yl]- benzoic acid; Figure 1.7). This compound belongs to the synthetic tridentate and iron-selective ligands of the bis-hydroxyphenyl-triazole class (Schroterova et al., 2004). Using the hypertransfused rat model, ICL670A was

able to remove iron from parenchymal iron stores 4 to 5 times greater than desferrioxamine, and combination of desferrioxamine and ICL670A demonstrated an additive effect at the lower dose range of 25 to 50 mg/kg (Hershko et al., 2001). Phase I and II clinical trials of ICL670A were successful in patients with transfusional iron overload (Nisbet-Brown et al., 2003). However, a recent study on neonatal rat cardiac myocytes showed that ICL670A was unable to protect these cells from doxorubicin-mediated cardiotoxicity as measured by lactate dehydrogenase release, while dexrazoxane significantly prevented this (Hasinoff et al., 2003). The reason for inability of ICL-670A to prevent anthracycline mediated cardiotoxicity is puzzling, but it could be related to its inability to access appropriate pools of iron that could be the potential targets of anthracyclines. Understanding why some chelators are protective against anthracycline-mediated cardiotoxicity while others are not is important for the rationale design of new cardioprotective agents and understanding the mechanism of action of these drugs.

1.5 SUMMARY

Anthracyclines avidly bind iron and form anthracycline-iron(III) complexes that may serve as a regulator of cellular iron homeostasis, by generally decreasing IRP-RNA-binding activity. However, the precise molecular mechanism of this effect remains controversial with the doxorubicin-iron complex and/or doxorubicinol, being involved. Another molecular target of doxorubicin includes the iron-storage protein ferritin. Recent experiments suggest that anthracyclines prevent ferritin iron mobilisation through a mechanism which may involve inhibition of lysosomal function that is involved in ferritin degradation. The prevention of iron release from ferritin may be detrimental to the cell due to the importance of iron for DNA synthesis and energy

metabolism. On the other hand, it has been suggested that doxorubicin-mediated ferritin iron accumulation is a protective effect against anthracycline-induced free radical generation.

Due to the role of iron in anthracycline-mediated cardiotoxicity, both dexrazoxane and other chelators such as desferrioxamine have proven to be successful cardioprotective agents. Because these two chelators have limitations, including myelotoxicity and a cumbersome administration regimen, respectively, other chelators that are orally effective are being developed. Indeed, the ligands PIH, SIH and ICL670A are under investigation and their ability to alleviate anthracycline-mediated cardiotoxicity is important to evaluate in further studies.

CHAPTER 2:

GENERAL MATERIALS

AND METHODS

2.1 REAGENTS

2.1.1. General Reagents

Catalase, ebselen, ferric ammonium citrate (FAC), horse spleen ferritin, menadione, sodium thiosulfate ($Na_2S_2O_3$) and superoxide dismutase (SOD) were obtained from Sigma-Aldrich (St. Louis, MO, USA). The Mn(III) tetrakis (4-benzoic acid) porphyrin complex (MnTBAP) was obtained from MP Biomedicals (Aurora, Ohio, USA). A polyclonal anti-ferritin antibody was obtained from the In-Vitro Technologies (VIC, Australia). All other chemicals were of analytical reagent quality.

2.1.2. Anthracyclines and Analogue

Doxorubicin (DOX), daunorubicin (DAU) and epirubicin (EPI) were obtained from Pharmacia (Sydney, Australia). An anthracycline analogue, mitoxantrone, was obtained from Sigma-Aldrich (St. Louis, MO, USA). Another analogue named 5-iminodaunorubicin (5-i-DAU) was kindly provided by Dr. Ven L. Narayanan, Drug Synthesis and Chemistry Branch, National Cancer Institute, Bethesda, MD, USA.

The anthracycline-Fe complexes (DOX-Fe, DAU-Fe and EPI-Fe) were synthesized under acidic conditions as previously described (Garnier-Suillerot and Gattegno, 1988; Gianni et al., 1985; Kostoryz and Yourtee, 2001; Zweier et al., 1986). Briefly, anthracyclines were diluted to 1 mM in 140 mM NaCl and $FeCl_3 \cdot 6H_2O$ was diluted to 1 mM in 1 mM HCl. Then 3 volumes of 1 mM anthracycline was mixed reacted with 1 volume of 1 mM $FeCl_3$ to synthesize the anthracycline-Fe (3:1) complex. The reaction was allowed to proceed for 15 min in the dark, resulting in a purple brown solution. These solutions were then adjusted to pH 7.4 and spectroscopic analysis performed between 350 and 800 nm. The DOX-Fe complex demonstrated a

hypochromic shift at 480 nm and the Fe complex charge-transfer band was demonstrated at around 600 nm as demonstrated previously (Garnier-Suillerot and Gattegno, 1988; Gianni et al., 1985; Kostoryz and Yourtee, 2001; Zweier et al., 1986).

2.1.3. Iron Chelators

Desferrioxamine (DFO) was obtained from Novartis Pharmaceutical Co. (Basel, Switzerland). The chelators pyridoxal isonicotinoyl hydrazone (PIH) and the PIH analogue, 2-hydroxy-1-naphthylaldehyde isonicotinoyl hydrazone (311), were synthesized using standard procedures (Richardson et al., 1995). Briefly, a Schiff base condensation was performed between pyridoxal isonicotinoyl hydrazone or 2-hydroxy-1-naphthyladehyde and isonicotinic acid hydrazide to yield PIH or 311, respectively (Richardson et al., 1995).

PIH was dissolved in dimethyl sulphoxide (DMSO) as 10 mM stock solution immediately prior to an experiment and then diluted in medica containing 10% foetal calf serum (FCS) giving a final DMSO concentration of less than or equal to 0.5% (v/v). Solutions were mixed vigorously to ensure total solubilisation.

2.2 CELL CULTURE

Human DMS-53 lung carcinoma, human IMR-32 neuroblastoma, human SK-Mel-28 melanoma, human SK-N-MC neuroepithelioma, human MCF-7 breast cancer, rat H9c2 cardiomyocyte were obtained from the American Type Culture Collection (Rockville, MD, USA). The murine fibroblast cell line from homozygous *hypoxia inducible factor-1α* (*HIF-1α*) knockout mice and its wild-type counterparts were obtained from Dr R. Johnson (University of California, San Diego). All cell lines, except rat H9c2

cardiomyocytes, were grown in Eagle's modified minimum essential medium (MEM; Gibco BRL, Sydney, Australia) containing 10% fetal bovine serum (Gibco), 1% non-essential amino acid (Gibco), streptomycin (Gibco; 100 μg/mL), penicillin (Gibco; 100 U/mL) and fungizone (Squibb Pharmaceuticals, Montreal, Canada; 0.28 μg/mL).

Rat H9c2 cardiomyocytes were grown in Dulbecco's modified Eagle's medium (DMEM; Gibco) with 10% fetal bovine serum, 1% non-essential amino acid, streptomycin (100 μg/mL), penicillin (100 U/mL) and fungizone (0.28 μg/mL).

2.3 CELL PROLIFERATION ASSAY

At the end time-point of proliferation experiments, the cells were removed from the plate with 1 mM EDTA. The cells were pelleted at 1390 rpm for 5 min and the supernatant aspirated. Pelleted cells were then resuspended in fresh media. Trypan blue (50 μL; Sigma Aldrich) was added to a 50 μL aliquot of cell suspension and allowed to stain for 2-3 min. A visual cell count was next performed using a haemocytometer and light microscope.

2.4 RNA ISOLATION AND SEMI-QUANTITATIVE RT-PCR

2.4.1 Isolation of RNA from Whole Cells

Total RNA was isolated from whole cells using TRIzol® Reagent (Sigma-Aldrich). Whole cell pellets were resuspended in a 1 mL volume of TRIzol®. Briefly, the cell lysates were incubated at room temperature for 5 min, then 0.2 mL of chloroform was added and the samples shaken vigorously. After another incubation period, the samples were centrifuged at 12,000 x*g* for 15 min at 4°C, and the aqueous phase transferred to a 0.5 mL volume of isopropanol (Sigma-Aldrich). After a further 10 min incubation, the

samples were centrifuged, the supernatant removed and the RNA pellet washed in 75% RNA-grade EtOH. RNA pellets were resuspended in DEPC-treated water and concentrations determined by UV-Vis spectrophotometry at 260 nm. The quality of the RNA was also assessed by 1.5% formaldehyde gel electrophoresis and the bands visualised by ethidium bromide (EtBr) staining.

2.4.2 Reverse Transcriptase-Polymerase Chain Reaction

Isolated total RNA was used to perform semi-quantitative reverse-transcriptase polymerase chain reaction (RT-PCR). A typical reaction follows: 0.3 μg of RNA was incubated with gene specific oligonucleotides (0.2 μM final primer concentration) in a 25 μL volume containing 12.5 μL of 2x Reaction Mix (1.6 mM $MgSO_4$ and 200 μM dNTP) and 1 μL SuperScript™ III RT/ Platinum® *Taq* Mix for 30 min at 56°C. After reverse transcription the samples were initially denatured for 3 min at 94°C. The reactions were then amplified for 23–36 PCR cycles that included a 94°C denaturation step for 30 s, 56°C annealing step for 30 – 60 s and a 68°C extension step for 60 s, with a final extension time of 5 min. As an internal control, the house-keeping gene *β-actin* was amplified from the same samples. All RT-PCR amplifications were performed with a no template control that was always negative. To minimise non-specific amplification of genomic DNA, primers were designed to span exons where possible. All RT-PCR reaction products were analysed by 1.5% agarose gel electrophoresis and visualised with EtBr staining.

2.5 DETECTION OF PROTEIN USING WESTERN BLOT ANALYSIS

2.5.1 Antibodies

The mouse monoclonal anti-human β-actin antibody (Sigma-Aldrich; clone AC-15) was used at a dilution of 1:5,000. The anti-human TfR1 antibody was used ay a concentration of 1:4,000 (Sigma-Aldrich). The rabbit monoclonal anti-human Ndrg1 antibody was used at a dilution of 1:500 (Zymed, Carlsbad, California). The sheep monoclonal anti-human ferritin antibody was used at a dilution of 1:1,000 (In-Vitro Technologies, Australia). Anti-mouse, anti-rabbit and anti-sheep IgG antibodies conjugated with horseradish peroxidase (0.03-0.1 mg/mL; Sigma-Aldrich) were used at a dilution of 1:5,000.

2.5.2 Extraction of Protein from Whole Cells

Cells grown on the flasks were washed with phosphate buffered saline (PBS) and stored at -80°C overnight. The cells were thawed on ice and scraped with 250 µL of ice-cold lysis solution [150 mM NaCl, 10 mM Tris-HCl (pH 7.4), 1.5% Triton X-100, 0.5% SDS, 1 mM EDTA, 1mM EGTA, 40 µM NaF and EDTA-free protease inhibitor cocktail (Roche, Penzberg, Germany)]. Whole cells were vigorously suspended in lysis solution and incubated on ice for 30 min. The samples were subjected to multiple 2 sec bursts of sonication on ice and centrifuged at 16,000 x*g* for 45 min at 4°C. The protein lysate supernatants were retained and the protein concentrations were determined using the Bio-Rad protein assay reagent (Bio-Rad, Hercules, CA, USA) as described in the manufacturer's directions.

2.5.3 Western Blot Analysis

Protein lysates were heat denatured at 90°C for 5 min, mixed with loading buffer under

non-reducing conditions and then added (100 μg/lane) to a non-reducing PAGE gel. This consisted of 4% stacking and 12% separating gels (SDS-PAGE stacking or separating buffers with 30% bis-acrylamide, 10% ammonium persulphate (Sigma-Aldrich), N,N,N',N'-tetramethyl-ethylenediamine (TEMED; Bio-Rad, Hercules, CA, USA) and de-ionised water. Protein standards (Bio-Rad) were run on each gel. Following electrophoresis in SDS-PAGE running buffer, proteins were electroblotted at 30 V onto polyvinyl-difluoride (PVDF) membranes (Amersham Biosciences, Buckinghamshire, United Kingdom) overnight at 4°C in 90% SDS-PAGE transfer buffer/10% MeOH using standard transfer protocols (Sambrook et al., 1989). The membrane was stained with Ponceau S (Sigma-Aldrich) to ensure that all lanes contained equal amounts of protein and that the transfer of proteins to the membrane had been complete. In all experiments, only membranes with equal protein loads were used. As an additional check of protein loading, membranes were also probed for β-actin. All incubation and washing steps were performed using a platform rocker (Bioline, Edwards Instrument Co., Australia).

Membranes were soaked in MeOH and blocked with 5% skim milk in Tris buffered saline (TBS) for 2 h at room temperature. The membranes were then washed four times with TBS containing 0.1% Tween 20 (Sigma-Aldrich) (TBST). Monoclonal antibodies were added to TBS containing 5% skim milk and incubated for 2 h or overnight at room temperature. Membranes were then washed four times with TBST. Following washing, a secondary antibody conjugated to horseradish peroxidase was incubated with the membranes for 1 h at room temperature. After washing, the membranes were developed using the Enhanced chemiluminescence (ECL) Plus™ Western blot detection reagent (GE Healthcare, Bucks, UK) and exposed to X-ray film. The films

were scanned and assembled in Adobe Photoshop then analysed using the densitometric software, Quantity One (Bio-Rad). All densitometric data were normalised to β-actin loading controls.

2.6 CELLULAR IRON UPTAKE AND MOBILISATION EXPERIMENTS

2.6.1 Preparation of ^{59}Fe-Transferrin

Human apotransferrin (apo-Tf; Sigma-Aldrich) was labeled with ^{59}Fe (Dupont NEN, MA) to produce $^{59}Fe_2$-transferrin (^{59}Fe-Tf), as described (Kwok and Richardson, 2003). Briefly, apo-Tf was labeled with Fe using the ferric-nitrilotriacetate complex at a ratio of 1 Fe to 10 NTA. This complex was prepared in 0.1 M HCl and then this solution adjusted to pH 7.4 using 1.4% $NaHCO_3$. This solution was added to apo-Tf and then incubated for 1 h at 37^{o}C. Unbound Fe was removed by exhaustive vacuum dialysis against 150 mM NaCl adjusted to pH 7.4 using 1.4% $NaHCO_3$. The saturation of Tf with Fe was monitored by UV-Vis spectrophotometry with the absorbance at 280 nm (protein) being compared with that at 465 nm (Fe-binding site). In all studies, fully saturated diferric Tf was used.

2.6.2 Effect of Anthracyclines on ^{59}Fe Efflux from Prelabelled Cells

Iron efflux experiments examining the ability of various agents to mobilise ^{59}Fe from cells were performed using established techniques (Richardson et al., 1995). Briefly, cells were prelabelled with ^{59}Fe-Tf ([Tf] = 0.75 μM; [Fe] = 1.5 μM) for 3 h at 37°C. This medium was aspirated and the cell monolayer washed four times with ice-cold PBS. The cells were then reincubated for 3 to 24 h at 37°C with minimum essential medium in the presence or absence of the agents to be tested. After this incubation, the overlying media containing released ^{59}Fe were collected in γ-counting tubes. The cells

were removed from the Petri dishes and placed in a separate set of tubes. Radioactivity was measured in both the cell pellet and supernatant using a Wallac Wizard 1480 3" γ-counter (Turku, Finland).

2.6.3 The Ability of Iron Chelators and Anthracyclines to Mobilise ^{59}Fe from the Cell Lysates

The ^{59}Fe mobilisation assay was performed to examine the ability of the chelators or anthracyclines to chelate ^{59}Fe from the cell lysates using standard procedures (Watts and Richardson, 2002). Briefly, cells grown to near confluence in culture flasks were labelled with ^{59}Fe-Tf (0.75 μM) for 3 h at 37 °C, placed on a tray of ice, the medium decanted and the cell monolayer washed six times with ice-cold BSS. The cells were lysed by one freeze-thaw cycle and then detached from the flask using a Teflon spatula in the presence of the nonionic detergent Triton X-100 (1.5%) at 4°C. These samples were then centrifuged at 16,000 x*g* for 30 min at 4 °C and the cytosol removed and assessed for radioactivity using the γ-counter described above. The cytosolic samples were then incubated for 3 h at 37°C with the agents of interest for 24 h. After this incubation, the samples were then subjected to centrifugation at 4°C through a 5-kDa NMWL exclusion filter unit (Millipore, Billerica, MA, USA). After centrifugation, the eluent and eluate were taken to estimate ^{59}Fe levels by the γ-counter.

2.6.4 Effect of Anthracyclines on ^{59}Fe Uptake from Transferrin by Cells

To examine the ability of various agents to inhibit cellular ^{59}Fe uptake from ^{59}Fe-Tf, experiments were performed using standard procedures (Richardson et al., 1995). Briefly, cells were incubated with ^{59}Fe-Tf (0.75 μM; *i.e.*, [Tf] = 0.75 μM; [Fe] = 1.5 μM) together with the agents of interest for 3 to 24 h at 37°C. This medium

was then aspirated and the cell monolayer washed four times with ice-cold PBS. Cells were then harvested on ice using a plastic spatula and placed in γ-counting tubes. As a measure of cellular density, protein concentrations were assessed using the Bio-Rad protein reagent (Bio-Rad, Hercules, CA, USA). The data are expressed as counts per minute of ^{59}Fe/mg of protein. Separate experiments demonstrated that cell number was directly proportional to protein concentration.

2.7 CELLULAR IRON DISTRIBUTION STUDIES

2.7.1 Cell Treatments

To examine cellular ^{59}Fe distribution during ^{59}Fe efflux, cells were pre-labelled with ^{59}Fe-Tf (0.75 μM) for 3 h at 37°C. Cells were then washed four times with ice-cold PBS and reincubated in the presence or absence of agents of interest for 3 to 24 h at 37°C. Following the reincubation, media was removed and cells stored in -80°C. To examine ^{59}Fe distribution during cellular Fe uptake, cells were labelled with ^{59}Fe-Tf (0.75 μM), in the presence or absence of the agents of interest, for 3-24 h at 37°C. Cells were then washed four times with ice-cold PBS and stored at -80°C.

2.7.2 Cell Lysates

Cells stored at -80°C were then thawed on ice and then lysed by scraping in the presence of 100 μL ice-cold 1.5% Triton X-100 containing 2 mM PMSF (Sigma), followed by one freeze-thaw cycle. Samples were then vortexed and spun at 16,000 x*g* for 45 min at 4°C to separate the stromal mitochondrial membrane (SMM) fraction from the cytosolic fraction. Under these conditions, the SMM fraction contains the disrupted plasma and nuclear membranes, intracellular membranes and a variety of organelles including mitochondria and lysosomes (Rickwood and Patel, 1995).

2.7.3 Determination of Intracellular Iron Distribution using Native-PAGE-^{59}Fe-Autoradiography

Native-gradient-PAGE-^{59}Fe-autoradiography was performed using established techniques (Babusiak et al., 2005). Briefly, cells labelled with ^{59}Fe-Tf (0.75 μM) were lysed at 4^{o}C in buffer containing 1.5% Triton X-100, 140 mM NaCl and 20 mM HEPES (pH 8) supplemented with an EDTA-free protease inhibitor cocktail (Roche, Penzberg, Germany). Samples were then vortexed and centrifuged at 16,000 x*g* for 45 min at 4°C. The supernatants were loaded onto a native 3-12% gradient PAGE gel (100 μg protein/lane) and electrophoresis was performed at 20 mA/gel overnight at 4°C. Gels were subsequently dried and autoradiography was performed. Bands on X-ray film were quantified by scanning densitometry and analysed using the program, Quantity One (Bio-Rad, Hercules, CA).

Super-shift experiment was performed as previously described (Kwok and Richardson, 2003). Briefly, cell lysates were incubated with the anti-ferritin antibody (In-Vitro Technologies, VIC, Australia) for 1 h at 37°C. The mixture was then separated using the native gradient PAGE.

2.8 ^{3}H-LEUCINE INCORPORATION ASSAY

To assess cellular protein synthesis, ^{3}H-leucine incorporation assay was performed using standard procedures (Richardson and Milnes, 1997). Cells were seeded onto petri dishes overnight and then incubated with the agents of interest for 22 h at 37°C. The cells were then labelled with ^{3}H-leucine (1 μCi/dish) for 2 h at 37°C. After the incubation, media was removed and the cells washed four times with ice-cold PBS. Cells were then scraped from the plates using 1 mL PBS into scintillation vials along

with 4 mL of scintillant and removed into a 5 mL scintillation tube. Radioactivity was measured by a Beckman LS 6000 TA β-counter (Beckman Instruments, Irvine, CA). Binding of isotope to the plastic wells was corrected for by the preparation of blank wells containing all additions apart from the cells.

2.9 TWO DIMENSIONAL GEL ELECTROPHORESIS

2.9.1 Animals

The KO and WT animals were obtained from Drs. H. Puccio and M. Koenig (Institut de Genetique et de Biologie Moleculaire et Cellulaire, CNRS/INSERM, Universite Louis Pasteur, Strasbourg, France). These animals were bred and handled using a protocol approved by the University of Sydney Animal Ethics Committee. Genotyping was performed using tail DNA *via* standard techniques (Puccio et al., 2001).

2.9.2 Protein Extraction from Mice Hearts or Cells

Mice hearts were cut into small pieces, washed in PBS buffer and homogenized in a buffer for 2D gel electrophoresis (7 M urea, 2 M thiourea and 1% C7bZO) or in a buffer for Western blot analysis (50 mM Tris-HCl, 1.5% Triton X100, EDTA-free Protease Inhibitor Cocktail (Roche, Penzberg, Germany), pH 7.2). For human SK-Mel-28 cells, proteins were extracted and homogenized using the buffers mentioned above. Homogenisation was performed using a Dounce glass tissue grinder (approximately 10 strokes, small clearance pestle; Sigma-Aldrich Chemical Co., St. Louis, MO USA) followed by sonication (2 x 5 sec, 50% intensity) and then pelleted at 16,000 x*g*.

2.9.3 Two dimensional Gel Electrophoresis

The supernatants after protein extraction were reduced and alkylated in 5 mM tributylphosphine and 10 mM acrylamide monomer for 60 min at 20°C. The reaction was quenched by adding 10 mM DTT. Protein concentration was determined using Bio-Rad protein assay (Bio-Rad, Hercules, CA, USA). Immobilised pH gradient strips (IPG strips, 11 cm, pH 5–8, Bio-Rad) were re-hydrated in 500 µg sample protein extract for 6 h at room temperature. The re-hydrated strips were focused using the ElectrophoretIQ^3 system (Proteome Systems, Boston, MA USA) for a total of 120 kVh. IPG strips were then equilibrated using equilibration buffer and loaded onto SDS-PAGE gels (GelChip™, 2D, 8–16%, 10 cm × 15 cm; Proteome Systems) for second dimension separation by the ElectrophoretIQ^3 system (50 mA/gel, 15 °C for 120 min; Proteome Systems). The gel was fixed in a solution consisting of 25% methanol and 10% acetic acid and stained using colloidal Coomassie Blue (Proteome Systems). All experiments were repeated five times using samples from five different mice.

2.9.4 Image Analysis

Gels were analyzed using Phoretix 2D Expression software (Nonlinear Dynamics Ltd, Newcastle, UK). Following background subtraction and volume normalization of all gels (normalization was based on total spot density), average gels were created for each pentaplicate. To verify the expression differences (spot volume) between the control and frataxin-deleted group, one-way analysis of variance (ANOVA) was performed. Spots of interest were recovered for identification by mass spectrometry.

2.9.5 Mass Spectrometry (MS) and Database Searching

Protein spots were cut and de-stained using 25 mM NH_4HCO_3/ 60% acetonitrile (ACN) for 2 × 30 min at 37°C. Each gel piece was incubated with 12.5 ng/mL trypsin (sequencing grade; Promega, Madison, WI, USA) in buffer containing 25 mM NH_4HCO_3/0.1% trifluroacetic acid for 45 min at 4°C followed by incubation at 37°C for 2 h. The peptide mixtures were purified from the supernatant using C-18 purification tips (Eppendorf). The samples were eluted from the purification tip onto a MALDI sample plate with 3 μL of matrix (5 mg/mL solution of α-cyano-4-hydroxy-cinnamic acid in 70% ACN/ 0.1% TFA) and allowed to air dry. Samples were then analyzed using Qstar XL Excell Hybride MS system (Applied Biosystems, Foster City, CA, USA) in positive reflector mode, with delayed extraction. Peak lists in XML data format were created using Analysis QS 1.1 (Applied Biosystems).

The peak lists were searched using the MASCOT search engine against the MSDB database subset of mouse proteins with the following search settings: peptide tolerance of 0.2 Da, missed cleavage site value set to one, and variable modifications including oxidation (HW), oxidation (M) and propionamide (C). No restrictions on protein molecular weight or p*I* value were applied. Positive protein identifications were based on a significant MOWSE score and sequence coverage.

CHAPTER 3:

IRON CHELATION BY CLINICALLY RELEVANT ANTHRACYCLINES: ALTERATIONS IN EXPRESSION OF IRON REGULATED GENES AND ATYPICAL CHANGES IN INTRACELLULAR IRON DISTRIBUTION AND TRAFFICKING

This work has been published in:

Xu, X., Sutak, R. and Richardson, D. R. (2008) Iron chelation by clinically relevant anthracyclines: alteration in expression of iron-regulated genes and atypical changes in intracellular iron distribution and trafficking. *Mol Pharmacol*. 73(3):833-44

3.1 INTRODUCTION

Anthracyclines are known iron (Fe) chelators (Figure 3.1A), but their effects on cellular Fe metabolism are poorly understood (for review, see Xu et al., 2005). These compounds have high activity against hematological malignancies and a variety of other tumours (Xu et al., 2005). However, a major problem is their cardiotoxic effect at high cumulative doses that limit their clinical use (Gianni and Myers, 1992). The mechanism of anthracycline-mediated cardiotoxicity is unclear (Kaiserova et al., 2007), probably because of the multiple effects of these agents, including DNA-binding, intercalation, alkylation, inhibition of topoisomerase II and the generation of reactive oxygen species (ROS; Gianni and Myers, 1992).

Previous studies have indicated that interactions of anthracyclines with cellular Fe pools are of great importance in their cardiotoxic effects and ability to induce apoptosis (Hershko et al., 1993; Kotamraju et al., 2002). Anthracyclines such as doxorubicin (DOX) can directly chelate Fe(III) forming an Fe complex with an overall association constant of 10^{33} (Beraldo et al., 1985; May et al., 1980). Hershko and associates demonstrated that Fe-loading potentiates the cardiotoxic effects of anthracyclines (Hershko et al., 1993; Link et al., 1996) and some chelators can prevent this (Kaiserova et al., 2007). In fact, the clinical intervention for anthracycline cardiotoxicity involves the chelator, dexrazoxane (Xu et al., 2005). Hence, understanding the mechanisms of how anthracyclines interfere with Fe metabolism is a key for preventing cardiotoxicity.

Iron is transported by its binding to transferrin (Tf) and is delivered to cells *via* binding to the transferrin receptor 1 (TfR1; Xu et al., 2005). After this, Tf is internalized by receptor-mediated endocytosis and the Fe is released. Iron is then transported into the cell and becomes part of the intracellular Fe pool. Iron that is not used for metabolic

requirements is stored in ferritin, a polymeric protein consisting of H- and L-subunits (Minotti et al., 2004a).

The translation of TfR1 and ferritin are regulated by the binding of iron regulatory proteins (IRPs) to iron-responsive elements (IREs) present in the 5'- or 3'-untranslated regions of *TfR1* and *ferritin* mRNAs (Xu et al., 2005). There are two IRPs, IRP1 and IRP2, and anthracyclines have been shown to decrease their mRNA-binding activity in most cell types (Kwok and Richardson, 2002; Minotti et al., 2001).

Apart from the effect of anthracyclines on IRP-mRNA-binding activity, these agents have been shown to affect a variety of molecules and metabolic pathways involved in Fe metabolism (Minotti et al., 2004a). For instance, DOX is known to directly bind Fe and has been reported to remove Fe from isolated ferritin, Tf and microsomal membranes (Xu et al., 2005). However, using intact cells, we showed that incubation of many cell types with anthracyclines (Figure 3.1A) such as doxorubicin (DOX), daunorubicin (DAU) or epirubicin (EPI) induced ferritin Fe-loading, due to their ability to prevent Fe release from this protein (Kwok and Richardson, 2003; Kwok and Richardson, 2004). The precise mechanism by which anthracyclines prevent ferritin-Fe mobilisation was not clear, but inhibition of protein synthesis and/or proteasomal/lysosomal activity were suggested to be involved (Kwok and Richardson, 2004). Incubation of cells with DOX also increased ferritin expression (Corna et al., 2004; Kwok and Richardson, 2003) and this was suggested to act as a protective response against the ability of DOX to generate ROS (Corna et al., 2004).

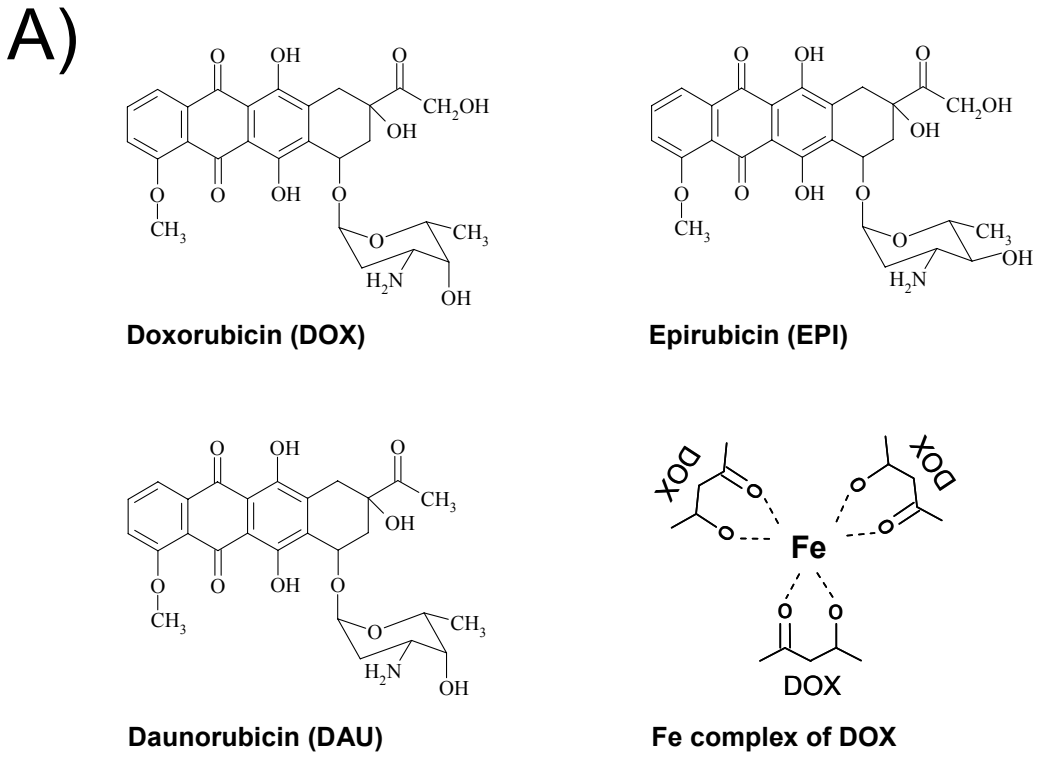

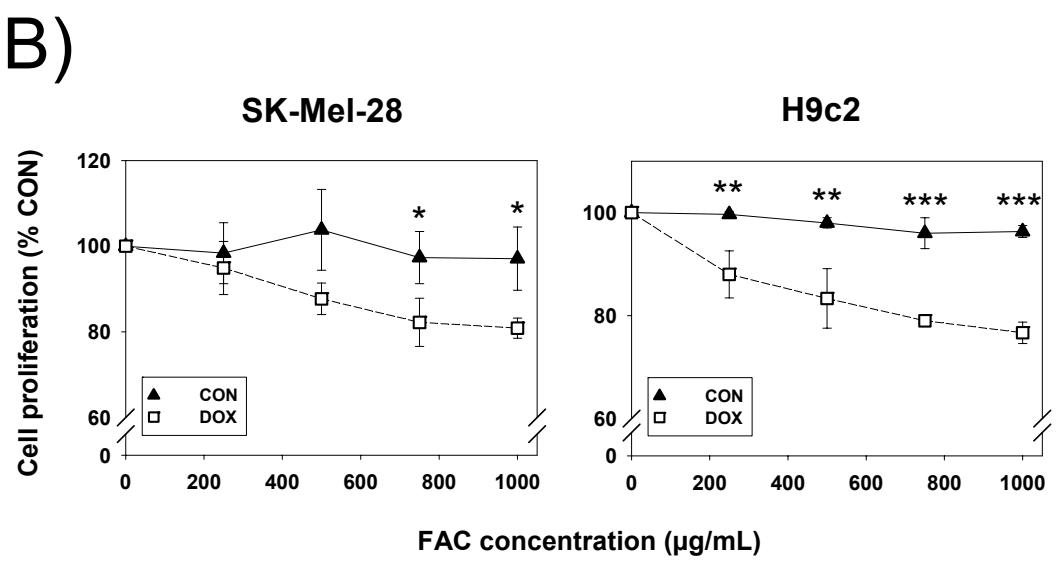

Figure 3.1 (A) Schematic illustration of doxorubicin (DOX), epirubicin (EPI), daunorubicin (DAU) and the Fe complex of DOX. (B) Pre-incubation with DOX could not protect cells from the toxicity of subsequent Fe-loading by ferric ammonium citrate (FAC). Human SK-Mel-28 melanoma cells or rat H9c2 cardiomyocytes were pre-incubated with control medium (CON) or DOX (5 µM) for 24 h at 37°C and then washed. The cells were then reincubated for 16 h at 37°C with CON containing increasing concentrations of FAC (250, 500, 750 and 1000 µg/mL). Cell viability was examined using Trypan blue staining. The percentage of viable cells in control or DOX pre-treated group was plotted comparing to the relative control, which was set as 100%. Results are mean ± SD (3 experiments). *$p < 0.05$, **$p < 0.01$ and ***$p < 0.001$ versus control values (Student's *t*-test).

In the present study, we demonstrate for the first time that anthracyclines act as atypical chelators, having a number of effects on cellular Fe metabolism and the expression of Fe-regulated genes, including *TfR1*, *Ndrg1* and *ferritin*. While Fe chelation mediated by anthracyclines increased *TfR1* and *Ndrg1* mRNA expression, the protein levels of these molecules were decreased. Paradoxically, ferritin protein expression increased after incubation with DOX as did ferritin Fe accumulation, suggesting that anthracyclines have a selective effect on gene expression. The effects of anthracyclines on cellular Fe metabolism were complex, probably since they act on multiple molecular targets.

3.2 MATERIALS AND METHODS

3.2.1 Reagents

All reagents used are listed in Section 2.1. The anthralcyline-metal complexes were prepared as previousely described (Garnier-Suillerot and Gattegno, 1988; Gianni and Myers, 1992) in Section 2.1.2. Pyridoxal isonicotinoyl hydrazone (PIH) was synthesized and characterised by standard methods (Ponka et al., 1979b; Richardson et al., 1995).

3.2.2 Cell Culture

Cell lines were obtained from the American Type Culture Collection (Manassas, VA). Murine embryonic fibroblasts (MEFs) from wild-type and homozygous *hypoxia inducible factor-1*α (*HIF-1*α) knockout mice were obtained from Dr. R. Johnson (University of California, San Diego, USA). All cells were grown as described in Section 2.2.

3.2.3 Effect of Anthracyclines on ^{59}Fe Efflux from Intact Prelabelled Cells

Experiments examining the ability of agents to mobilise cellular-^{59}Fe were performed using standard techniques (Richardson et al., 1995) as described in Section 2.6.2.

3.2.4 Assay for Examining the Ability of Anthracyclines to Bind ^{59}Fe from Cell Lysates

Established methods (Watts and Richardson, 2002) were used to determine the efficacy of anthracyclines at mobilising ^{59}Fe from SK-Mel-28 cell lysates (see Section 2.6.3).

3.2.5 Fast Pressure Liquid Chromatography (FPLC) and Native Gradient PAGE

SK-Mel-28 cells were incubated with or without DOX (2 μM) in the presence of ^{59}Fe-Tf (0.75 μM). Cells were then washed 4-times and lysed on ice in 20 mM HEPES/140 mM NaCl/1.5% Triton X-100 (pH 8). Cell lysates were centrifuged at 16,000 x*g* and the supernatant was loaded onto a Superdex 200 10/300 GL column (GE Healthcare, Bucks, UK) and proteins eluted with 20 mM HEPES/140 mM NaCl (pH 8) using FPLC (Bio-Rad, Hercules, CA). Fractions (1 mL) were collected and radioactivity examined using the γ-counter above. Fractions were concentrated and desalted using the microfilter units described above with a 5 kDa molecular mass (M_r) cut-off. Concentrated fractions were then separated and examined *via* native-gradient-PAGE-^{59}Fe-autoradiography (Babusiak et al., 2005).

3.2.6 Statistical Analysis

Data were compared using the Student's *t*-test. Results were considered statistically significant when $p < 0.05$.

3.2.7 Other Experimental Methods

All other methods including Western blot, RT-PCR, ^{3}H-leucine incorporation assay and Native-PAGE-^{59}Fe-Autoradiography were performed as described in Chapter 2.

Table 3.1 Primers for amplification of human and mouse mRNA

Pair No.	Organisms	Target Gene	Accession No.	Oligonucleotides (5'-3')		Product Size (bp)
				Forward	Reverse	
1	*Homo sapiens*	*β-actin*	NM_001101	CCCGCCGCCAGCTCACCATGG	AAGGTCTCAAACATGATCTGGGTC	397
2		*Ndrg1*	NM_006096	CCCTCGCGTTAGGCAGGTGA	AGGGGTACATGTACCCTGCG	370
3		*TfR1*	NM_003234	GCTCGGCAAGTAGATGGC	TTGATGGTGCTGGTGAAG	359
4	*Mus musculus*	*β-actin*	NM_007393	CCCGCCACCAGTTCGCCATGG	AAGGTCTCAAACATGATCTGGGTC	397
5		*HIF-1α*	NM_010431	CTGGATGCCGGTGGTCTAGACAGT	CGAGAAGAAAAAGATGAGTTCTGAACGTCG	217
6		*Ndrg1*	NM_008681	TGCTTGCTCATTAGGTGTGTGATAGC	CCATCCTGAGATCTTAGAGGCAGC	581
7		*TfR1*	NM_011638	TCCCGAGGGTTATGTGGC	GGCGGAAACTGAGTATGATTGA	324
8		*VEGF1*	NM_009505	CCATGCCAAGTGGTCCCAG	GTCTTTCTTTGGTCTGCATTCACAT	346

3.3 RESULTS

3.3.1 Challenge of DOX-Treated Cells with Iron Leads to Decreased Viability

Incubation of cells with anthracyclines leads to alterations in Fe metabolism (Corna et al., 2004; Kwok and Richardson, 2003; Xu et al., 2005). Initial experiments examined if DOX altered the ability of cells to protect against a challenge with excess Fe. In these studies, SK-Mel-28 melanoma cells or H9c2 cardiomyocytes were preincubated for 24 h at 37^{o}C with DOX (5 μM) and then reincubated for 16 h at 37^{o}C with increasing concentrations of ferric ammonium citrate (FAC; 250-1000 μg/mL), that donates Fe to cells (Corna et al., 2004). Direct cell counts and viability were then assessed using Trypan blue staining. These incubation conditions were identical to those used by others to demonstrate the protective effect against an Fe challenge of preincubating H9c2 cells with DOX (Corna et al., 2004).

In contrast to results by others (Corna et al., 2004), preincubation with DOX did not protect against an Fe challenge. In fact, it resulted in significantly decreased viability of H9c2 and SK-Mel-28 cells at FAC concentrations >500 μg/mL (Figure 3.1B). Hence, DOX decreased the ability of cells to appropriately accomodate the Fe load and prevent its cytotoxic effects.

3.3.2 DOX Increases mRNA Expression of the Fe-Responsive Genes, *TfR1* and *Ndrg1*

To further understand how DOX affects Fe metabolism, we investigated the effect of DOX on *TfR1* expression (Figure 3.2). To examine this, SK-Mel-28 human melanoma cells were initially used (Figure 3.2A) as their Fe metabolism is well characterised and these cells were previously utilised to assess the effects of DOX on Fe

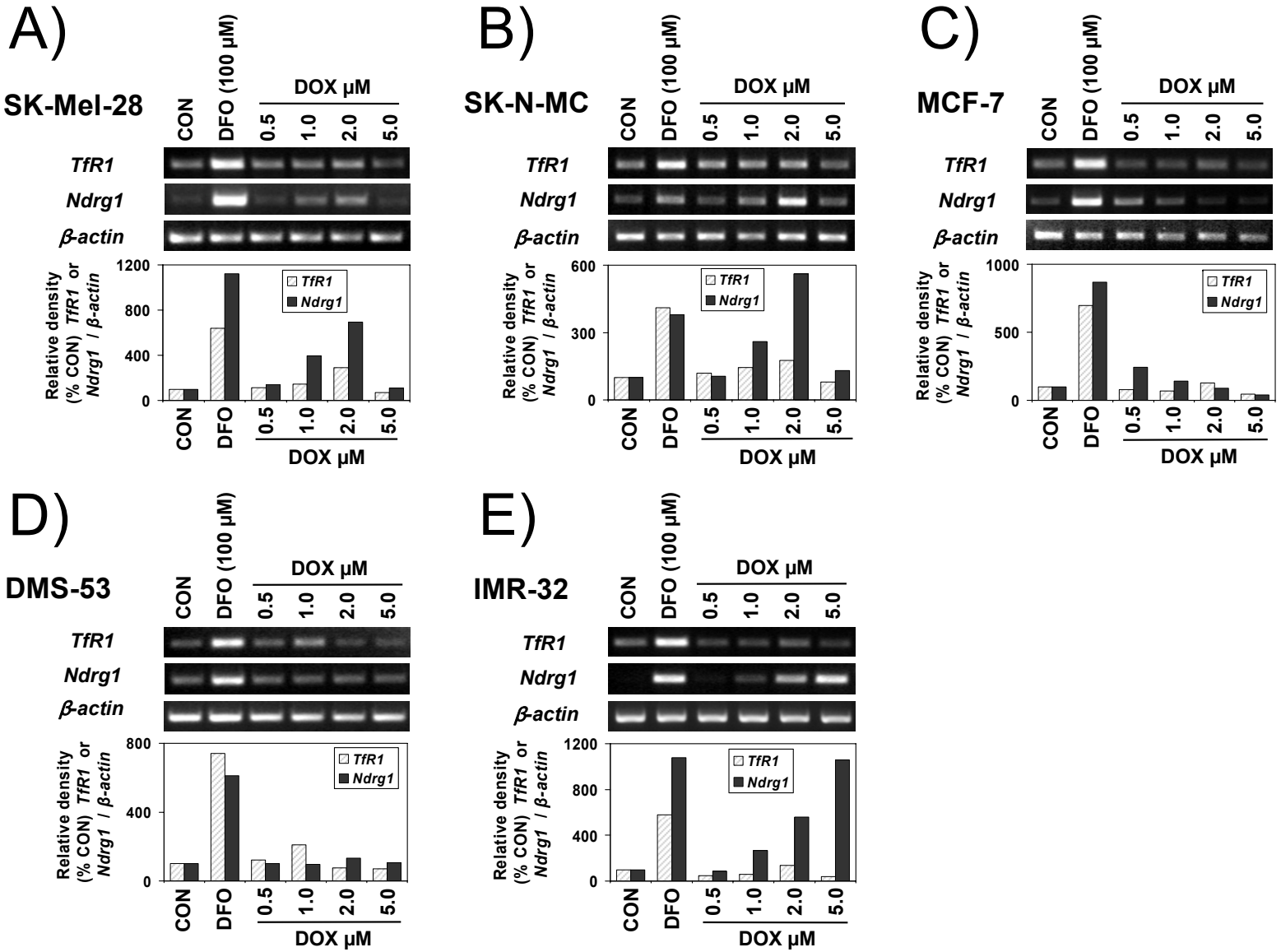
A)
SK-Mel-28
B)
SK-N-MC
C)
MCF-7
D)
DMS-53
E)
IMR-32
CON
DFO (100 μM)
DOX μM
0.5
1.0
2.0
5.0
TfR1
Ndrg1
β-actin
Relative density (% CON) TfR1 or Ndrg1 / β-actin
TfR1
Ndrg1
DOX μM

trafficking (Kwok and Richardson, 2002; Kwok and Richardson, 2003; Kwok and Richardson, 2004).

Incubation of cells for 24 h at 37^{o}C with the Fe chelator, desferrioxamine (DFO; 100 μM), was used as a positive control as it increases *TfR1* mRNA and protein expression (Hentze and Kuhn, 1996). Incubation of SK-Mel-28 cells with DFO increased *TfR1* expression >6-fold compared to the control (Figure 3.2A). DOX (0.5-5 μM) induced a dose-dependent increase in *TfR1* mRNA up to 2 μM where its expression was 3-fold greater than the control (Figure 3.2A). The up-regulation of *TfR1* mRNA after incubation with DOX was relatively marked considering the dose maximally up-regulating its expression (2 μM) was 50-fold lower than DFO (100 μM; Figure 3.2A). At 5 μM DOX, *TfR1* expression then decreased and this down-regulation may be related to the drug acting as a transcriptional inhibitor (Tarr and van Helden, 1990).

The increase in *TfR1* mRNA after incubation of SK-Mel-28 cells with DOX may be mediated *via* its ability to act as an Fe chelator (Gianni and Myers, 1992; May et al., 1980). Examination of four other cell types also demonstrated that DOX increased *TfR1* mRNA, although the dose-dependence and extent of up-regulation was different for each cell type (Figure 3.2B-E). Generally, maximum *TfR1* mRNA expression was found at 1-2 μM DOX.

Typically, Fe chelation is known to up-regulate *TfR1* mRNA by the IRP-IRE mechanism (Hentze and Kuhn, 1996). However, the lower DOX concentrations (1-2 μM) used in this study have little effect on IRP-mRNA-binding activity in SK-Mel-28 cells (Kwok and Richardson, 2002). Thus, it was unclear if this mechanism was

responsible for DOX-mediated up-regulation of *TfR1* mRNA (Figure 3.2A). Apart from the IRPs, other Fe-sensing mechanisms could be responsible for altering *TfR1* mRNA expression. Considering this, HIF-1α protein expression is known to increase after Fe chelation or hypoxia and can transcriptionally up-regulate *TfR1* and other genes (Beerepoot et al., 1996; Bianchi et al., 1999; Le and Richardson, 2004; Lok and Ponka, 1999).

To determine if HIF-1α activity is affected by anthracyclines, we examined the effect of DOX on HIF-1α target gene expression. These studies investigated the metastasis suppressor, *N-myc downstream regulated gene-1* (*Ndrg1*), that is known to be up-regulated after Fe chelation by HIF-1α (Le and Richardson, 2004). This gene was important to assess as its anti-proliferative and -metastatic effects could be relevant to DOX activity (Kovacevic and Richardson, 2006). Similarly to *TfR1*, DOX also increased *Ndrg1* mRNA expression in SK-Mel-28 cells (Figure 3.2A). Assessment of 4 other cell types demonstrated that as for SK-Mel-28 cells, DFO increased *Ndrg1* mRNA (Figure 3.2B-E). Again, the response of *Ndrg1* mRNA levels to increasing DOX concentrations was variable in terms of dose-response and the extent of up-regulation between cell types (Figure 3.2A-E). The differences in gene expression between these cell types may relate to variation in the uptake and metabolism of DOX. Of interest, the mRNA levels of another HIF-1α target gene, namely *Nip3* (Bruick, 2000), was also up-regulated by DOX in a similar way to *TfR1* and *Ndrg1* (data not shown). Further studies then examined the effect of other anthracyclines on Fe metabolism using the SK-Mel-28 cell type.

3.3.3 Daunorubicin and Epirubicin also Increase *TfR1* and *Ndrg1* mRNA Expression

DAU and EPI are structurally-related to DOX (Figure 3.1A) and also increased *TfR1* and *Ndrg1* mRNA in a dose-dependent manner (Figure 3.3A). However, the response of SK-Mel-28 melanoma cells to each of the anthracyclines was different (Figure 3.3A). Daunorubicin gradually increased *TfR1* and *Ndrg1* mRNA up to 5 μM, with the effect at this latter concentration being similar to 2 μM DOX (Figure 3.3A). As found for DOX, EPI increased *TfR1* and *Ndrg1* mRNA up to 2 μM and then at the highest EPI concentration assessed (*i.e.*, 5 μM), the expression of these genes decreased (Figure 3.3A). Generally, these results demonstrated that DOX, DAU and EPI increased *TfR1* and *Ndrg1* mRNA up to a concentration of 1-2 μM.

3.3.4 Anthracyclines Increase *TfR1* and *Ndrg1* Expression as a Function of Time

The effect of anthracyclines on *TfR1* and *Ndrg1* mRNA was then assessed as a function of incubation time. The optimal anthracycline concentration that up-regulated gene expression in SK-Mel-28, namely 2 μM (Figure 3.2A), was incubated with this cell type for 3-24 h at 37^{o}C. The effect of DOX was compared to the positive control, DFO (100 μM). In these studies, DFO increased *TfR1* and *Ndrg1* mRNA expression after 6 h (Figure 3.3B). This was in agreement with previous studies using DFO and other cell types (Le and Richardson, 2004). A significant ($p < 0.05$) increase in *TfR1* mRNA expression after incubation with the anthracyclines was evident after 18 h. However, the anthracyclines increased *Ndrg1* mRNA expression after only 6 h to a comparable or greater extent than DFO (Figure 3.3B).

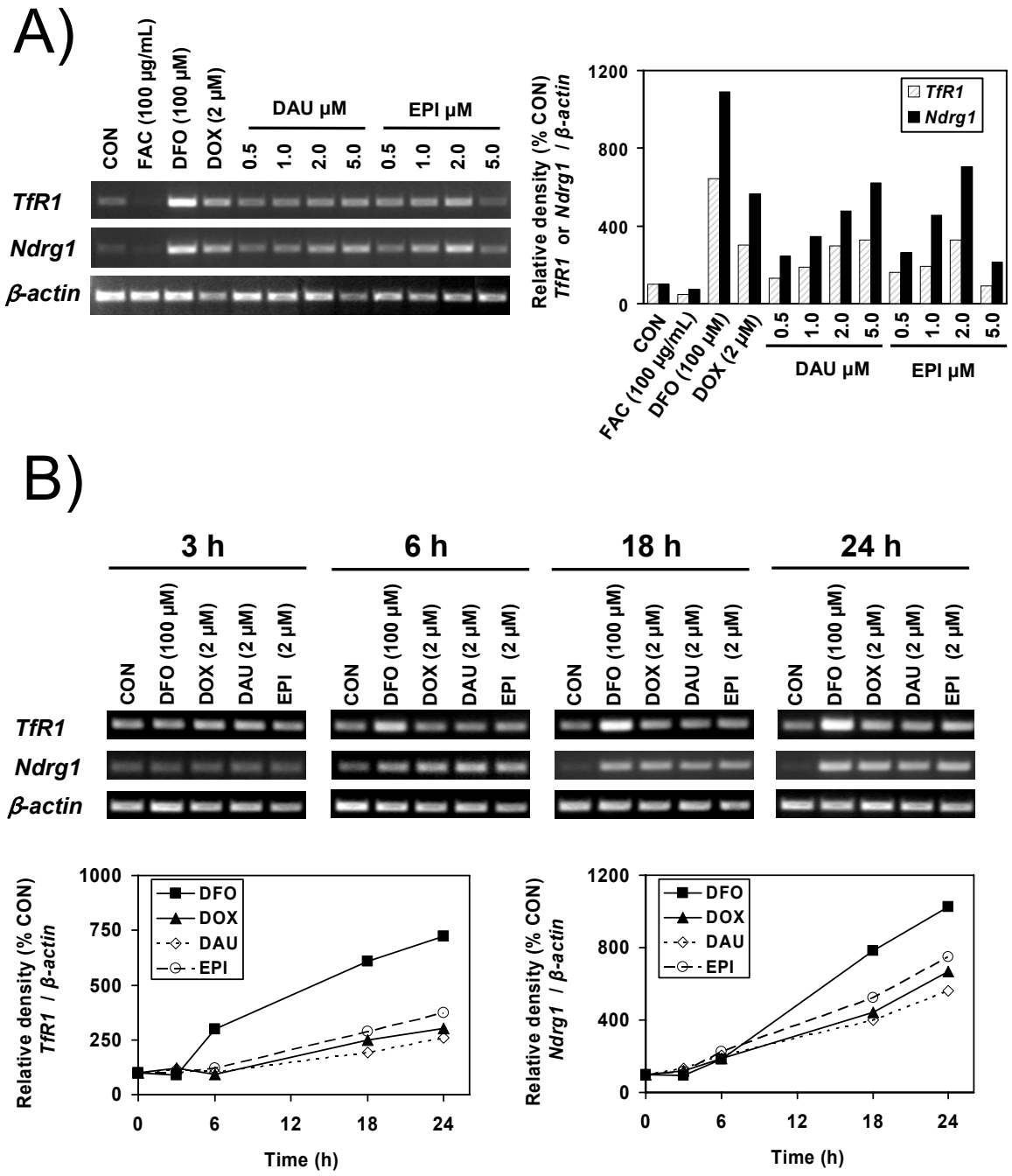

Figure 3.3 Anthracyclines increase *TfR1* and *Ndrg1* mRNA expression in a (A) dose-dependent and (B) time-dependent manner in SK-Mel-28 melanoma cells. (A) Cells were incubated for 24 h at 37°C with control medium (CON), ferric ammonium citrate (FAC; 100 µg/mL), desferrioxamine (DFO; 100 µM), doxorubicin (DOX; 2 µM), or daunorubicin (DAU) or epirubicin (EPI; 0.5, 1, 2 and 5 µM). The expression of *TfR1* and *Ndrg1* mRNA levels were evaluated using RT-PCR. **(B)** Cells were incubated with CON, DFO (100 µM), DOX (2 µM), DAU (2 µM) or EPI (2 µM) for 3, 6, 18 and 24 h. The expression of *TfR1* and *Ndrg1* mRNA levels were evaluated using RT-PCR. Gene expression was then calculated relative to the *β-actin* control. Results are typical from 3 separate experiments performed.

3.3.5 The DOX-Mediated Increase in *TfR1* and *Ndrg1* mRNA is Iron-Dependent

DOX, DAU and EPI possess the same Fe-binding sites (carbonyl and hydroxyl moieties) that are necessary for Fe chelation (Figure 3.1A). The ability of these agents to bind Fe was shown in the "test tube" (May et al., 1980), but not in intact cells. Certainly, these compounds may be acting as chelators to deplete Fe pools and increase *TfR1* and *Ndrg1* mRNA. To examine this, the effect of DFO (2 μM) was compared to the anthracyclines at the same concentration. Furthermore, the efficacy of the anthracyclines at increasing *Ndrg1* and *TfR1* was also compared to their pre-formed 3:1 ligand-Fe(III) complexes (Figure 3.4A).

After a 24 h incubation, DFO clearly increased *TfR1* and *Ndrg1* mRNA expression (Figure 3.4A). The 1:1 DFO-Fe complex largely prevented *TfR1* and *Ndrg1* up-regulation that was observed with DFO. The anthracyclines, DOX, DAU and EPI all increased both *TfR1* and *Ndrg1* mRNA expression, while their Fe complexes were significantly ($p < 0.001$) less effective over 3 experiments. Hence, this suggested that up-regulation of *TfR1* and *Ndrg1* was due to anthracyclines binding cellular Fe (Figure 3.4A). Interestingly, the effect of the anthracyclines at inducing *Ndrg1* expression was more pronounced than that observed with *TfR1* (Figure 3.4A).

Further experiments assessed whether DOX-mediated up-regulation of *TfR1* and *Ndrg1* could be reversed by Fe added as FAC (100 μg/mL; Figure 3.4B, C). SK-Mel-28 cells were pre-incubated with control medium (CON), DFO (100 μM) or DOX (2 μM) for 20 h (primary incubation), and then re-incubated for another 20 h (secondary incubation) with CON, FAC (100 μg/mL), DFO (100 μM) or DOX (2 μM).

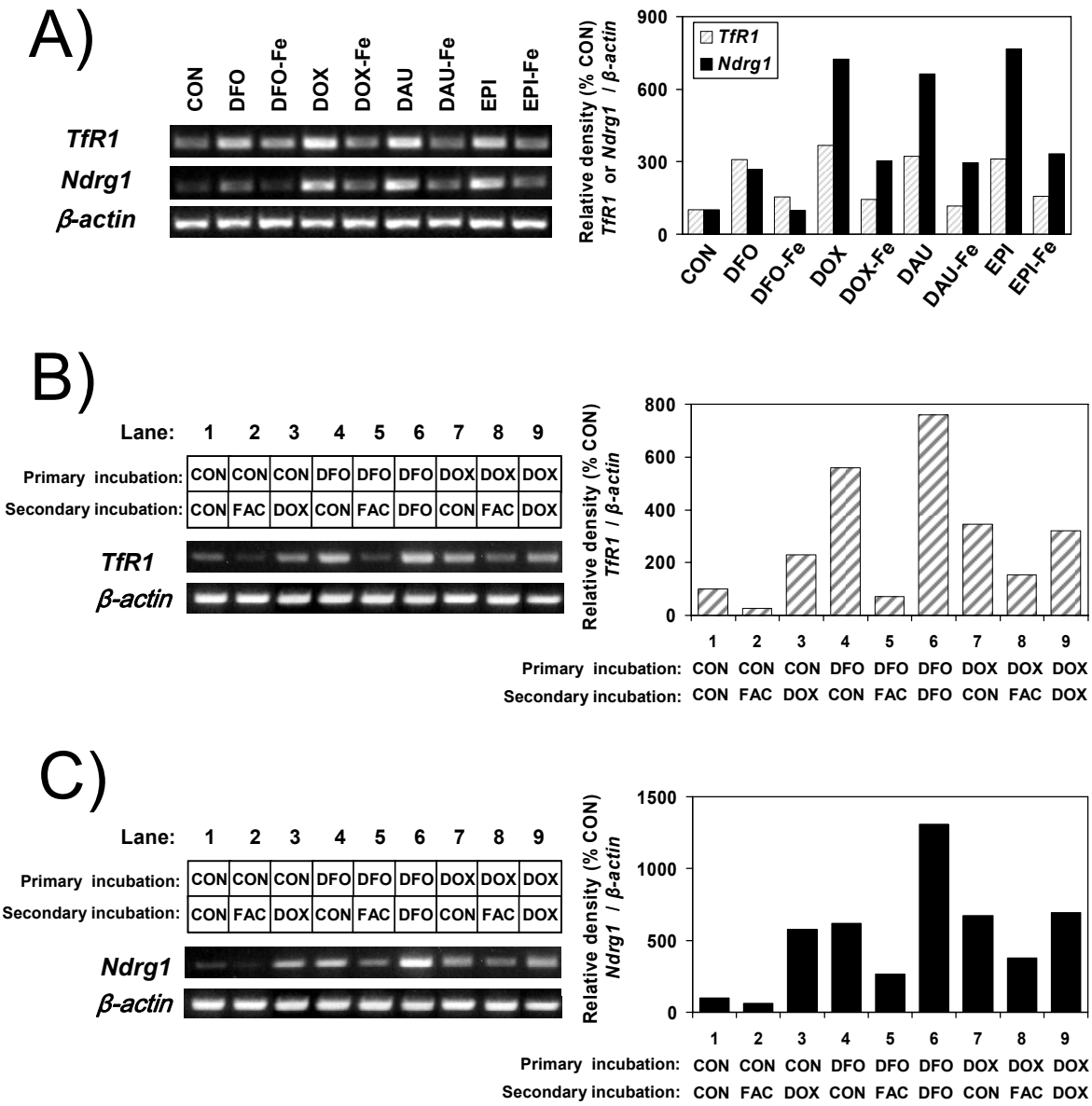

Figure 3.4 Anthracyclines up-regulate *TfR1* and *Ndrg1* mRNA levels by Fe-deprivation. (A) Anthracycline-Fe complexes are far less active than their parent ligands at increasing gene expression. (B, C) The soluble Fe salt, ferric ammonium citrate (FAC), decreases (B) *TfR1* and (C) *Ndrg1* mRNA expression after incubation with anthracyclines. (A) SK-Mel-28 cells were incubated for 24 h at 37°C with control medium (CON), DFO (2 μM), the 1:1 DFO-Fe complex (2 μM), DOX (2 μM), 3:1 DOX-Fe complex (2 μM), DAU (2 μM), 3:1 DAU-Fe complex (2 μM), EPI (2 μM) or 3:1 EPI-Fe complex (2 μM). **(B and C)** SK-Mel-28 cells were pre-incubated with CON, DFO (100 μM) or DOX (2 μM) for 20 h at 37°C (Primary Incubation), followed by a 20 h re-incubation at 37°C with CON, FAC (100 μg/mL), DFO (100 μM) or DOX (2 μM) (Secondary Incubation). The expression of *TfR1* and *Ndrg1* mRNA levels were evaluated using RT-PCR. Densitometric analysis was performed and gene expression was then calculated relative to the *β-actin* control. Results are typical of 3 experiments performed.

After primary incubation with CON, secondary incubation with FAC (Figure 3.4B, C; lane 2) decreased *TfR1* and *Ndrg1* mRNA levels compared to cells treated with CON (Figure 3.4B, C; lane 1). The treatment with FAC acted as a positive control to demonstrate both genes are Fe-regulated. Cells treated with DFO or DOX followed by CON (Figure 3.4B, C; lane 4, 7) led to increased *TfR1* and *Ndrg1* mRNA expression compared to the control (Figure 3.4B, C; lane 1). Depletion of cellular Fe by primary and secondary incubation with DFO resulted in more pronounced up-regulation of *TfR1* and *Ndrg1* levels (Figure 3.4B, C; lane 6) in comparison to DFO followed by CON (Figure 3.4B; lane 4). Primary and secondary incubation with DOX caused similar up-regulation of *TfR1* and *Ndrg1* (Figure 3.4B, C; lane 9) as DOX followed by CON (Figure 3.4B, C; lane 7). Importantly, primary incubation with DFO or DOX and reincubation with FAC (Figure 3.4B, C; lanes 5 and 8) significantly ($p < 0.01$) decreased *TfR1* and *Ndrg1* up-regulation compared to the relative control (Figure 3.4B, C; lanes 4 and 7). This further confirmed that anthracyclines increased *TfR1* and *Ndrg1* mRNA *via* Fe chelation and this up-regulation was reversible upon adding Fe.

3.3.6 DOX Does Not Induce Cellular Fe Mobilisation but Causes Intracellular Fe Re-distribution

To understand how DOX affected Fe metabolism to up-regulate *TfR1* and *Ndrg1* mRNA, studies examined its effects on cellular ^{59}Fe mobilisation. The ability of DOX (0.1-5 μM) at mobilizing ^{59}Fe was compared to the chelators, DFO (100 μM) and PIH (25 μM), over 24 h at 37^{o}C (Figure 3.5A). These DOX concentrations were chosen as they were used to examine *TfR1* and *Ndrg1* mRNA expression (Figures 3.2-3.4). Both DFO and PIH increased cellular-^{59}Fe mobilisation to 225 and 270% of the control, while DOX had no effect (Figure 3.5A). Further studies examined the ability of DOX

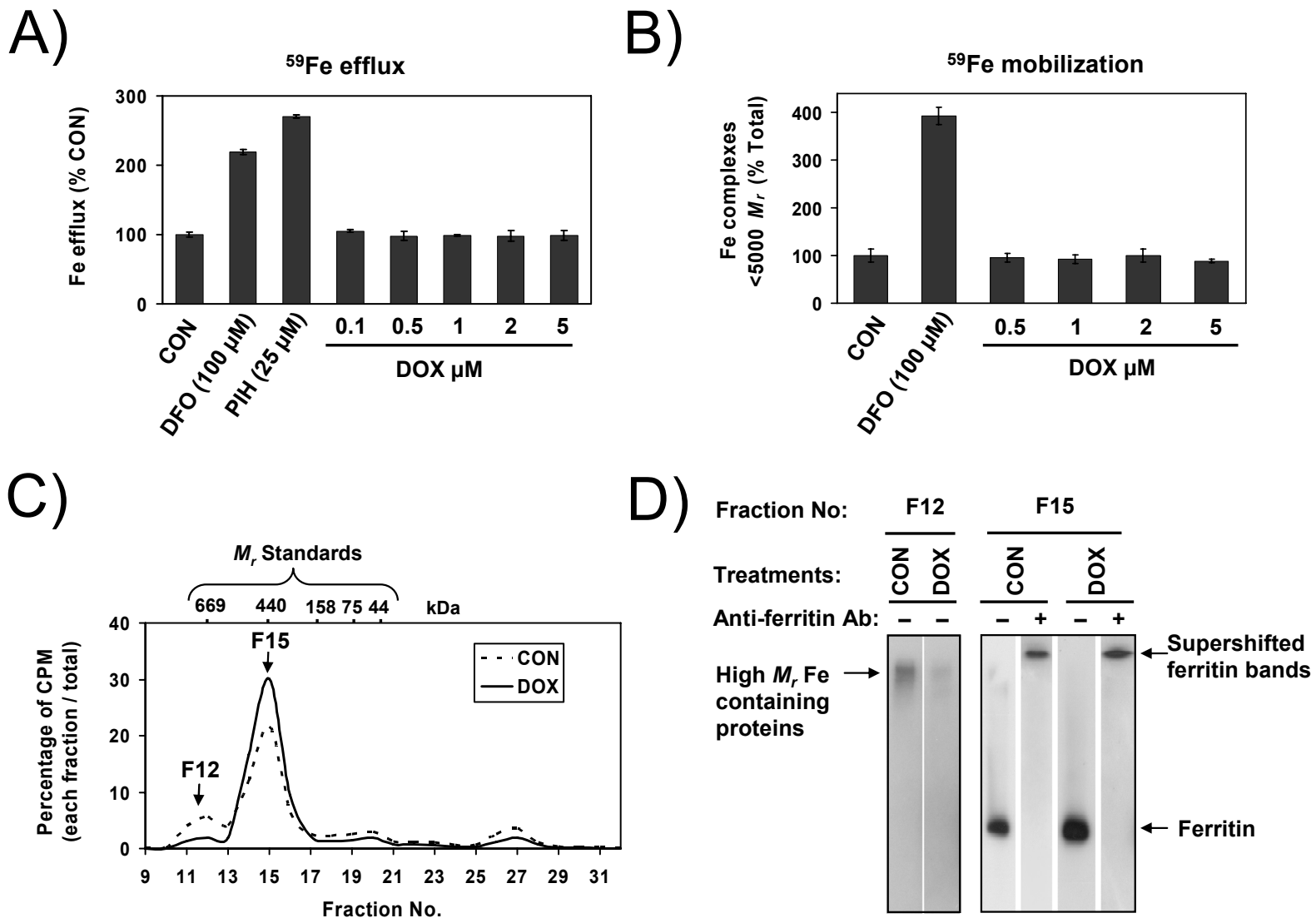
A)
59Fe efflux
Fe efflux (% CON)
300
200
100
0
CON
DFO (100 µM)
PIH (25 µM)
0.1
0.5
1
2
5
DOX µM
B)
59Fe mobilization
Fe complexes <5000 Mr (% Total)
400
300
200
100
0
CON
DFO (100 µM)
0.5
1
2
5
DOX µM
C)
Mr Standards
669
440
158
75
44
kDa
Percentage of CPM (each fraction / total)
40
30
20
10
0
F15
F12
CON
DOX
9
11
13
15
17
19
21
23
25
27
29
31
Fraction No.
D)
Fraction No:
F12
F15
Treatments:
CON
DOX
CON
DOX
Anti-ferritin Ab:
– –
– +
– +
High Mr Fe containing proteins
Supershifted ferritin bands
Ferritin

to mobilise ^{59}Fe from cell lysates. In contrast to the positive control, DFO (100 μM), which caused marked ^{59}Fe mobilisation from lysates, DOX (0.5-5 μM) had no effect (Figure 3.5B). Collectively, despite DOX having high Fe-binding affinity (May et al., 1980) and its ability to up-regulate *TfR1* and *Ndrg1* mRNA by Fe-depletion (Figure 3.4), it does not act like a typical chelator to induce Fe efflux.

Further studies were performed using FPLC to examine alterations in intracellular ^{59}Fe distribution (Figure 3.5C). Cells were labelled with ^{59}Fe-Tf (0.75 μM) in the presence or absence of DOX (2 μM) for 24 h at 37^{o}C, then washed, lysed and centrifuged. The supernatant was fractionated on a size-exclusion column and the fractions measured for ^{59}Fe. In control cells, two major high M_r peaks were detected (Figure 3.5C). According to the column calibration, the first peak at fraction 12 (F12) represented ^{59}Fe-containing molecules of ≈ 700 kDa. A second peak at fraction 15 (F15) co-migrated with horse spleen ferritin (≈ 400 kDa; Figure 3.5C). After incubation with DOX, ^{59}Fe in F12 was significantly ($p < 0.01$) decreased over 3 experiments. In contrast, in the ferritin fraction (F15) there was a significant increase in ^{59}Fe incorporation. There were two other lower M_r peaks eluting at fractions 20 and 27, although there was no significant difference between them comparing control and DOX-treated cells (Figure 3.5C).

To further elucidate the nature of the ^{59}Fe-containing molecules, F12 and F15 were concentrated and separated using native-gradient PAGE (Figure 3.5D). These studies showed that DOX decreased ^{59}Fe incorporation into high M_r proteins (F12), while there was ferritin-^{59}Fe accumulation (F15). The ferritin-^{59}Fe loading was confirmed by addition of anti-ferritin antibody to the latter fraction leading to a super-shifted ferritin

band (Figure 3.5D). These data demonstrated re-distribution of ^{59}Fe between ferritin and other ^{59}Fe-containing proteins, extending our previous observations (Kwok and Richardson, 2003; Kwok and Richardson, 2004). This ferritin-^{59}Fe accumulation leads to cytosolic Fe-deficiency that may up-regulate *TfR1* and *Ndrg1* mRNA (Figures 3.2, 3.3).

3.3.7 HIF-1α-Independent Mechanisms are Involved in Up-Regulation of *TfR1* and *Ndrg1* after Incubation with DOX

The up-regulation of *TfR1* mRNA by anthracyclines could occur by the classical IRP mechanism (Hentze and Kuhn, 1996) and/or also *via* HIF-1α since the *TfR1* promoter contains a hypoxia response element (HRE; Bianchi et al., 1999; Lok and Ponka, 1999). The increase in *Ndrg1* mRNA expression after Fe chelation by DFO was previously shown to occur by HIF-1α-dependent and -independent mechanisms (Le and Richardson, 2004).

To examine the role of HIF-1α in *TfR1* and *Ndrg1* up-regulation after incubation with DOX, we utilised *HIF-1α* knockout (*HIF-1α*$^{-/-}$) MEFs in comparison to wild-type (*HIF-1α*$^{+/+}$) MEFs (Ryan HE, 2000; Figure 3.6A). Both *HIF-1α*$^{+/+}$ and *HIF-1α*$^{-/-}$ MEFs were incubated with DFO (100 μM; positive control) or DOX (2 μM) for 8 h and then *TfR1*, *Ndrg1* and *HIF-1α* mRNA expression was assessed (Figure 3.6A). Incubation of *HIF-1α*$^{+/+}$ or *HIF-1α*$^{-/-}$ cells with DFO or DOX increased *TfR1* mRNA levels irrespective of *HIF-1α* status, suggesting another mechanism was responsible. For DFO, this could be mediated by the IRPs (Hentze and Kuhn, 1996). Previous studies examining SK-Mel-28 cells demonstrated that at high DOX concentrations (*ie.*, 20 μM), IRP-mRNA-binding activity was reduced (Kwok and Richardson, 2002).

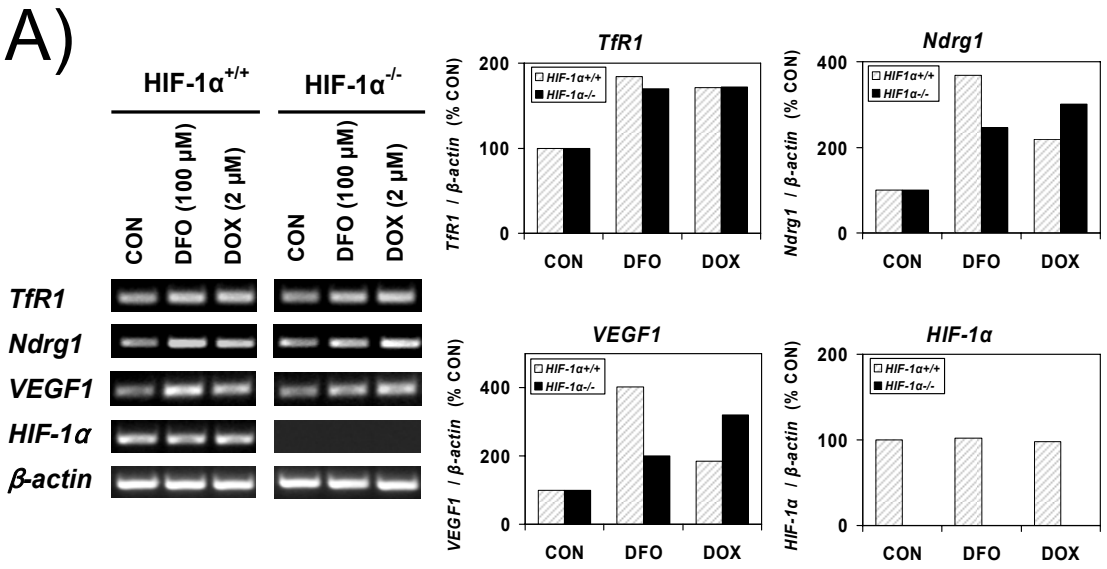

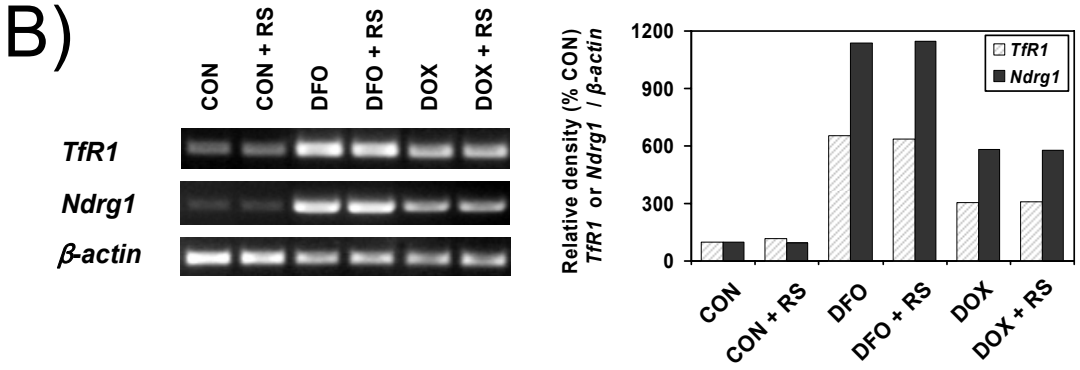

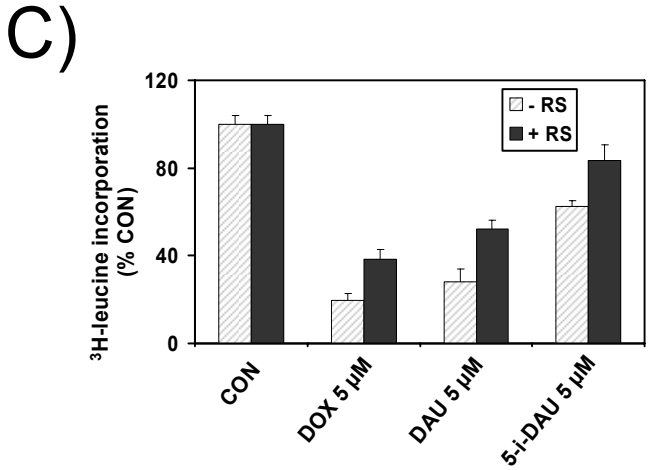

Radical Scavenger Combination (RS):

- catalase (1000 U/ml)
- ebselen (15 µM)
- MnTBAP (200 µM)
- SOD (1000 U/ml)

However, at low concentrations (1 μM), IRP-binding was not markedly affected (Kwok and Richardson, 2002). This suggested the DOX-induced *TfR1* mRNA up-regulation at 1-2 μM in SK-Mel-28 cells (Figure 3.2A) may not be mediated by IRPs.

The expression of *Ndrg1* mRNA was more significantly up-regulated ($p < 0.05$) by DFO in *HIF-1α*$^{+/+}$ cells than their *HIF-1α*$^{-/-}$ counterparts (Figure 3.6A), in agreement with previous studies (Le and Richardson, 2004). This suggests that HIF-1α is important in up-regulating *Ndrg1* mRNA after Fe chelation, but that a HIF-1α-independent mechanism was also present (Le and Richardson, 2004). The up-regulation of *Ndrg1* mRNA after incubation of DOX occurred in *HIF-1α*$^{-/-}$ and *HIF-1α*$^{+/+}$ cells (Figure 3.6A), suggesting the response was HIF-1α-independent. In fact, in 3 experiments, *Ndrg1* mRNA up-regulation was significantly ($p < 0.045$) more marked in *HIF-1α*$^{-/-}$ than *HIF-1α*$^{+/+}$ cells (Figure 3.6A).

The effect of DOX and DFO was also examined on the expression of *vascular endothelial growth factor-1* (*VEGF1*) mRNA (Figure 3.6A) which is a typical HIF-1α-regulated gene (Beerepoot et al., 1996). The ability of DFO at increasing *VEGF1* mRNA was more pronounced in *HIF-1α*$^{+/+}$ than *HIF-1α*$^{-/-}$ cells. Hence, similarly to *Ndrg1*, this indicates HIF-1α is important in up-regulating *VEGF1* mRNA after DFO, but that a HIF-1α-independent mechanism was also present. After incubation with DOX, *VEGF1* mRNA was more highly expressed in *HIF-1α*$^{-/-}$ cells than *HIF-1α*$^{+/+}$ cells, indicating the anthracycline was up-regulating this gene *via* a HIF-1α-independent mechanism.

As an appropriate control, HIF-1α status was examined in *HIF-1α*$^{+/+}$ and *HIF-1α*$^{-/-}$ cell

types. In these studies, *HIF-1α* mRNA expression was clearly evident in *HIF-1α*$^{+/+}$ cells and not markedly affected by the incubation with DFO or DOX. In contrast, and as expected, no transcript was detected in *HIF-1α*$^{-/-}$ cells (Figure 3.6A).

3.3.8 Activity of Free Radical Scavengers on *Ndrg1* and *TfR1* Expression after Incubation with Anthracyclines

Anthracyclines are well known to generate radicals (Corna et al., 2004) and increased TfR1 protein expression occurs after oxidant stress, at least in part, through IRP activation (Pantopoulos and Hentze, 1995). To determine the role of anthracycline-induced oxidant stress in *TfR1* and *Ndrg1* mRNA expression, we assessed the effect of radical scavengers (RS) on DOX-induced *TfR1* and *Ndrg1* mRNA expression (Figure 3.6B) and also the ability of DOX to inhibit protein synthesis (Figure 3.6C). In these experiments, we combined superoxide dismutase (SOD; 1000 U/mL) and catalase (1000 U/mL) with the cell-permeable glutathione peroxidase mimetic ebselen (15 μM) and cell-permeable SOD mimetic, MnTBAP (200 μM), as these agents alone and in combination are effective RS (Kotamraju et al., 2002; Kwok and Richardson, 2002). The addition of the RS had no significant effect on the up-regulation of either *TfR1* or *Ndrg1* mRNA by either DOX or DFO over 3 experiments (Figure 3.6B). This suggested *TfR1* and *Ndrg1* mRNA up-regulation was not due to anthracycline-induced oxidant stress.

As a positive control to demonstrate that RS reduced ROS generation and the cytotoxic effects of anthracyclines, experiments were performed with various anthracyclines to assess their ability to inhibit protein synthesis (^{3}H-leucine incorporation) in the presence and absence of the same combination of RS (Figure 3.6C). In these studies,

DOX and DAU were compared to 5-imino-daunorubicin (5-i-DAU), that generates less ROS than the former anthracyclines (Corna et al., 2004).

All anthracyclines were effective at reducing ^{3}H-leucine incorporation (Figure 3.6C). From the anthracyclines examined, DOX was the most effective, while 5-i-DAU demonstrated the least ability to inhibit ^{3}H-leucine incorporation (Figure 3.6C). This could be because 5-i-DAU is less redox active than DOX (Corna et al., 2004). For all anthracyclines, the combination with RS significantly ($p < 0.05$) increased ^{3}H-leucine incorporation compared to their relative controls (Figure 3.6C). Hence, the RS could partially rescue the effects of anthracyclines at depressing ^{3}H-leucine incorporation.

3.3.9 DOX Inhibits the Translation of TfR1 and Ndrg1 mRNA into Protein, while Ferritin Protein Expression Increases

The ability of DOX to prevent ^{3}H-leucine incorporation into protein suggested mRNA translation could be inhibited. These data agree with our earlier studies using SK-Mel-28 cells where DOX markedly inhibited ^{3}H-leucine incorporation (Kwok and Richardson, 2004). Hence, it was important to investigate if up-regulation of *TfR1* and *Ndrg1* mRNA after incubation with DOX (Figure 3.2 and 3.3) leads to increased protein expression.

At the lowest DOX concentration (0.5 μM), a slight but not significant increase in TfR1 protein expression occurred in SK-Mel-28 melanoma cells relative to the control (Figure 3.7A). At the same concentration, a more pronounced and significant ($p < 0.04$) increase in Ndrg1 protein expression was found relative to the control (Figure 3.7B). However, at higher DOX concentrations (5 and 7.5 μM), TfR1 and Ndrg1 protein

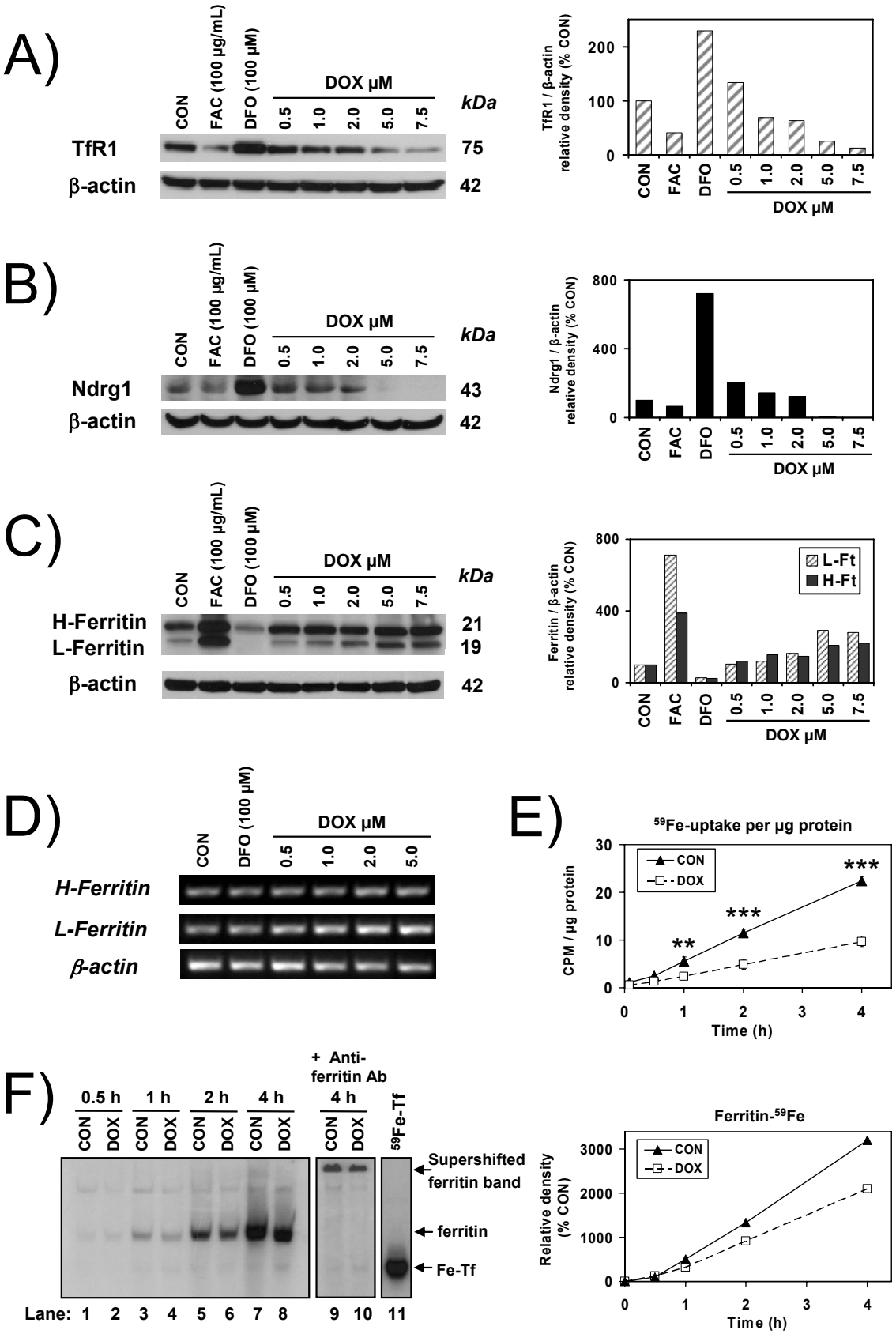
A)
CON
FAC (100 µg/mL)
DFO (100 µM)
DOX µM
0.5
1.0
2.0
5.0
7.5
kDa
TfR1
75
β-actin
42
TfR1 / β-actin relative density (% CON)
200
100
0
CON
FAC
DFO
0.5
1.0
2.0
5.0
7.5
DOX µM
B)
CON
FAC (100 µg/mL)
DFO (100 µM)
DOX µM
0.5
1.0
2.0
5.0
7.5
kDa
Ndrg1
43
β-actin
42
Ndrg1 / β-actin relative density (% CON)
800
400
0
CON
FAC
DFO
0.5
1.0
2.0
5.0
7.5
DOX µM
C)
CON
FAC (100 µg/mL)
DFO (100 µM)
DOX µM
0.5
1.0
2.0
5.0
7.5
kDa
H-Ferritin
21
L-Ferritin
19
β-actin
42
Ferritin / β-actin relative density (% CON)
800
400
0
L-Ft
H-Ft
CON
FAC
DFO
0.5
1.0
2.0
5.0
7.5
DOX µM
D)
CON
DFO (100 µM)
DOX µM
0.5
1.0
2.0
5.0
H-Ferritin
L-Ferritin
β-actin
E)
59Fe-uptake per µg protein
CPM / µg protein
30
20
10
0
CON
- DOX
**
***
***
0
1
2
3
4
Time (h)
F)
0.5 h
1 h
2 h
4 h
+ Anti-ferritin Ab
4 h
CON
DOX
59Fe-Tf
Supershifted ferritin band
ferritin
Fe-Tf
Lane: 1 2 3 4 5 6 7 8 9 10 11
Ferritin-59Fe
Relative density (% CON)
3000
2000
1000
0
CON
- DOX
0
1
2
3
4
Time (h)

expression decreased, potentially due to inhibition of protein synthesis (Figure 3.6C). In contrast, ferritin-H and -L protein levels increased in the presence of DOX (Figure 3.7C), in agreement with previous studies (Corna et al., 2004; Kwok and Richardson, 2003). It is also of interest that *ferritin –H* and *–L* mRNA increased as a function of DOX concentration up to 5 μM (Figure 3.7D), which is in contrast to *TfR1* and *Ndrg1* mRNA which decreased at this latter concentration (Figure 3.2A). This indicated differential effects of DOX on gene expression.

3.3.10 Preincubation with DOX followed by Labelling with ^{59}Fe-Transferrin Decreases Cellular ^{59}Fe Uptake

Considering the decreased TfR1 protein expression at higher DOX concentrations (Figure 3.7A), studies were performed to examine the effect of DOX on ^{59}Fe uptake from ^{59}Fe-Tf (Figure 3.7E). After a 24 h preincubation with DOX (2 μM), cells were incubated with ^{59}Fe-Tf (0.75 μM) for 0.5-4 h. There was a significant ($p < 0.05$) decrease in ^{59}Fe uptake after 1-4 h in cells preincubated with DOX compared to control medium (Figure 3.7E). The intracellular distribution of ^{59}Fe was then assessed using native-gradient-PAGE-^{59}Fe-autoradiography (Babusiak et al., 2005; Figure 3.7F). Again, cells were preincubated for 24 h at 37^{o}C with control medium or DOX (2 μM), washed and then incubated with ^{59}Fe-Tf (0.75 μM) for up to 4 h at 37^{o}C. Most ^{59}Fe was incorporated into a band in the middle of the gel which was shown to be ferritin by super-shift studies with an anti-ferritin antibody (Figure 3.7F; lanes 9 and 10). Transferrin migrated below ferritin as demonstrated using purified ^{59}Fe-Tf (Figure 3.7F; lane 11). The ferritin-^{59}Fe uptake was linear up to 4 h, with less ^{59}Fe being incorporated into cells preincubated with DOX.

Preincubation with DOX decreased both ^{59}Fe-Tf uptake (Figure 3.7E) and ^{59}Fe incorporation into ferritin (Figure 3.7F). This was in contrast to studies with no preincubation period, where DOX and ^{59}Fe-Tf were incubated together for 24 h, leading to ferritin-^{59}Fe accumulation (Figure 3.5C, D). Clearly, preincubation with DOX before the addition of ^{59}Fe-Tf inhibits protein synthesis (Figure 3.6C) which is a crucial secondary event that decreases TfR1 and thus ^{59}Fe uptake.

3.4 DISCUSSION

Anthracyclines bind Fe and act as bidentate chelators *via* their carbonyl and hydroxyl groups (Figure 3.1A; May et al., 1980). The same ligating sites are involved in Fe chelation by the effective chelator, deferiprone (Kalinowski and Richardson, 2005), and thus the effects of anthracyclines on Fe metabolism are important to dissect. However, the effects of anthracyclines on metabolism are complex since these agents have multiple molecular targets (Minotti et al., 2004a; Xu et al., 2005). In this study, we demonstrate for the first time that anthracyclines act as atypical chelators, having a number of effects on Fe metabolism and the expression of Fe-regulated genes.

Previous work suggested that preincubation with DOX protected cells from an Fe challenge due to increased ferritin expression (Corna et al., 2004). In this investigation, we repeated this experiment and demonstrated that preincubation with DOX followed by an Fe challenge did not protect cells. In fact, it was detrimental, resulting in decreased cellular viability (Figure 3.1B). The reason for this observation is probably related to several factors. First, it was shown by Link and colleagues (Link et al., 1996) that Fe-loading potentiates the cytotoxic effect of DOX, which is probably through the generation of a redox-active DOX-Fe complex (Gianni and Myers, 1992). Second, we previously demonstrated that incubation of cells with DOX prevented ferritin Fe release (Kwok and Richardson, 2004), which may be related to its ability to act as a protein synthesis inhibitor and/or inhibit lysosomal and proteasomal activity (Kwok and Richardson, 2004). The inability of ferritin to release Fe for essential metabolic processes would not be beneficial and could play a role in the cytotoxicity of anthracyclines. Third, in combination with the other well characterised cytotoxic effects of anthracyclines *e.g.*, inhibition of topoisomerase II, DNA intercalation *etc*

(Minotti et al., 2004b), the multiple effects of preincubating cells with DOX markedly affects cellular metabolism, leading to an ineffective response to an Fe challenge.

While chemical studies have shown that anthracyclines directly bind Fe (May et al., 1980), the intracellular consequences of this Fe-depletion have not been established. This is probably due to the complexity of their cellular interactions (Minotti et al., 2004a; Xu et al., 2005). In this study, we demonstrated that DOX, DAU and EPI could act like the well known chelator, DFO, increasing mRNA expression of the Fe-regulated genes, *TfR1* (Hentze and Kuhn, 1996) and *Ndrg1* (Le and Richardson, 2004). This effect was marked, as at an equimolar concentration to DFO (2 μM), all the anthracyclines were as, or more effective at increasing *TfR1* and *Ndrg1* mRNA (Figure 3.4A). The high Fe chelation efficacy of the anthracyclines is probably related to their marked lipophilicity (Miura et al., 1991), which enables rapid intracellular access in comparison to DFO which is hydrophilic and poorly penetrates cells (Richardson and Milnes, 1997).

In the current investigation, increased expression of *TfR1* and *Ndrg1* mRNA acted as a sensitive indice of intracellular Fe chelation and could be inhibited by pre-saturating the Fe-binding site of anthracyclines with Fe (Figure 3.4A). These Fe complexes still entered cells as they are highly hydrophobic (Miura et al., 1991) and this was obvious from the red colour of the cell pellets which are usually white. Hence, the formation of the Fe complex prevented intracellular Fe chelation, but did not stop cellular access.

The nature of the Fe pools that regulate TfR1 and Ndrg1 expression remains unknown. However, these Fe pools influence IRP mRNA-binding activity which post-

transcriptionally regulates *TfR1* mRNA (Hentze and Kuhn, 1996) and HIF-1α that transcriptionally up-regulates *TfR1*, *Ndrg1* and *VEGF1* (Beerepoot et al., 1996; Bianchi et al., 1999; Kalinowski and Richardson, 2005; Le and Richardson, 2004; Lok and Ponka, 1999). The DOX concentrations which up-regulate *TfR1* mRNA in SK-Mel-28 cells (*ie*., 1-2 μM; Figure 3.2A) were previously shown not to markedly affect IRP-mRNA-binding activity in this cell type (Kwok and Richardson, 2002), suggesting it was not an IRP response. Considering this, we also assessed the role of HIF-1α in regulating gene expression using HIF-1α knockout (*HIF-1α*$^{-/-}$) MEFs compared to their wild-type counterparts (*HIF-1α*$^{+/+}$). These studies suggested up-regulation of *TfR1*, *Ndrg1* and *VEGF1* mRNA by DOX occurred *via* an HIF-1α-independent mechanism, as regulation was comparable in the presence or absence of this transcription factor. Other studies examining HIF-1α activation by hypoxia also demonstrated that regulation of its target genes occurred irrespective of HIF-1α status in MEFs (Helton et al., 2005). Moreover, we showed using MEFs that DFO increased *Ndrg1* mRNA expression by HIF-1α-dependent and -independent mechanisms (Le and Richardson, 2004). Collectively, the current work and previous studies (Helton et al., 2005; Le and Richardson, 2004) indicated functional redundancy in the control of HIF-1α target gene expression, with a HIF-1α-independent mechanism responding to Fe chelation. This is of interest, as HIF-1α-independent pathways have been identified to be involved in the up-regulation of genes by hypoxia (Wood et al., 1998) and may also respond to Fe-depletion. Potentially, such pathways could be mediated by molecules related to HIF-1α, such as HIF-2α (Hu et al., 2003) and HIF-3α (Gu et al., 1998).

While anthracyclines could act like typical chelators such as DFO to bind Fe and induce up-regulation of Fe-responsive genes, the effect on cellular ^{59}Fe mobilisation

and intracellular ^{59}Fe distribution were atypical compared to other ligands. For instance, in contrast to DFO and PIH that induce cellular Fe efflux (Ponka et al., 1979b; Richardson and Milnes, 1997), DOX had no effect on ^{59}Fe release from cells or cellular lysates at the same concentrations that up-regulated *TfR1* and *Ndrg1* mRNA. This suggests the high lipophilicity of DOX and its ^{59}Fe complex leads to marked retention in membranes and organelles, as shown by others (Hurwitz et al., 1997; Jung and Reszka, 2001; Miura et al., 1991).

The multi-functional activity of DOX was shown by FPLC to lead to ferritin-^{59}Fe accumulation and prevent ^{59}Fe incorporation into high M_r compartments. This work confirmed and extended our previous observations demonstrating anthracyclines inhibit ferritin-Fe mobilisation, which is probably mediated through inhibition of protein synthesis (Kwok and Richardson, 2003; Kwok and Richardson, 2004). Moreover, considering the alteration in ^{59}Fe distribution, it can be suggested that anthracycline-mediated Fe-deprivation which up-regulates *TfR1* and *Ndrg1* mRNA could not only be due to direct Fe chelation, but also to inhibition of ferritin-Fe mobilisation.

An interesting observation which also demonstrated the multi-functional effect of DOX was that it acted as an effective protein synthesis inhibitor. This potentially could be responsible for the observed decrease in TfR1 and Ndrg1 protein as a function of DOX concentration. However, it was paradoxical that increasing DOX concentrations led to elevated ferritin protein expression, suggesting selective targeting of gene expression or. This finding was surprising, but was in accordance with previous studies demonstrating the effect of DOX at differentially targeting the expression of other

genes (Chen et al., 1999; Ito et al., 1990). This selective activity of DOX has not been reported for genes involved or modulated by Fe metabolism. Alternatively, the observed ferritin up-regulation could be induced *via* hampered lysosomal degradation of ferritin, since DOX may interfere with normal lysosomal function (Kwok and Richardson, 2004; Persson et al., 2001). At present, it remains uncertain what precise molecular mechanism leads to DOX inhibiting TfR1 and Ndrg1 protein expression and increasing ferritin protein synthesis. The apparent selectivity in altering gene expression could be important for understanding the complex pharmacological effects of DOX.

As discussed above, the marked inhibition of TfR1 protein expression by DOX in SK-Mel-28 cells may be due to the depression of protein synthesis. Hence, this appeared to be a secondary response unrelated to Fe chelation which occurred after long preincubations with DOX that led to decreased Fe uptake from Tf. Certainly, the decreased TfR1 and increased ferritin protein expression observed after incubation with DOX is opposite to that found with typical Fe chelators such as DFO (Hentze and Kuhn, 1996) that are not potent protein synthesis inhibitors (Richardson and Milnes, 1997). Our current observations with neoplastic cells were in contrast to results using endothelial cells, where anthracyclines induced Fe uptake *via* increasing TfR1 protein (Kotamraju et al., 2002). These latter authors suggested that DOX-mediated apoptosis was accompanied by increased Fe uptake *via* TfR1 that was responsible for inducing apoptosis (Kotamraju et al., 2002). This result is controversial, as decreased intracellular Fe is generally associated with apoptosis and inhibiting proliferation (Kalinowski and Richardson, 2005).

In summary, anthracyclines act as atypical chelators up-regulating the mRNA expression of the Fe-regulated genes, *TfR1* and *Ndrg1* by their chelation of intracellular Fe. However, this complexation of Fe did not lead to increased TfR1 or Ndrg1 protein levels, nor did DOX induce cellular Fe mobilisation. The lack of anthracycline-mediated Fe efflux was probably because of the high lipophilicity of the so-formed Fe complexes that remained intracellular. Considering the effect of anthracyclines on TfR1 and Ndrg1 expression, it was surprising and paradoxical that DOX increased ferritin protein expression and led to ferritin Fe accumulation. Hence, the effect of anthracyclines on Fe metabolism was multi-faceted, probably due to their complicated chemical properties which leads to multiple mechanisms of action.

CHAPTER 4:

INVESTIGATION OF NOVEL

FERRITIN PARTNER PROTEIN(S)

4.1 INTRODUCTION

The iron (Fe) storage protein, ferritin, plays a key role in Fe detoxification and storage in almost all mammalian cells (Arosio et al., 1978). Ferritin is composed of a protein shell that can accommodate up to 4500 atoms of Fe in its internal cavity (for review, see Harrison and Arosio, 1996; Richardson and Ponka, 1997). The protein shell is made up of 24 symmetrically related subunits of two types, a light subunit (L-ferritin) of about 19 kDa and a heavy subunit (H-ferritin) of about 21 kDa (Hentze et al., 1987). In mammals, major Fe storage sites include liver (about one-third), spleen and bone marrow (Harrison and Arosio, 1996).

Anthracyclines are effective anti-cancer agents which are widely used for the treatment of cancer (for review, see Xu et al., 2005). It has been suggested that the cardiotoxic effects of anthracyclines were related to their ability to bind Fe (Garnier-Suillerot and Gattegno, 1988). Previous studies showed that incubation of cells in culture with the anthracycline, doxorubicin (DOX) led to ferritin-Fe accumulation at very low concentrations (1 μM; Kwok and Richardson, 2003). The increase in ferritin-^{59}Fe was shown to be due to a decrease in the release of Fe from the protein (Kwok and Richardson, 2003).

Interestingly, a protein synthesis inhibitor, cycloheximide (CHX), was also shown to markedly increase ferritin-Fe accumulation in a similar way to DOX (Kwok and Richardson, 2004). Therefore, we hypothesised that DOX may impair the Fe release pathway by preventing ferritin trafficking to lysosomes where degradation and Fe release is thought to occur (Radisky and Kaplan, 1998) or alternatively DOX could inhibit the synthesis of essential ferritin partner proteins that induce Fe release. In cells,

many biological processes are catalysed by protein-protein complexes, *e.g.* haem synthesis (Babusiak et al., 2005). Similarly, the process of ferritin-Fe release may require other proteins to catalyse a series of cascade processes that leads to the release of Fe from the protein. However, the mechanisms behind Fe mobilisation from ferritin remain obscure.

It has been argued that release of Fe from ferritin requires the proteolytic degradation of the ferritin shell, and this process takes place within lysosomes by the action of lysosomal enzymes operating at acidic pH (Kidane et al., 2006; Persson et al., 2001; Yu et al., 2003). Intra-lysosomal ferritin degradation is preceded by lysosomal autophagy of cytosolic ferritin, seemingly being a non-specific or at least a non-saturable process (Persson et al., 2001; Yu et al., 2003). Depression of lysosomal activity via the enzyme inhibitors, E64d and leupeptin, or the lysosomotropic agents, ammonium chloride, chloroquine and methylamine, lead to marked ferritin-^{59}Fe accumulation compared to the control (Kwok and Richardson, 2004). Additionally, the proteasome inhibitors, MG132 and lactacystin, also significantly increased ferritin-^{59}Fe levels compared to the control (Kwok and Richardson, 2004). In summary, these results suggest that lysosomes and proteosomes play an important role in ferritin-Fe release.

In the present study, we designed a native protein purification technique in an attempt to isolate ferritin-binding partners that could potentially play a role in ferritin-Fe mobilisation. These techniques included ultra-centrifugation, anion-exchange chromatography, size exclusion chromatography and native gel electrophoresis. In addition to cells in culture (namely, SK-Mel-28 melanoma cells), liver taken from the mouse was used as a physiological *in vivo* model, as this organ is a major source of

ferritin (Aisen and Listowsky, 1980; Drysdale and Munro, 1966). After several initial experiments utilising some/all of these techniques, we obtained ferritin protein preparations containing potential ferritin-binding partners. Ferritin containing bands were sent for liquid chromatography – mass spectrometry (LC-MS), and various potential partner proteins were identified along with ferritin. These included aldehyde dehydrogenase 1 (family member L1; ALDH1L1) and aspartyl aminopeptidase.

4.2 MATERIALS AND METHODS

4.2.1 Purification of Ferritin and Ferritin Associated Proteins Using Native Techniques Combining FPLC and Gradient Gel Electrophoresis

4.2.1.1 Protein Extraction from Cells and Mouse Liver

SK-Mel-28 melanoma cells were seeded onto petri dishes (145 mm^2, Greiner Bio-One, Frickenhausen, Germany) and allowed to adhere overnight. The cells were then labelled with ^{59}Fe-Tf (0.75 μM) in the presence of agents of interest for 24 h at 37°C. The monolayer was then washed four times with ice-cold PBS (pH 7.4), and lysed on ice by 100 uL lysis buffer (20 mM HEPES, pH 8) supplemented with an EDTA-free protease inhibitor cocktail (Roche, Penzberg, Germany). Cell lysates were collected and thoroughly homogenised using a Dounce glass tissue grinder (approximately 10 strokes, small clearance pestle; Sigma-Aldrich Chemical Co., St. Louis, MO USA).

Mice were injected with 0.6 mg ^{59}Fe-Tf *via* the tail vein. After 24 h, the mice were sacrificed, the livers surgically removed, cut into pieces and homogenised using 20 mM HEPES (pH 8) supplemented with an EDTA-free protease inhibitor cocktail. The homogenised cell samples and liver samples were centrifuged at 16,000 x*g* for 45 min at 4°C to obtain the soluble protein fractions. After centrifugation, the supernatant was collected and the pellet was discarded.

4.2.1.2 Ultra-Centrifugation

The cell or liver proteins after centrifugation (Section 4.2.1.1) were filtered using a 0.22 μM filter (Millipore, Billerica, MA, USA) to remove particulate matter. The flow-through was diluted to 22 mL using 20 mM HEPES (pH 8), and then placed in an ultra-centrifugation tube (Beckman, Fullerton, CA, USA). The tubes containing cell or liver

lysates were carefully balanced and inserted into the Type Ti-60 rotor (Beckman). Ultra-centrifugation was performed at 38,000 rpm (102,000 x*g*) for 70 min at 4°C. After centrifugation, a brown pellet was formed at the bottom of the tube, which was confirmed to be a protein mixture containing ferritin. The supernatant was discarded and the brown pellet was diluted according to the requirements of the next experiment. For anion-exchange chromatography, the pellet was diluted in 5 mL HEPES buffer (20 mM, pH 8), while for size-exclusion chromatography, the pellet was dissolved in 0.5 mL HEPES buffer (20 mM, pH 8) with 140 mM NaCl. The diluted sample was centrifuged at 16,000 x*g* for 5 min at 4°C to remove any insoluble materials before loading onto the column.

4.2.1.3 Anion Exchange Fast Pressure Liquid Chromatography (FPLC)

Anion exchange liquid chromatographic separation was performed at room temperature using the medium-pressure BioLogic Duo Flow system (Bio-Rad, Hercules, CA, USA). In these studies, cell lysates from extraction procedures (Section 4.2.1.1) or from the ultra-centrifugation step (Section 4.2.1.2) were diluted to 5 mL and then loaded onto the Mono Q HR 5/5 anion exchange column (GE Healthcare, Bucks, United Kingdom) using 20 mM HEPES (pH 8). Proteins and protein complexes trapped on the column were eluted with a linear gradient of sodium chloride from 0–1 M (flow rate 1 mL/min). The elution of ^{59}Fe-labelled proteins was monitored by the γ-counter. Generally, samples with the highest amount of radioactivity were concentrated and desalted using a 5-kDa nominal molecular weight cut-off (NMWL) Microcon filter unit (Millipore, Billerica, MA, USA). The concentrated fractions were collected for later experiments, *e.g.* size exclusion chromaography or native gel electrophoresis.

4.2.1.4 Size Exclusion Fast Pressure Liquid Chromatography (FPLC)

Size exclusion chromatography was performed at room temperature using the BioLogic Duo Flow system (Bio-Rad, Hercules, CA, USA). The purified cell lysates (450 uL, after ultra-centrifugation or anion-exchange chromatography) were loaded onto a Superdex 20 10/300 GL column (GE Healthcare, Bucks, United Kingdom) and proteins were eluted according to their size using 20 mM HEPES (pH 8.0, containing 140 mM NaCl). The column was calibrated using the High Molecular Weight Gel Filtration Calibration Kit (GE Healthcare) containing thyroglobulin (669 kDa), ferritin (440 kDa), aldolase (158 kDa), conalbumin (75 kDa), ovalbumin (44 kDa). Fractions (1 mL) were collected and radioactivity was measured using the γ counter. Generally fractions with the highest levels of radioactivity were concentrated and desalted using Microcon filter units with a 5-kDa NWML (Millipore, Billerica, MA, USA).

4.2.1.5 Native Gradient PAGE

Concentrated radioactive fractions were separated on a linear gradient (3–12%) polyacrylamide gel in the presence of the nonionic detergent Triton X-100, in Tris-glycine buffer as previously described (Vyoral and Petrak, 1998; Vyoral et al., 1998). Exernal cooling was set to 15°C. The separation on Hoefer SE600 glass plates (GE Healthcare) proceeded for 12 h at a constant current of 20 mA per gel. Horse spleen ferritin (Sigma-Aldrich) was used as control. After electrophoresis, the gel was sandwiched between two cellophane foils (soaked and washed four times in 200 mL of double distilled water) and vacuum dried for 3 h at 50°C. The dried gels were exposed to the X-ray film for 1-7 days. The films were scanned and then analysed using the densitometric software, Quantity One (Bio-Rad).

4.2.1.6 Silver Staining

To localise and demonstrate the purity of the Fe-containing bands, a small portion of the sample (10%) was separated by the native-gradient PAGE for silver staining (Vyoral et al., 1998). Majority of the sample (90%) was loaded onto another gel and after the electrophoresis, the radioactive bands were cut for liquid chromatography – mass spectrometry (LC-MS). Briefly, the gel for silver staining was fixed in 50% methanol, 12% acetic acid (HAc), 0.05% formalin for 2 h, followed by 3 washes in 35% ethanol (20 min each). The gel was sensitised to 0.01% $Na_2S_2O_3$ for 2 min (Sigma-Aldrich) and then washed three times with H_2O (5 min each). After the washing, the gel was stained by 0.2% $AgNO_3$/0.076% formalin for 20 min, and then washed 2 times with H_2O. The gel was developed in 6% Na_2CO_3, 0.05% formalin and 0.0004% $Na_2S_2O_3$ until the bands were visible and clear. The staining process was stopped by the addition of 50% methanol, 12% HAc for 5 min. The final gel was stored in 1% HAc at 4°C degree.

4.2.1.7 Tryptic Digestion and MS Analysis

Tryptic digestion and LC-MS analysis were kindly performed by Dr. Mark Raftery (Bioanalytical Mass Spectrometry Facility, University of New South Wales, Australia). Briefly, detected radioactive protein bands were excised from the gel. The gel slices were rehydrated, cellophane removed, cut into small pieces and sonicated for 10 min in 20 mM DTT, 50 mM Tris-HCl, pH 8.5 in 50% acetonitrile (AcN) to achieve reduction of cysteine residues. Proteins were alkylated with 15% acrylamide in 50 mM Tris-HCl, pH 8.5 for 40 min at room temperature. The gel pieces were successively sonicated for 10 min in AcN, water, 50% AcN and dried. Dry gel pieces were reconstituted in cleavage buffer containing 0.01% 2-mercaptoethanol, 0.1 M 4-ethylmorpholine acetate,

1 mM $CaCl_2$, 10% AcN and sequencing grade trypsin (50 ng/mL; Promega, Madison, WI, USA).

Digested peptides were separated by nano-LC using a Cap-LC autosampler system (Waters, Milford MA). Samples (5 µL) were concentrated and desalted onto a micro C18 precolumn (500 µM x 2 mm, Michrom Bioresources, Auburn, CA) with H_2O:AcN (98:2, 0.05% heptafluorobutyric acid) at 15 uL/min. After a 4 min wash, the pre-column was automatically switched (Valco 10 port valve, Houston, TX) into line with a fritless nano column (Gatlin, et al., 1998). Peptides were eluted using a linear gradient of H_2O:AcN (98:2, 0.1 % formic acid) to H_2O:AcN (55:45, 0.1 % formic acid) at ~300 nL/min over 30 min. The precolumn was connected via a fused silica capillary to a low volume tee (Upchurch Scientific, Munich, Germany) where high voltage (2400 V) was applied and the column tip positioned ~ 1 cm from the Z-spray inlet of a QTof Ultima API hybrid tandem mass spectrometer (Micromass, Manchester, UK). Positive ions were generated by electrospray and the QTof was operated in data dependent acquisition mode (DDA). A Tof MS survey scan was acquired (m/z 350-1700, 1 s) and the 2 largest multiple charged ions (counts > 20) were sequentially selected by Q1 for MS-MS analysis. Argon was used as the collision gas and an optimum collision energy was chosen (based on charge state and mass). Tandem mass spectra were accumulated for up to 2 s (m/z 50-2000). Peak lists were generated by MassLynx (version 4.0 SP4, Micromass) using the Mass Measure program and submitted to the database search program Mascot (version 2.2, Matrix Science, London, England). Search parameters were: Precursor and product ion tolerances ± 0.25 and 0.2 Da respectively; Met(O) specified as variable modification, enzyme specificity was trypsin, 1 missed cleavage was possible and the $NCBI_{nr}$ database searched.

4.2.2 Other Experimental Methods

All other experimental methods were performed as described in Chapter 2.

4.3 RESULTS

4.3.1. Examination of Potential Ferritin Partner Protein(s)

4.3.1.1 DOX and CHX Altered Cellular Protein Profile and ^{59}Fe Distribution

A well known protein synthesis inhibitor, cycloheximide (CHX), induced ferritin-Fe accumulation in the same manner as DOX (Kwok and Richardson, 2004). Both of these agents are known to inhibit protein synthesis within cells and it is possible that the effect of DOX is due to it acting by this mechanism (Kwok and Richardson, 2004). In addition, many biological processes are catalysed by protein-protein complexes, such as haem synthesis (Babusiak et al., 2005). Therefore, we hypothesized that ferritin has one/several partner protein(s) which is/are involved in ferritin degradation, such as ferritin trafficking to lysosomes or ferritin-Fe release. To examine the existence of ferritin partner protein(s), ferritin was purified from cells to assess the presence of associated molecules.

Considering the effect of DOX and CHX on ferritin Fe-loading (Kwok and Richardson, 2003), our study focused on the effect of these agents on the alterations of ferritin-^{59}Fe levels in SK-Mel-28 cells, as the Fe metabolism of this cell type has been well characterised (Kwok and Richardson, 2003). In this study, SK-Mel-28 cells (100 x 10^6) were treated with DOX (5 μM) or CHX (70 μM) in the presence of ^{59}Fe-Tf (0.75 μM) for 24 h at 37°C. The cell lysates were then loaded onto a MonoQ anion-exchange column and the distribution of ^{59}Fe in the sample was examined using FPLC.

As the ionic strength (0-1M NaCl) of the elution buffer increased, proteins were eluted according to their charge (Figure 4.1A). For all samples, the UV-absorbance sharply increased at fraction 5, which represented the beginning of elution. The majority of

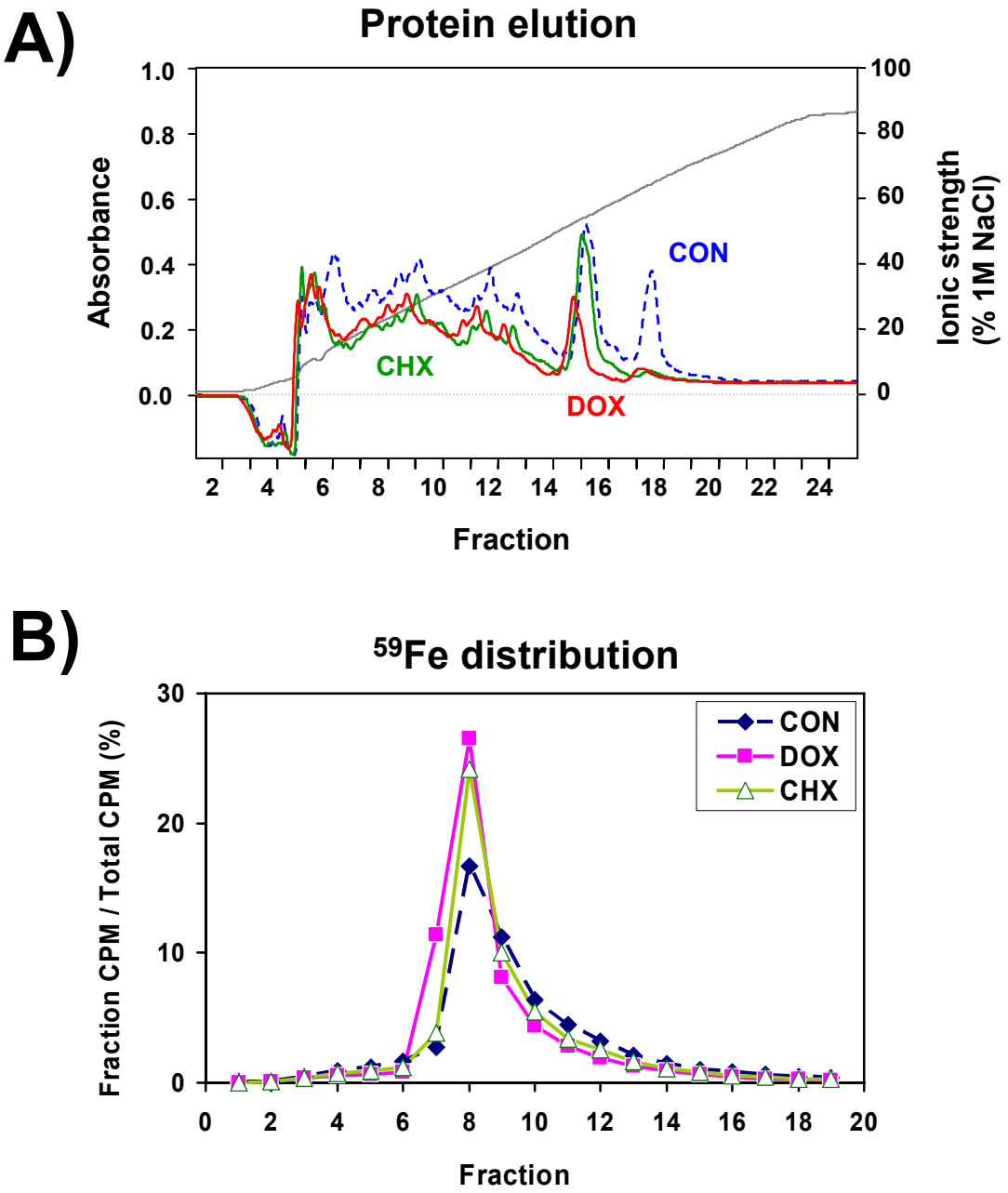

Figure 4.1 Incubation of SK-Mel-28 melanoma cells with DOX and cycloheximide alters: (A) UV-Vis absorbance and (B) ^{59}Fe distribution within cellular lysates. (A) UV-Vis absorbance trace at 280 nm measured during the protein elution process from anion exchange chromatography using FPLC. SK-Mel-28 cells were incubated with control media, DOX (5 μM) or CHX (70 μM) in the presence of ^{59}Fe-Tf (0.75 μM) for 24 h at 37°C. Cells were lysed and cellular proteins were separated using anion-exchange chromatography *via* FPLC. **(B)** The fractions obtained from (A) were assessed to determine the amount of ^{59}Fe in each fraction using the γ-counter. Results are typical from 3 separate experiments performed.

proteins in all samples were eluted in a series of peaks in fractions 5 to 19. These include several small peaks, such as at fractions 6, 8, 9, 12 and 13 (Figure 4.1A). Several more intense peaks were identified at approximately fractions 15 and 18 (Figure 4.1A).

Interestingly, CHX and DOX-treated samples showed a similar protein elution profile as the control, but the absorbance was generally slightly lower than the control (Figure 4.1A). These observations agree with the role of CHX and DOX as protein synthesis inhibitors (Kwok and Richardson, 2003). From the DOX profile, it is clear that when compared to control cells, the peak in fraction 5 is slightly higher, while the peaks at fractions 6 and 7 were diminished compared to the control (Figure 4.1A). Generally, the whole elution pattern in the DOX-treated sample from fractions 7 to 14 was similar to the control. DOX reduced UV-absorbance at fraction 15 to half the control value and led to the elimination of a peak at fraction 18 (Figure 4.1A). The protein elution pattern from CHX-treated cells was similar to that from cells incubated with DOX, except that the UV-absorbance peak at fraction 15 was doubled in intensity (Figure 4.1A).

The ^{59}Fe content of each fraction was then examined and expressed as a percentage of the total ^{59}Fe found in all fractions (Figure 4.1B). For all samples, fraction 8 contained the largest amount of ^{59}Fe and in control samples this was equal to 17% of the total ^{59}Fe eluted from the column. Treatment of cells with CHX or DOX increased the amount of ^{59}Fe in this fraction to 24% and 26% respectively. Fraction 8 was later proven to be ferritin as demonstrated by native-gradient PAGE and super-shift analysis using anti-ferritin antibodies (see Section 2.7). Thus, the increase in ^{59}Fe content in fraction 8 after incubation with CHX or DOX was consistent with studies

demonstrating that these agents induce ferritin-^{59}Fe loading in a similar manner (Kwok and Richardson, 2003). Apart from fractions 7 and 8, the percentage of ^{59}Fe in other fractions from DOX-treated cells was lower compared to the control (Figure 4.1B). This observation is consistent with previous results showing that DOX prevented ^{59}Fe redistribution from ferritin to other cellular compartments (see Section 3.3.6).

In summary, these data above strongly support our hypothesis that DOX and CHX induce ferritin-Fe accumulation in a similar manner, preventing Fe release from ferritin and decreasing the amount of Fe for cellular use.

4.3.1.2 Ferritin-^{59}Fe Distribution is Markedly Changed by DOX and CHX

Fractions 7-12 in Figure 4.1B from control-, DOX- and CHX-treated cells were concentrated using the Microcon filter units with a 5-kDa nominal molecular weight cut-off (Section 4.2.1.3) to a final volume of 100 µL. These samples were then separated using 3-12% native-gradient PAGE. After electrophoresis, the gels were vacuum dried and exposed to X-ray films (Figure 4.2 A, B, C). The radioactive bands were visible and the density confirmed the ^{59}Fe distribution data (Figure 4.1B) with the majority of ^{59}Fe being observed in fraction 8. These bands were confirmed to be ferritin, as they co-migrated with purified horse spleen ferritin and they were super-shifted by an anti-ferritin antibody (data not shown).

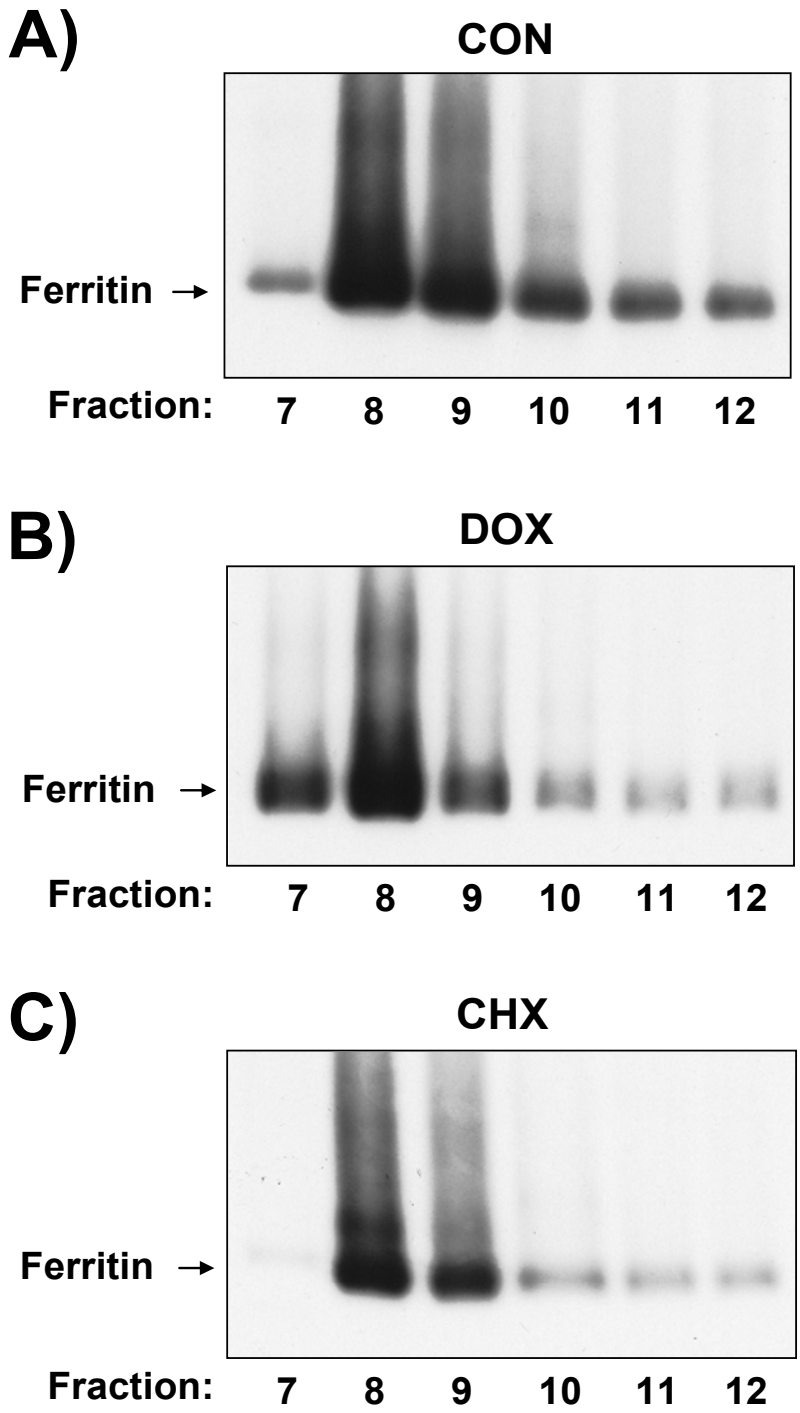

Figure 4.2 The distribution of ^{59}Fe in fractions obtained from anion-exchange chromatography (see Figure 4.1) determined using native-gradient-PAGE. After FPLC (anion-exchange chromatography), fractions from: **(A)** control, **(B)** DOX (5 μM) and **(C)** CHX (70 μM) were concentrated and separated by the 3-12% native-gradient-PAGE. Gels were subsequently dried and autoradiography performed. The bands represent ferritin which was confirmed by super-shift studies using an anti-ferritin antibody. Results are typical from 3 separate experiments performed.

The reason for ferritin being eluted in each fraction may be explained by differential glycosylation of ferritin and subunit composition which will result in differences in the charge of the protein and its molecular weight and shape (Alpert, 1975; Suryakala and Deshpande, 1999).

In the DOX- and CHX-treated samples, the majority of ^{59}Fe-ferritin is eluted in fractions 7-9 and 7-8 respectively (Figure 4.2). In the control sample, although the majority of ^{59}Fe-ferritin is found in fractions 8-9, fractions 10-12 still contain a significant proportion of ferritin-^{59}Fe (Figure 4.2). In spite of the similarity in ^{59}Fe distribution between the 3 samples, in both DOX- and CHX-treated samples much less ferritin-^{59}Fe is found in fractions 10, 11, and 12 compared to the control (Figure 4.2). Thus, in accordance with our hypothesis, treatment with DOX or CHX may lead to less diverse forms of ferritin that are not involved in ^{59}Fe release.

4.3.1.3 Primary Investigation of Ferritin Associated Protein(s) by LC-MS

The radioactive bands shown in Figure 4.2 were carefully cut from the gel and sent for LC-MS analysis by Dr. Mark Raftery (Mass Spectrometry Facility, University of New South Wales, Australia). The detailed experimental procedures were described in Section 4.2. The LC-MS data from 3 different experiments were compiled and demonstrated a list of proteins that were identified along with ferritin (Table 4.1). Several proteins were commonly identified in most of the bands in all 3 treatments, including human elongation factor 2, vesicle amine transporter protein 1 homolog and heat shock protein 60 (Hsp60; Table 4.1).

Table 4.1 Proteins identified by LC-MS from ferritin bands obtained from SK-Mel-28 cells incubated with control media, DOX (5 µM) or CHX (70 µM) for 24 h at 37^{o}C. The presence of the proteins in the ferritin band between 3 different experiments is stated within brackets.

	CON	DOX	CHX
1	**Human elongation factor 2 (3/3)**	**Human elongation factor 2 (3/3)**	**Human elongation factor 2 (3/3)**
2	**Vesicle amine transporter protein 1 (3/3)**	**Vesicle amine transporter protein 1 (2/3)**	**Vesicle amine transporter protein 1 (3/3)**
3	**Heat shock protein 60 (2/3)**	**Heat shock protein 60 (3/3)**	**Heat shock protein 60 (2/3)**
4	Lysosome-associated membrane protein-2 (2/3)	Heat shock protein 70 (2/3)	L-lactate dehydrogenase B chain (1/3)
5	Alanyl-tRNA synthetase (1/3)	Gelsolin (1/3)	Gamma non-muscle actin (2/3)
6	Melanotransferrin precursor (1/3)	78 kDa glucose-regulated protein precursor (1/3)	Actin 1 (1/3)
7	Mutant beta-actin (1/3)	90 kDa heat shock protein (1/3)	Glucosidase II alpha subunit (1/3)
8	Eukaryotic translation elongation factor 1 γ (1/3)	Alpha-tubulin (1/3)	Protein kinase C substrate 80K-H (1/3)

Interestingly, Lysosome-associated membrane protein-2 (LAMP2) was found in the control sample twice, while it was not identified in DOX or CHX-treated samples (Table 4.1). Lysosome-associated membrane proteins are major lysosomal membrane proteins (Pillay et al., 2002) and it could be speculated that LAMP2 act as a dock protein, which facilitates ferritin uptake and degradation within lysosomes. Inhibition of LAMP2 expression by DOX or CHX may prevent ferritin uptake and degradation.

However, none of these proteins have been reported to correlate with mammalian Fe metabolism, suggesting these proteins may be contaminants. It should be noted that the accuracy of LC-MS analysis is limited by the abundance of target protein compared to its contaminating proteins.

In summary, treatment with DOX or CHX altered the cellular protein profile in a similar manner compared to the relevant control. The novel protein purification techniques are appropriate for ferritin purification. However, to assess the existence of ferritin partner proteins, it is necessary to increase their protein levels.

4.3.2 Ferritin Purification by Ultra-Centrifugation, Ion-Exchange FPLC, Size Exclusion FPLC and Native-Gradient PAGE.

Using the techniques above, it was unclear if the proteins present in the bands were ferritin-partner proteins or non-specific contaminants. To further define the molecular species that were present, another technique of ferritin purification was implemented to determine if the same molecular partners could be identified. In this case, ultra-centrifugation was implemented as a first step, as it has been previously proven to be effective for ferritin purification (Winzerling et al., 1995). Subsequent to this, anion-

exchange chromatography, size exclusion chromatography and native-gradient PAGE were performed.

The common protein purification method, immuno-affinity chromatography was not used as it will introduce a large amount of ferritin antibodies. The binding of ferritin antibody-ferritin may induce dissociation of ferritin associated proteins. Furthermore, the antibody will introduce a large amount of noise signal to the LS-MS analysis. Indeed, four commercially available anti-ferritin antibodies were tested using immuno-precipitation. However, all the antibodies appeared to bind to multiple targets apart from ferritin which had been proved by coomassie staining (data not shown). Therefore, immuno-affinity chromatography was not used.

4.3.2.1 Combination of Ultra-Centrifugation, Anion-Exchange and Size Exclusion Chromatography

SK-Mel-28 cells (1 x 10^9) were treated with the Fe donor, ferric ammonium citrate (FAC, 100 μg/mL), for 72 h at 37°C to elicit Fe-loading and ferritin expression. To identify ferritin-^{59}Fe, cells were subsequently incubated with ^{59}Fe-Tf (0.75 μM) for 24 h/37°C. The cells were then harvested and homogenised as described in Section 4.2.1. Cellular proteins were collected and diluted in HEPES buffer (20 mM, pH 8.0) before ultra-centrifugation. A brown pellet was obtained after ultra-centrifugation at 37,000 xg/70min/4^{o}C (Figure 4.3), which may contain ferritin, ferritin-associated proteins, large molecular weight protein complexes and membranes. This pellet was then dissolved in 5 mL of HEPES buffer (20 mM, pH 8.0) and loaded onto an anion-exchange chromatography column as described in Section 4.2 (Figure 4.4A). In the elution profile, there were three major peaks at fractions 5, 19 and 27. The first peak

was flow-through which did not bind to the column, while the next two peaks were possibly ^{59}Fe-ferritin-containing proteins. After examining the radioactivity of each fraction, peak 2 (fractions 18 and 19) was confirmed to be the major ^{59}Fe-containing peak, with 800 and 2400 cpm, respectively (Figure 4.4A). These two fractions were combined and concentrated by a 5 kDa NMWL filter (see Section 4.2).

The sample was concentrated to a final volume of 500 µL and then separated using size-exclusion chromatography as described in Section 4.2.1.4. This purification step was successful, resulting in a major peak at fractions 14 and 15 (Figure 4.4B). Consistent with the protein elution profile, the ^{59}Fe distribution confirmed that these two fractions contained the majority of ^{59}Fe (Figure 4.4B). Considering this, fractions 14 and 15 were combined and concentrated to 100 µL using the 5-kDa NMWL filter units.

Figure 4.3 Isolation of ferritin by ultra-centrifugation using lysates obtained from SK-Mel-28 melanoma cells incubated with the Fe-donor, ferric ammonium citrate. Molecules including ferritin with large M_r were pelletd by ultra-centrifugation (38,000 x*g*, 70 min, 4°C). In these studies, cells were incubated with FAC (100 μg/mL) for 72 h at 37°C. Then ^{59}Fe-Tf (0.75 μM) was added to trace label ferritin for the last 24 h of the incubation. Cells were washed, harvested, homogenised and centrifuged (16,000 x*g* for 45 min at 4^{o}C) to remove nuclei, plasma membrane, mitochondria and cell debris. The supernatant was collected and ultra-centrifugation performed. A brown pellet formed at the bottom of the tube that was consistent with ferritin. Results are typical from 3 separate experiments performed.

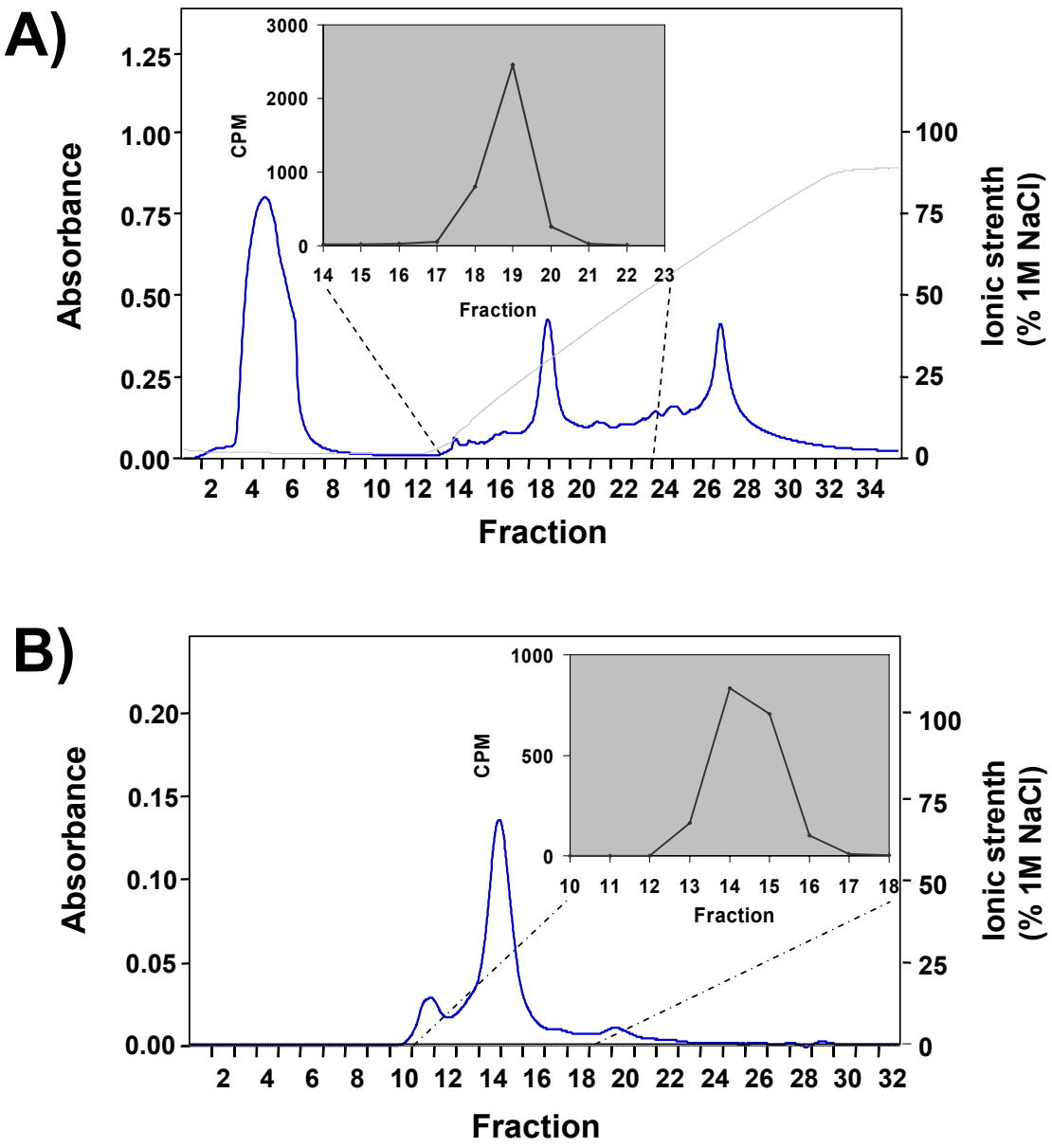

Figure 4.4 Anion-exchange chromatography (A) followed by (B) size exclusion chromatography of samples obtained from ultra-centrifugation of lystates from SK-Mel-28 cells loaded with Fe using the Fe donor, FAC, for 72 h and trace labelled with ^{59}Fe-Tf (0.75 µM) for the final 24 h. (A) The brown pellet from ultra-centrifugation (Figure 4.3) was dissolved in 20 mM HEPES (pH 8) and loaded onto a MonoQ anion exchange column and separated *via* FPLC. Proteins were eluted using increasing ionic strength (0-1 M NaCl/20 mM HEPES, pH 8). Radioactivity of each fraction was examined using a γ-counter. **(B)** Fractions 18 and 19 from (A) were concentrated by a Micron filter unit and separated by size-exclusion chromatography (Superdex 20 10/300 GL column) using FPLC. 1 mL fractions were collected and radioactivity of each fraction examined. Results are typical from 3 separate experiments performed.

4.3.2.2 Native-Gradient PAGE and Silver Staining Confirmed Ferritin

Two 3-12% native-gradient gels were prepared as described in Section 4.2.1.5. A small proportion (10 μL; 10%) of the sample from size exclusion chromatography was loaded onto one gel for silver staining. The silver staining result showed a single band, which co-migrated with purified horse spleen ferritin (data not shown). The majority of the sample (90 μL; 90%) was separated on another gel and the radioactive bands were cut for LC-MS analysis. It was noted that after electrophoresis, a brown band was visible on the gel (data not shown), which had the same colour compared to the pellet that was observed after ultra-centrifugation (Figure 4.3). This brown band was thought to be ferritin. To further confirm the identity of the band, autoradiography was performed. On the X-ray film, a dark band was visible which corresponded to the brown band on the native gel (data not shown). This ^{59}Fe-containing band was excised and sent for LC-MS analysis.

4.3.2.3 Ferritin Identified by LC-MS Analysis

The LC-MS analysis detected ferritin in the brown band. However, no partner protein or co-migrating molecules were detected (data not shown). Compared to the experiments in Section 4.3.1, we used two extra purification steps in addition to anion-exchange chromatography and native-gradient PAGE, namely ultra-centrifugation and size exclusion FPLC. It could be suggested that these extra steps lead to ultra-purified ferritin where ferritin-partner proteins may have disassociated during these extra purification procedures. Considering this, further experiments employed less purification steps and also utilised mouse liver which was rich in ferritin and this was compared to ferritin purified from SK-Mel-28 melanoma cells cultured *in vitro*.

4.3.3 Ferritin Purification from SK-Mel-28 Cells and Mouse Liver, by Efficient Native Separation Techniques

The previous studies described above showed either a large amount of potential ferritin partner proteins (Section 4.3.1) or over-purification of ferritin (Section 4.3.2). Therefore, a new combination of native purification techniques was utilised. Considering this, the ultra-centrifugation step proved highly successful in enabling separation of small molecular weight proteins from high molecular weight molecules (including ferritin and/or associate partner proteins). Indeed, ultra-centrifugation alone was shown to be a very successful ferritin purification procedure leading to a brown pellet at the bottom of the tube (Figure 4.3) and appeared to be an important step in the ferritin purification process.

However, the next step in the purification procedure of ferritin involving ion-exchange chromatography separated ferritin-^{59}Fe in several fractions (Figure 4.2) instead of one fraction and this markedly increased the chance of dissociation of ferritin and ferritin partner protein(s). Thus, we decided to remove the anion-exchange FPLC step from the procedure in 4.3.2 to enable identification of potential ferritin partner proteins.

4.3.3.1 Ultra-Centrifugation and Size Exclusion Chromatography are Efficient Procedures to Separate Ferritin

In these studies, mouse liver was used because it is rich in ferritin (Aisen and Listowsky, 1980; Drysdale and Munro, 1966). The SK-Mel-28 cell line was still used as a control, since we have successfully purified ferritin from these cells in Section 4.3.2.

In this investigation, nine-week-old mice were injected with ^{59}Fe-Tf (0.6 mg) *via* the tail vein and 24 h later the mice were sacrificed to isolate the radioactive liver. The livers were homogenised and cytosolic proteins were extracted as described in Section 4.2.1. SK-Mel-28 cells were treated as described in Section 4.3.2. Briefly, SK-Mel-28 cells were grown to confluence in the presence of the Fe-donor, FAC (100 μg/ml), for 72 h at 37°C and then incubated with ^{59}Fe-Tf (0.75 μM) to trace label the Fe stores for the last 24 h at 37°C. The cells were then homogenised and the proteins extracted.

The two samples obtained after homogenisation (*i.e.*, mouse liver lysate and cell lysate) were diluted in HEPES buffer (20 mM, pH 8.0) and then ultra-centrifugation was performed (Section 4.2.1). Consistently, a brown pellet formed at the bottom of the tube from both samples (Figure 4.5). This suggested that ferritin was successfully isolated.

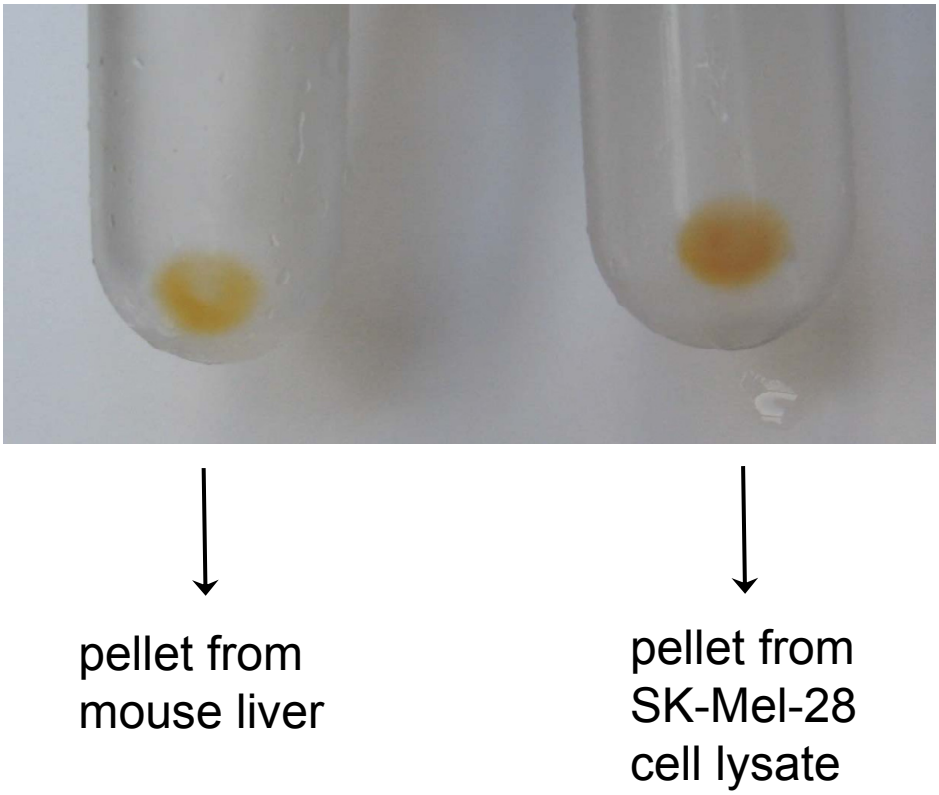

Figure 4.5 Ferritin from mouse livers and iron loaded SK-Mel-28 cells was isolated using ultra-centrifugation. SK-Mel-28 cells were incubated with the Fe donor, FAC (100 μg/ml), for 72 h at 37°C and trace labelled with ^{59}Fe-Tf (0.75 μM) for the final 24 h of this incubation. Mice were injected with ^{59}Fe-Tf (0.6 mg) *via* the tail vein and sacrificed 24 h later to isolate the radioactive liver. SK-Mel-28 cells and mouse liver were homogenised and centrifuged (16,000 x*g* for 45 min/4°C) to obtain cytosol. The cytosol was dissolved in 20 mM HEPES (pH 8) and ultra-centrifugation was performed (38,000 x*g*, 70 min, 4°C). Brown pellets were obtained that were consistent with ferritin. This result is typical from three experiments performed.

The pellets were then dissolved in 0.5 mL of HEPES buffer (20 mM, pH 8) containing 140 mM NaCl and separated by size exclusion column chromatography using FPLC. The SK-Mel-28 cell lysates showed a broad elution peak in fractions 10-15 (Figure 4.6A). The UV-absorbance began to decrease at fraction 14, but formed a small plateau between fraction 14 and 15, before the absorbance decreased at fractions 16 and 17 (Figure 4.6A). The radioactivity of each sample was examined and the majority of ^{59}Fe was in fractions 14, 15 and 16. Previous data using the same chromatography conditions showed ferritin was eluted at fraction 15 (Section 3.3.6), which agreed with the present result where the greatest radioactivity was found in fraction 15 (Figure 4.6A inset). Hence, ultra-centrifugation purified the sample removing all small molecular weight molecules < ~200 kDa, as no peaks were visible after fraction 16 (Figure 4.6A).

Similarly, the mouse liver sample showed a major UV-Vis absorption peak in fractions 10-13 (Figure 4.6B). However, this peak was less pronounced compared to the cell sample (Figure 4.6 A). A second peak was also observed at fraction 15. In line with the results in Figure 4.6A, the majority of liver ^{59}Fe was in fraction 14 and 15 (Figure 4.6B inset). To minimise contamination, fraction 15 was selected for native PAGE analysis.

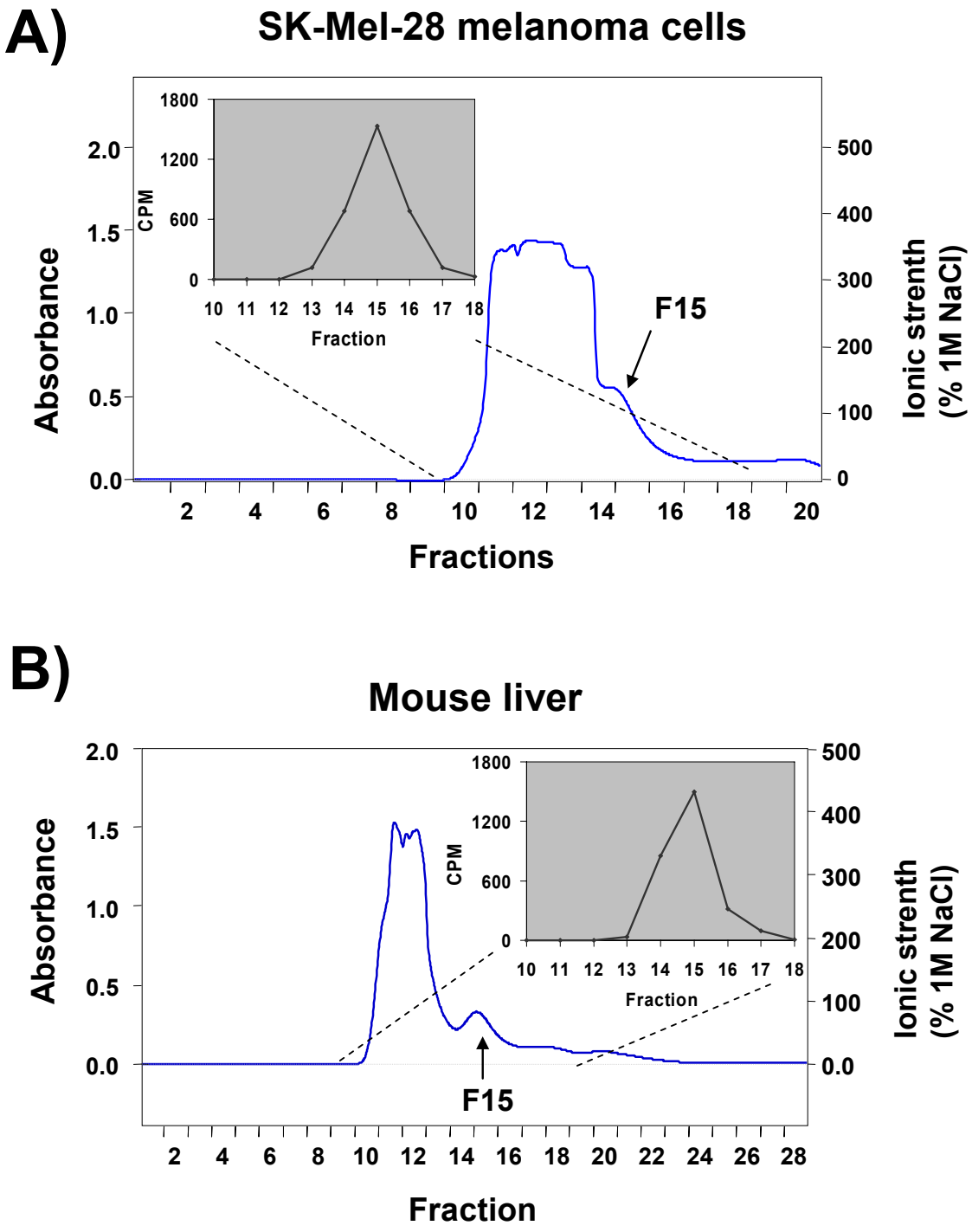

Figure 4.6 Size exclusion chromatography of samples obtained from ultra-centrifugation of lystates from (A) Fe-loaded SK-Mel-28 cells and (B) mouse liver. (A) Fe-loaded SK-Mel-28 cells and (B) mouse liver were homogenised and ultra-centrifuged to obtain a ferritin pellet (see Figure 4.5). The pellets were dissolved in 20 mM HEPES/140 mM NaCl (pH 8) and then separated by size exclusion chromatography (Superdex 20 10/300 GL column) using FPLC. The amount of ^{59}Fe in each fraction was examined using a γ-counter. Results are typical from 3 separate experiments.

After concentration of fraction 15 from the cell and mouse liver samples using the 5-kDa NMWL units, these were then separated using 3-12% native-gradient PAGE. A small portion (10%) of both samples was separated by native PAGE and then silver staining perfomed (Figure 4.7). Lysates from SK-Mel-28 cells showed a major brown band (Figure 4.7, lane 2) that co-migrated with dialysed horse spleen ferritin (Figure 4.7, lane 1). This band was later confirmed to contain human ferritin by LC-MS. The purified mouse liver ferritin presented a different pattern (Figure 4.7, lane 3) compared to commercial horse spleen ferritin and also ferritin SK-Mel-28 cells (Figure 4.7). The purified mouse liver ferritin was located at a higher position (Figure 4.7, lane 3) in the gel compared to horse spleen ferritin (Figure 4.7, lane 1). Later LC-MS analysis proved that the former band was murine ferritin (Table 4.2).

After size-exclusion FPLC, approximately 90% of the sample from SK-Mel-28 melanoma cells and mouse liver was separated by native-gradient PAGE. Two brown bands were visible on the gel (data not shown), which was consistent with the ferritin pattern shown by silver staining (Figure 4.7). These brown bands were directly excised from the gel and sent for LC-MS analysis. Both SK-Mel-28 cell and mouse liver ferritin samples were selected from fraction 15 derived from size exclusion FPLC, which suggested they had a similar molecular weight. However, their migration on native PAGE was dissimilar (Figure 4.7), suggesting differences in charge or shape.

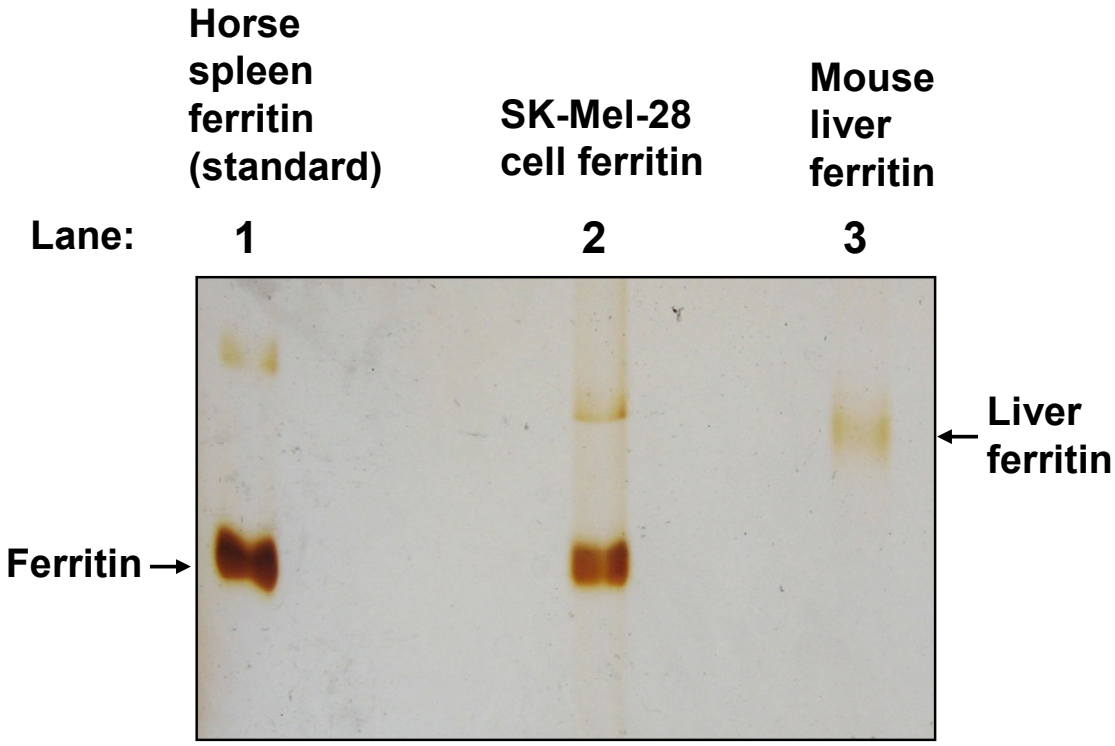

Figure 4.7 Ferritin from SK-Mel-28 melanoma cells and mouse liver was isolated by ultra-centrifugation and size exclusion chromatography (Figure 4.6) was separated by native-gradient PAGE and visualised by silver staining. After size-exclusion chromatography, fractions containing ^{59}Fe-ferritin were concentrated using the 5 kDa NMWL ultra-filtration units and then separated by native-gradient PAGE. Silver staining was performed and ferritin bands were visualised. Dialysed horse spleen ferritin was used as a standard (Lane 1). Results are typical from 3 separate experiments performed.

4.3.3.2 Proteins of Interest after LC-MS Analysis

The ^{59}Fe-ferritin band from mouse liver that was prepared above in Section 4.3.3.1 was excised from the gel and sent for LC-MS analysis, which confirmed the presence of mouse ferritin. These experiments were repeated three times and interestingly, several proteins that consistently co-migrated with ferritin were identified, including: aldehyde dehydrogenase 1 (member L1; ALDH1L1), UDP-glucose pyrophosphorylase 2, glutamine synthetase and aspartyl aminopeptidase (Table 4.2).

Table 4.2 Proteins identified by LC-MS using ferritin-containing samples from mouse livers that were isolated using ultracentrifugation, size-exclusion chromatography and native-gradient PAGE.

	Mice 1	Mice 2	Mice 3
1	**Ferritin light chain**	**Ferritin light chain**	**Ferritin light chain**
2	**Aaldehyde dehydrogenase 1, member L1**	**Aldehyde dehydrogenase 1, member L1**	**Aldehyde dehydrogenase 1 , member L1**
3	**UDP-glucose pyrophosphorylase 2**	**UDP-glucose pyrophosphorylase 2**	**UDP-glucose pyrophosphorylase 2**
4	**Glutamine synthetase**	**Glutamine synthetase**	**Glutamine synthetase**
5	**Aspartyl aminopeptidase**	**Aspartyl aminopeptidase**	**Aspartyl aminopeptidase**
6	**Ferritin heavy chain**	**Ferritin heavy chain**	**Ferritin heavy chain**
7	ATP citrate lyase	Alpha glucosidase 2 alpha	Tripeptidyl peptidase II
8	C1-tetrahydrofolate synthase	40S ribosomal protein S7	UDP glucuronosyltransferase 2
9	Glutamate dehydrogenase 1	Ribosomal protein L27	Cytochrome P450, family 2, subfamily d
10	SEC24 related gene family, member D	Retinol dehydrogenase 7	Formiminotransferase cyclodeaminase
11	Betaine-homocysteine methyltransferase	Transitional endoplasmic reticulum ATPase	Proteasome subunit beta type 4

4.4 DISCUSSION

Ferritin degradation is important for Fe recycling, but the mechanisms by which Fe is released from ferritin for metabolic use are poorly understood (Kwok and Richardson, 2004). Previous and current studies showed that incubation of cells with anthracyclines leads to ^{59}Fe accumulation within ferritin (Kwok and Richardson, 2003, 2004; Xu et al., 2007). This was shown to be due to the effect of anthracyclines at preventing Fe release from this molecule, while the exact molecular mechanism was not clear (Kwok and Richardson, 2003). In addition, the protein synthesis inhibitor, CHX, also mediated ferritin-^{59}Fe accumulation in a similar manner to anthracyclines (Kwok and Richardson, 2003).

It has been suggested that ferritin degradation within lysosomes is essential for Fe release (Persson et al., 2001; Radisky and Kaplan, 1998; Roberts and Bomford, 1988). Furthermore, recent studies employing a variety of well-characterised lysosomal enzyme inhibitors (E64d and leupeptin), lysosomotropic agents (ammonium chloride, chloroquine and methylamine) and proteasomal inhibitors (MG132 and lactacystin) all lead to marked Fe accumulation within ferritin (De Domenico et al., 2006; Kwok and Richardson, 2004). Therefore, ferritin degradation may occur within lysosomes or proteasomes.

Collectively, we hypothesised that DOX prevented Fe release from ferritin by inhibiting the expression of ferritin partner protein(s) which facilitate ferritin trafficking to lysosomes or ferritin-Fe release. Therefore, examination of novel ferritin partner protein(s) became important.

We first identified that treatment with DOX or CHX altered the cellular protein profile using anion exchange chromatography *via* the FPLC technique (Figure 4.1A). SK-Mel-28 cells treated with DOX (5 μM) or CHX (70 μM) lead to lower UV-absorbance compared to the control, suggesting protein synthesis was inhibited by these two agents (Figure 4.1A). However, the proportion of ^{59}Fe within ferritin was markedly increased by incubating cells with DOX or CHX compared to the control (Figure 4.1B), which was consistent with previous studies showing that DOX and CHX lead to ferritin-^{59}Fe accumulation (Kwok and Richardson, 2003).

After separation by anion exchange FPLC, ^{59}Fe containing fractions from control-, DOX- and CHX-treated samples were examined by native-gradient PAGE. Consistent with the ^{59}Fe profile (Figure 4.1B), the ferritin-^{59}Fe bands were visible by autoradiography (Figure 4.2). Interestingly, treatment with DOX and CHX led to a narrower distribution of ^{59}Fe-ferritin with the majority being found in 2 and 3 fractions, respectively (Figure 4.2). In contrast in control cells, ^{59}Fe-ferritin was spread over 5 fractions. Considering this, several hypotheses can be made to explain these observations. First, it could be speculated that in control cells, ferritin could exist in equilibrium between several states, that are involved in Fe-release or Fe-uptake processes. However, treatment with DOX or CHX may largely decrease the ability of ferritin to convert or exist in these forms. Second, it has been shown that ferritin is a glycoprotein and the effect of DOX and CHX on these glycosylation processes may result in alterations of the charge and shape of ferritin (Alpert, 1975; Suryakala and Deshpande, 1999). Third, DOX and CHX could potentially inhibit the expression of ferritin partner proteins, and subsequently lead to a narrower range of ferritin protein complexes.

After anion-exchange chromatography and native-gradient PAGE, a number of proteins were commonly identified by LC-MS in control, DOX and CHX treated samples, including elongation factor 1, vesicle amine transporter protein 1 and heat shock protein 60. However, assessment of the literature demonstrated no correlation between these proteins with cellular Fe metabolism. Moreover, none of the proteins were identified in later experiments using more refined ferritin purification techniques (see below).

To verify the presence of the potential ferritin partner proteins identified by anion exchange chromatography, native PAGE and LC-MS, another purification protocol was important to examine. To do this, ultra-centrifugation, size exclusion FPLC and native-gradient PAGE were utilised (see Section 4.3.3). Using normal mouse liver, four potential ferritin partner proteins were consistently identified over 3 separate experiments, including ALDH1L1, UDP-glucose pyrophosphorylase 2, glutamine synthetase and aspartyl aminopeptidase. Below is a discussion on the molecular properties and potential roles of these proteins in cellular iron metabolism.

Aldehyde dehydrogenase 1 family, member L1

Aldehyde dehydrogenase 1 family, member L1 (ALDH1L1, 10-formyltetrahydrofolate dehydrogenase; EC 1.5.1.6) is developmentally regulated in the cerebellum (Kuhar et al., 1993). ALDH1L1 is a tetramer with a $M_r \sim 440$ kDa, which is very similar to ferritin and thus there is some concern that this protein could be a contaminant due to its similar size (Schirch et al., 1994). It is one of the most abundant enzymes involved in folate metabolism, comprising about 1% of the total pool of soluble cell protein in liver cytosol (Kisliuk, 1999).

ALDH1L1 catalyses the NADP-dependent oxidation of 10-formyltetrahydrofolate (10-FTHF) to tetrahydrofolate (THF; Vasiliou et al., 2000). 10-FTHF represents one of the major forms of folate in the cell which is involved in the de novo purine biosynthesis (Krupenko and Wagner, 1999) and the methylation potential of the cell (Anguera et al., 2006). The ALDH1L1-catalysed reaction is important for recycling the excess 10-FTHF in the cell (Krupenko and Wagner, 1999). This process appears to be important for the clearance of formate protecting the cell from formate intoxication (Tephly, 1991). Furthermore, ALDH1L1 is significantly down-regulated in several different tumours (Krupenko and Oleinik, 2002; Oleinik and Krupenko, 2003). However, the precise physiological role of ALDH1L1 *in vivo* is unclear .

Interestingly, it has been reported that iron deficiency decreased serum folate levels in rats and humans (Oppenheim et al., 2001). Moreover, increased ferritin H-subunits induced the expression of the folate-dependent enzyme, cytoplasmic serine hydroxyl-methyltransferase (cSHMT; Oppenheim et al., 2001). This enzyme catalyses the THF-dependent interconversion of glycine and serine, which is an important pathway involved in the circulation of 10FTHF/THF.

The latter authors suggested that cSHMT is a key regulatory enzyme in folate metabolism and responded to the altered Fe status and metabolism (Oppenheim et al., 2001; Oppenheim et al., 2000). The precise molecular mechanism of Fe altered folate metabolism needs to be further clarified. However, considering the significance of ALDH1L1 in folate metabolism it is possible to speculate upon some association between this molecule and ferritin where formation of a high molecular weight complex could be beneficial in the efficient coupling of metabolic intermediates.

UDP-glucose pyrophosphorylase

UDP-glucose pyrophosphorylase (EC 2.7.7.9), also known as glucose-1-phosphate uridylyl-transferase or UGPase, catalyses the formation of UDP-glucose from glucose-1-phosphate and UTP (Holden et al., 2003; Thoden and Holden, 2007). This protein has not yet been shown to correlate with cellular Fe metabolism. Furthermore, this molecule has a M_r around 450 kDa (Aksamit and Ebner, 1972; Turnquist et al., 1974), suggesting it may be a co-migrating contaminant.

Aspartyl aminopeptidase and glutamine synthetase

Aspartyl aminopeptidase (EC 3.4.11.21) has been reported to be the major aminopeptidase in rabbit brain homogenates that degrades N-terminal acidic acid-containing peptides (Kelly et al., 1983; Wilk et al., 1998). It has been shown that this protein has a M_r of 440 kDa, which is similar to ferritin (Wilk et al., 1998). Furthermore, glutamine synthetase (EC 6.3.1.2) is a large molecule with $M_r \sim 600$ kDa (Blanco et al., 1989; Yin et al., 1998). The high molecular weight of these two molecules suggests that they may be contaminants.

It should be noted that the four potential ferritin partner proteins described above from mouse liver were not observed in initial studies using human SK-Mel-28 melanoma cells where we identified elongation factor 1, vesicle amine transporter protein 1 and heat shock protein 60 as potential ferritin partners. This could be explained by the fact that different cell types were used and the separation procedure was also distinct.

In conclusion, ferritin was purified along with several high molecular weight proteins. Among the possible ferritin partner proteins identified, ALDH1L1 was considered as

the most likely candidate for future study considering its involvement in 10FTHF/THF cycle, which could be regulated by ferritin H-subunit. Further studies need to be performed to clarify the correlation of this protein with cellular Fe metabolism.

CHAPTER 5

PROTEOMIC ANALYSIS OF HEARTS FROM FRATAXIN KNOCKOUT MICE: MARKED REARRANGEMENT OF ENERGY METABOLISM, A RESPONSE TO CELLULAR STRESS AND ALTERED EXPRESSION OF PROTEINS INVOLVED IN CELL STRUCTURE, MOTILITY AND METABOLISM

This work has been published in:

Sutak, R., Xu, X., Whitnall, M., Kasham, M. A., Vyoral, D and Richardson, D.R. (2008) Proteomic analysis of hearts from frataxin knockout mice: marked rearrangement of energy metabolism, a response to cellular stress and altered expression of proteins involved in cell structure, motility and metabolism. *Proteomics*. 8:1731-41

5.1 INTRODUCTION

Friedriech's ataxia (FA) is an autosomal recessive, progressively lethal disease affecting 1 in 50,000 caucasians (Lodi et al., 2006). It is the commonest form of inherited ataxia, with over 95% of patients having an abnormal expansion of a GAA triplet repeat in intron 1 of the FA gene on chromosome 9 (Campuzano et al., 1996; Lodi et al., 2006). The repeat expansion leads to a marked decrease in the expression of a 210-amino acid protein, frataxin, that has an N-terminal mitochondrial targeting sequence (Campuzano et al., 1997; Koutnikova et al., 1997).

The common features of cells with decreased frataxin expression are the presence of increased mitochondrial iron, decreased respiratory chain activity and oxidative damage (Pandolfo, 2006). The exact function of frataxin is still unknown and currently this is the subject of intense investigation (Lodi et al., 2006). Nevertheless, involvement of frataxin in mitochondrial iron metabolism is apparent, there being increased iron uptake by the mitochondrion in the absence of this molecule and decreased iron sulfur cluster (ISC) synthesis (Babcock et al., 1997; Becker et al., 2002; Foury and Cazzalini, 1997; Muhlenhoff et al., 2002; Napier et al., 2005; Nie et al., 2006; Pandolfo, 2006; Shan et al., 2007; Wilson, 2006). The decreased expression of frataxin and its homologs result in the deficiency of ISC-dependent enzyme activities (Muhlenhoff et al., 2002; Rotig et al., 1997), impairment of heme biosynthesis (Lesuisse et al., 2003) and accumulation of intra-mitochondrial iron (Babcock et al., 1997; Foury and Cazzalini, 1997; Puccio et al., 2001).

Whether frataxin is directly involved in iron detoxification remains unclear, although a number of studies have suggested that the molecule can directly bind iron (Cavadini

et al., 2002; Park et al., 2003). The oxidative damage associated with frataxin deficiency (Calabrese et al., 2005) could simply be a secondary effect of impaired iron homeostasis and respiratory chain dysfunction caused by defects in ISC and/or heme protein biosynthesis. However, mutations of frataxin have been described that increase the sensitivity of yeast cells to oxidative stress, but do not affect the activity of ISC-dependent enzyme aconitase or mitochondrial iron content (Gakh et al., 2006). This could suggest frataxin may be involved in iron detoxification independently of the biosynthesis of ISC and heme proteins (Gakh et al., 2006).

Cardiac involvement is present in most FA patients and therefore complications of cardiomyopathy are a frequent cause of death (Durr et al., 1996). To study this problem, a conditional gene targeting strategy has generated muscle creatine kinase (MCK) conditional frataxin knockout (KO) mice lacking a full-length frataxin transcript in the heart and skeletal muscle (Puccio et al., 2001). This mouse line exhibits classical phenotypic traits of the cardiomyopathy in FA, including cardiac hypertrophy, cytoplasmic vacuolization in myocytes and post-necrotic fibrosis (Puccio et al., 2001). Hence, it is an excellent model to study the molecular alterations that could play an important role in the pathogenesis of FA. In agreement with the hypothesis that frataxin functions in mitochondrial iron homeostasis, there is also mitochondrial iron accumulation and deficiency in ISC-dependent enzyme complexes observed in the hearts of these KO mice (Puccio et al., 2001). This cardiac pathology is not apparent in young animals (4-week-old), but becomes evident as they age (7-9 weeks-old) with death occurring at 10.9 $\pm$ 1.4-weeks (Puccio et al., 2001).

In the current study, we analysed the changes in the protein expression profile of

hearts from 4- and 9-week-old KO mice in comparison to their wild-type (WT) controls. We observed a pronounced rearrangement of energy metabolism pathways, some of which start at 4 weeks of age where no gross pathology was apparent (Puccio et al., 2001). Moreover, a marked increase in the expression of proteins functioning in cell stress protection as well as cellular structure, motility and general metabolism were demonstrated.

5.2 MATERIALS AND METHODS

5.2.1 Animals

The KO and WT animals were obtained from Drs. H. Puccio and M. Koenig (Institut de Genetique et de Biologie Moleculaire et Cellulaire, CNRS/INSERM, Universite Louis Pasteur, Strasbourg, France). These animals were bred and handled using a protocol approved by the University of Sydney Animal Ethics Committee. Genotyping was performed using tail DNA *via* standard techniques (Puccio et al., 2001).

5.2.2 Western Blot Analysis

The samples were separated on NuPAGE Bis–Tris 4–12%, 1.5 mm gels (Invitrogen, Carlsbad, CA, USA) and then transferred to Invitrolon™ PVDF membranes (Invitrogen). The polyclonal antibodies against Hsp25 (rabbit; Abcam, Cambridge, UK), SDHA (goat; Santa Cruz Ltd, Santa Cruz, CA, USA) and GAPDH (rabbit; Santa Cruz) were used at a 1:1000 dilution. The secondary antibodies used were anti-goat antibody (1:5,000 dilution, Santa Cruz) or anti-rabbit antibody (1:5,000 dilution, Sigma) conjugated with horseradish peroxidase. The protein bands were visualized using ECL reagent (Pierce Chemical Co., Rockford, IL, USA). Bands on X-ray film were quantified by scanning densitometry and analyzed using the program, Quantity One (Bio-Rad, Hercules, CA).

5.2.3 Statistics

Data was analysed using ANOVA except for the densitometric assessment of Western blots which implemented Student's t-test. Results were considered statistically significant when $p < 0.05$.

5.2.4 Other Experimental Methods

All other methods including two dimensional gel electrophoresis and proteomic analysis were performed as described in Chapter 2.

5.3 RESULTS

5.3.1 Two Dimensional Electrophoresis and Proteomic Analysis Reveals Marked Alterations in the Expression of Proteins Involved in Energy Metabolism and Response to Cellular Stress

In order to characterise the alterations in protein expression related to FA, we performed two dimensional electrophoresis analysis and proteomic analysis (Kashem et al., 2007) of cellular protein extracts from hearts of KO mice and compared them to their WT counterparts. For each group of animals, 5 different mice were utilised for statistical analysis. After differential analysis of protein profiles of hearts from 4- and 9-week-old KO mice and their WT controls, we analyzed the spots with statistically significant changes in volume ($p < 0.05$) by MALDI-TOF mass spectrometry.

Comparing 4-week-old, asymptomatic KO mice to their WT counterparts, we identified 6 differentially abundant spots (Figure 5.1). The corresponding proteins (Table 5.1) were identified as the components of NADH dehydrogenase (Ubiquinone), branched-chain ketoacid dehydrogenase and pyruvate dehydrogenase. Two spots corresponded to the flavoprotein of the succinate dehydrogenase complex (SDHA) and one protein was an unnamed protein product.

In 9-week-old KO animals that possessed severe pathology including cardiomyopathy, weight loss and mitochondrial iron accumulation (Puccio et al., 2001), the abundance of 51 spots was changed compared to their WT counterparts. The spots that showed a statistically significant difference in volume between KO and WT hearts are shown in

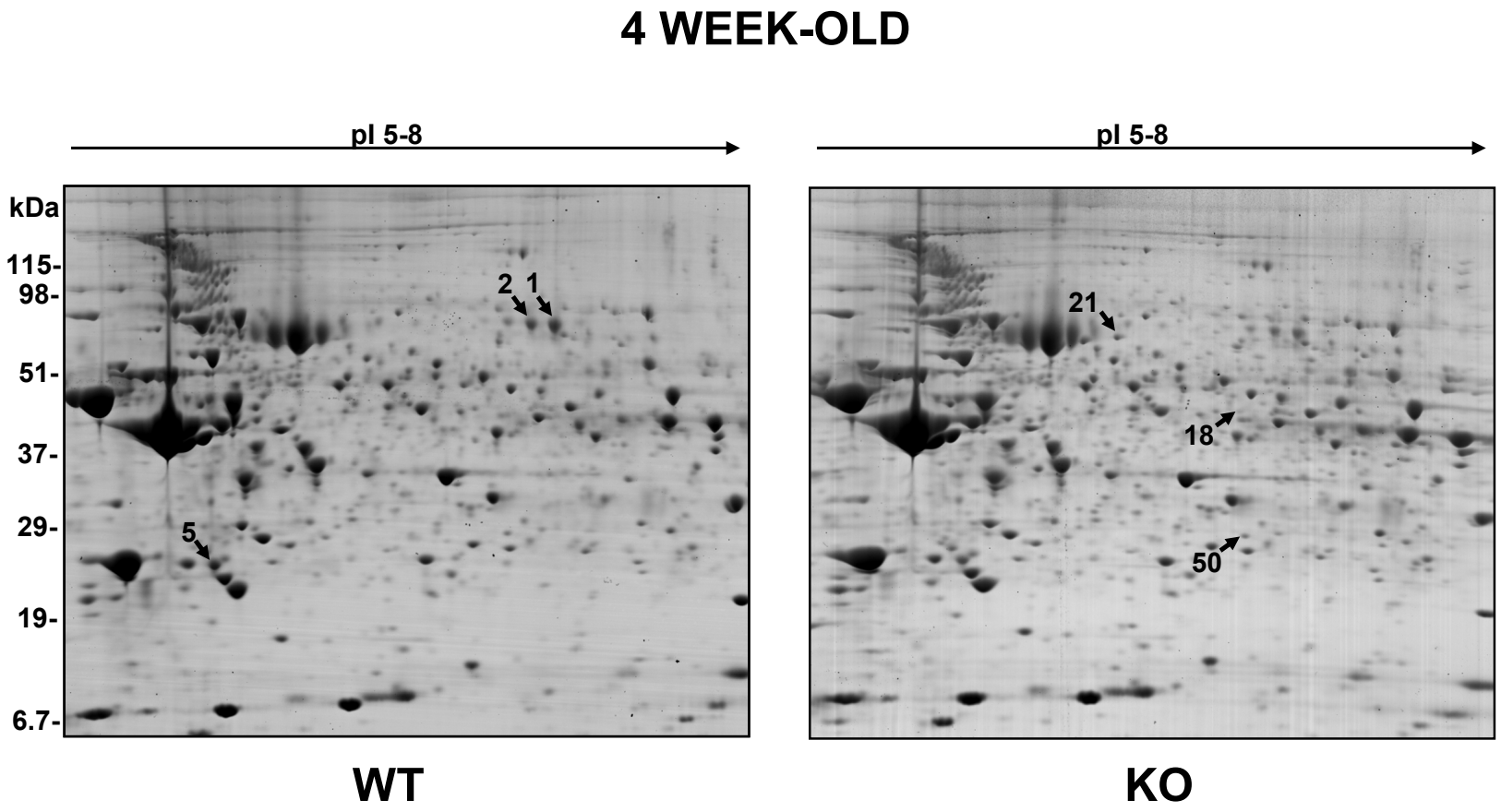

Figure 5.1. 2D gel electrophoresis analysis of proteins from wild type (WT) and frataxin knockout (KO) hearts taken from 4-week-old mice. Spots with significantly ($p < 0.05$) increased volume in WT mice are displayed in the WT gel. The spots with significantly ($p < 0.05$) increased volume in KO mice are displayed in the KO gel. The figure is a representative gel from 5 separate gels for each group of mice. Corresponding proteins are listed in Table 5.1.

Table 5.1 Heart proteins differentially expressed in 4- and 9-week-old KO mice relative to their corresponding WT controls.

Spot	Name	NCBI Accession number	Fold Change 9-week	4-week
	Energy metabolism			
1	succinate dehydrogenase, subunit A, flavoprotein	Q3UKP7	**-5.753**	**-1.258**
2	succinate dehydrogenase, subunit A, flavoprotein	Q3UKP7	**-9.161**	**-1.215**
3	succinate dehydrogenase, subunit A, flavoprotein	Q3UKP7	**-12.28**	
4	NADH dehydrogenase (ubiquinone) 1α, 10	BAC32674	**-4.302**	
5	NADH dehydrogenase (Ubiquinone) flavoprotein 2	Q8K2L0	**-13.182**	**-1.205**
6	NADH dehydrogenase (ubiquinone) Fe-S protein 3	Q8BTZ3	**-6.121**	
7	enolase 3, beta muscle	P21550	**-1.587**	
8	creatine kinase M chain	Q9D6U7	**-2.1**	
9	NADH dehydrogenase (ubiquinone) 1β, 5	BAB23279	**-7.994**	
10	malate dehydrogenase, cytoplasmic	P14152	**-1.633**	
11	NADH dehydrogenase (ubiquinone) Fe-S protein 2	Q99L23	**-5.169**	
12	enoyl coenzyme A hydratase 1, peroxisomal	AAB84224	**-2.097**	
13	malate dehydrogenase, cytoplasmic	P14152	**-3.256**	
14	NADH dehydrogenase (ubiquinone) Fe-S protein 3	Q8BTZ3	**-2.061**	
15	adenylate kinase 1	Q9R0Y4	**-2.088**	
16	E2 component of pyruvate dehydrogenase complex	Q91ZB1	**+25.695**	
17	E2 component of oxoglutarate dehydrogenase	Q4FK55	**+5.724**	
18	branched chain ketoacid dehydrogenase E1, α	Q99L69	**+5.334**	**+2.065**
19	succinyl-CoA:3-ketoacid-coenzyme A transferase 1	BAB27562	**+1.816**	
20	isocitrate dehydrogenase 3 (NAD+) α	BAB26679	**+1.402**	
21	E2 component of pyruvate dehydrogenase complex	Q91ZB1	**+31.816**	**+3.439**
22	mitochondrial acyl-CoA thioesterase	Q3T9C9	**+1.813**	
23	ATP synthase, mitochondrial F0 complex, subunit d	Q9DCX2	**+1.962**	
24	pyruvate dehydrogenase E1 component subunit β	Q9D051	**+2.113**	
25	pyruvate dehydrogenase E1 component subunit β	Q9D051	**+2.665**	
	Stress, protection and anti-oxidation			
26	peroxiredoxin-2	Q61171	**-1.852**	
27	glutathione S-transferase Ω 1	BAC25667	**+4.44**	
28	αB-crystallin	AAA37472	**+3.868**	
29	GrpE-like 1, mitochondrial	BAC33437	**+1.938**	
30	serine protease HTRA2	Q3TXN0	**+2.376**	
31	heat shock protein 25	AAA37862	**+3.151**	
32	heat shock protein 27	AAA18336	**+21.62**	
33	Prohibitin	AAH89034	**+1.874**	
34	protein DJ-1	Q99LX0	**+2.038**	
	Cell structure & motility			
35	Sarcalumenin	BAC29409	**-1.855**	
36	Sarcalumenin	BAC29409	**-1.593**	
37	fibrinogen, B β polypeptide	Q3TGR2	**-1.531**	
38	F-actin capping protein α-2 subunit	P47754	**-1.464**	
39	F-actin-capping protein subunit β	AAA52226	**-2.29**	
40	cardiac troponin T isoform A3b	AAA85352	**-7.195**	
41	moesin	AAA39728	**+4.724**	
42	moesin	P26041	**+2.797**	
43	glial fibrillary acidic protein	CAA26571	**+2.117**	
44	glial fibrillary acidic protein	CAA26571	**+1.419**	
	Miscellaneous			
45	nitrilase family, member 2	Q9JHW2	**-1.837**	
46	D-dopachrome decarboxylase	O35215	**-2.002**	
47	Transthyretin	Q5M9K1	**-1.435**	
48	unnamed protein product	Q8BTN3	**-4.567**	
49	proteasome (prosome, macropain) 28 subunit, α	Q5HZK3	**-1.5**	
50	unnamed protein product	BAC26453	**+2.084**	**+1.16**
51	purine-nucleoside phosphorylase	Q543K9	**+2.117**	

SUPPORTING INFORMATION

spot no.	NCBI accession no.	sequence coverage (%)	MOWSE score	peptides matched	change fold	normalised volume WT (SEM)	normalised volume KO (SEM)
9 weeks							
1	Q3UKP7	29	77	19	-5.753	0.124 (0.033)	0.022 (0.005)
2	Q3UKP7	31	84	23	-12.28	0.058 (0.010)	0.005 (0.001)
3	Q3UKP7	39	97	28	-9.161	0.128 (0.021)	0.014 (0.004)
4	BAC32674	50	97	34	-4.302	0.244 (0.040)	0.057 (0.005)
5	Q8K2L0	52	65	18	-10.182	0.225 (0.022)	0.022 (0.003)
6	Q8BTZ3	65	71	31	-6.121	0.333 (0.024)	0.054 (0.004)
7	P21550	58	138	37	-1.587	0.093 (0.010)	0.058 (0.005)
8	Q9D6U7	58	168	30	-2.1	0.182 (0.031)	0.087 (0.006)
9	BAB23279	41	92	8	-7.994	0.045 (0.008)	0.006 (0.003)
10	P14152	44	89	18	-1.633	0.209 (0.031)	0.128 (0.011)
11	Q99L23	70	120	38	-5.169	0.370 (0.036)	0.072 (0.011)
12	AAB84224	53	69	32	-2.097	0.621 (0.025)	0.296 (0.015)
13	P14152	43	75	14	-3.256	0.102 (0.019)	0.031 (0.009)
14	Q8BTZ3	33	84	10	-2.061	0.050 (0.005)	0.024 (0.003)
15	Q9R0Y4	55	63	9	-2.088	0.511 (0.048)	0.245 (0.070)
16	Q91ZB1	13	69	6	25.695	0.010 (0.005)	0.270 (0.033)
17	Q4FK55	46	77	27	5.724	0.035 (0.006)	0.203 (0.026)
18	Q99L69	45	60	28	5.334	0.008 (0.001)	0.044 (0.003)
19	BAB27562	60	143	35	1.816	0.043 (0.013)	0.077 (0.035)
20	BAB26679	37	108	16	1.402	0.269 (0.027)	0.377 (0.021)
spot no.	NCBI accession no.	sequence coverage (%)	MOWSE score	petides matched	change fold	normalised volume WT (SEM)	normalised volume KO (SEM)
21	Q91ZB1	19	85	12	31.816	0.011 (0.003)	0.340 (0.072)
22	Q3T9C9	62	97	40	1.813	0.218 (0.021)	0.395 (0.109)

SUPPORTING INFORMATION Table 5.1 - Continued

spot no.	NCBI accession no.	sequence coverage (%)	MOWSE score	petides matched	change fold	normalised volume WT (SEM)	normalised volume KO (SEM)
23	Q9DCX2	91	77	24	1.962	0.083 (0.014)	0.163 (0.014)
24	Q9D051	56	85	19	2.113	0.326 (0.040)	0.690 (0.031)
25	Q9D051	34	56	15	2.665	0.024 (0.008)	0.063 (0.016)
26	Q61171	37	104	9	-1.852	0.079 (0.012)	0.043 (0.005)
27	BAC25667	42	69	12	4.44	0.006 (0.001)	0.027 (0.007)
28	AAA37472	76	134	20	3.868	0.010 (0.003)	0.038 (0.008)
29	BAC33437	70	137	17	1.938	0.015 (0.005)	0.029 (0.002)
30	Q3TXN0	20	75	12	2.376	0.009 (0.002)	0.020 (0.005)
31	AAA37862	55	96	13	3.151	0.070 (0.010)	0.222 (0.016)
32	AAA18336	62	86	14	21.62	0.004 (0.002)	0.094 (0.008)
33	AAH89034	66	145	20	1.874	0.150 (0.016)	0.280 (0.023)
34	Q99LX0	34	77	11	2.038	0.008 (0.002)	0.016 (0.001)
35	BAC29409	50	75	31	-1.855	0.141 (0.009)	0.076 (0.013)
36	BAC29409	47	74	24	-1.593	0.258 (0.017)	0.162 (0.017)
37	Q3TGR2	67	80	70	-1.531	0.091 (0.010)	0.059 (0.004)
38	P47754	48	89	13	-1.464	0.024 (0.003)	0.016 (0.001)
39	AAA52226	59	135	21	-2.29	0.011 (0.002)	0.005 (0.001)
40	AAA85352	36	155	19	-7.195	0.356 (0.030)	0.050 (0.019)
41	AAA39728	42	70	31	4.724	0.012 (0.002)	0.058 (0.006)
42	P26041	34	88	25	2.797	0.023 (0.007)	0.064 (0.005)
43	CAA26571	65	67	34	2.117	0.042 (0.014)	0.089 (0.014)
44	CAA26571	65	67	34	1.419	0.404 (0.036)	0.284 (0.014)
45	Q9JHW2	42	86	12	-1.837	0.025 (0.004)	0.014 (0.002)
46	O35215	87	102	15	-2.002	0.038 (0.006)	0.019 (0.001)
47	Q5M9K1	67	76	9	-1.435	0.046 (0.005)	0.032 (0.001)
48	Q8BTN3	29	72	10	-4.567	0.018 (0.004)	0.004 (0.001)
49	Q5HZK3	48	114	15	-1.5	0.058 (0.006)	0.039 (0.003)

SUPPORTING INFORMATION Table 5.1 - Continued

50	BAC26453	35	105	13	2.084	0.021 (0.002)	0.044 (0.004)
51	Q543K9	36	76	12	2.117	0.005 (0.002)	0.011 (0.001)
4 weeks							
1	Q3UKP7	29	77	19	-1.258	0.293 (0.007)	0.233 (0.013)
2	Q3UKP7	31	84	23	-1.215	0.233 (0.012)	0.192 (0.013)
5	Q8K2L0	52	65	18	-1.205	0.242 (0.007)	0.201 (0.003)
18	Q99L69	44	89	18	2.065	0.022 (0.007)	0.046 (0.004)
21	Q91ZB1	19	85	12	3.439	0.042 (0.006)	0.146 (0.016)
50	BAC26453	35	105	13	1.16	0.104 (0.005)	0.120 (0.004)

Figure 5.2 and Table 5.1. Some proteins were identified in more than one spot (*e.g.*, SDHA; Figure 5.3), suggesting the presence of isoforms and/or post-translational modifications that affect the pI and/or molecular mass of the protein. The 51 differentially expressed proteins are involved in energy metabolism (49%), cell structure and motility (19%), stress protection and anti-oxidation (18%) and other functions (14%).

In hearts from 9-week-old KO animals relative to WT mice, we observed decreased expression of components of the iron-dependent complex I and II of the mitochondrial electron transport chain and enzymes involved in ATP homeostasis (creatine kinase, adenylate kinase; Stryer, 1980). Interestingly, the frataxin KO hearts displayed increased expression of enzymes participating in the citric acid cycle (isocitrate dehydrogenase, oxoglutarate dehydrogenase, pyruvate dehydrogenase; Stryer, 1980), catabolism of branched-chain amino acids (branched-chain ketoacid dehydrogenase E1; Stryer, 1980) and ketone body utilisation (succinyl-CoA:3-ketoacid-coenzyme A transferase 1; Stryer, 1980). Moreover, proteins functioning in protection against stress, such as glutathione S-transferase Ω 1 and a variety of chaperones also showed increased expression in the KO relative to the WT mice. Some of the spots displayed a 10- to 30-fold change in abundance between 9- week-old KO mice and their WT controls (Figure 5.3). These spots were identified as SDHA, NADH dehydrogenase flavoprotein 2, E2 component of pyruvate dehydrogenase complex and heat shock protein 27.

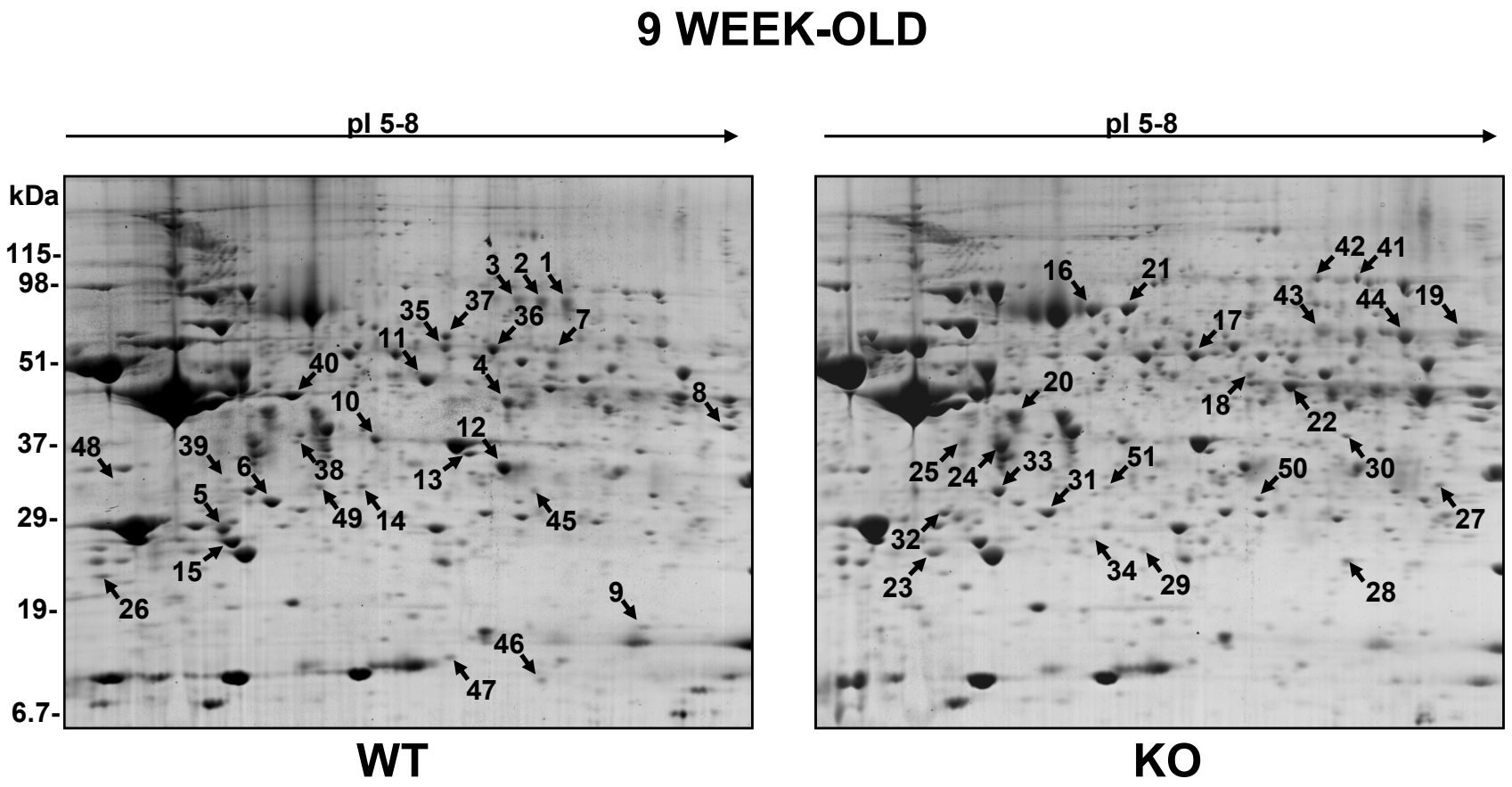

Figure 5.2 2D-gel electrophoresis analysis of proteins from WT and frataxin KO hearts taken from 9-week-old mice. Spots with significantly ($p < 0.05$) increased volume in WT mice are displayed in the WT gel. The spots with significantly ($p < 0.05$) increased volume in KO mice are displayed in the KO gel. The figure is a representative gel from 5 separate gels for each group of mice. Corresponding proteins are listed in Table 5.1.

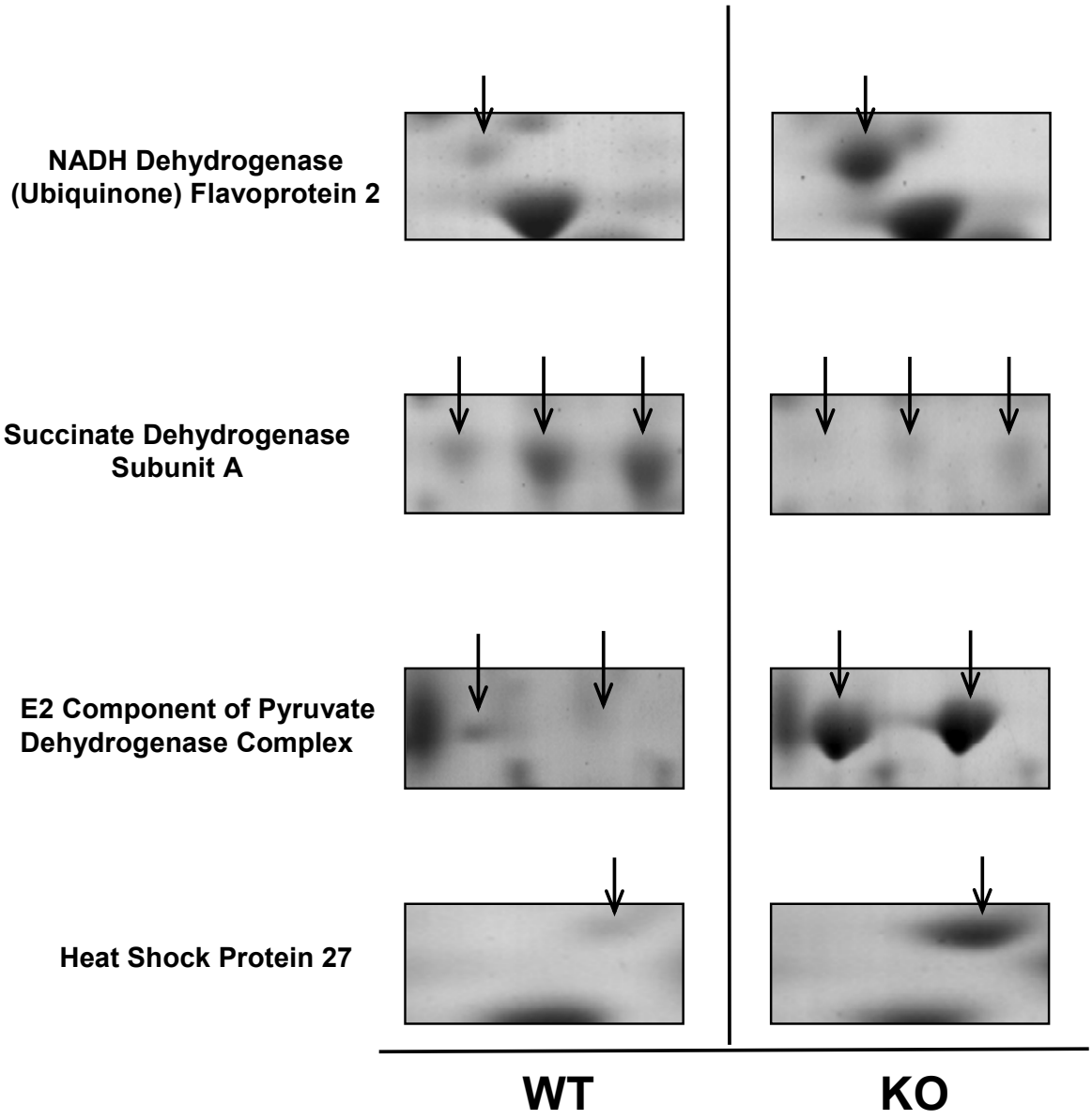

Figure 5.3 Spots with greater than a 10-fold volume change taken from a representative 2D-gel of WT and KO hearts from 9-week-old mice. The figure is a representative gel from 5 separate gels for each group of mice.

5.3.2 Western Blot Analysis Confirms Decreased Expression of SDHA and Up-Regulation of Hsp25

The significant alterations in protein expression from two dimensional electrophoresis analysis above were obtained from 5 individual animals in each group. As a further validation check of the expression changes observed, we performed western blot analysis using antibodies against SDHA and heat shock protein 25 (Hsp25; Figure 5.4). Validation of all 51 alterations in protein expression was not possible due to cost considerations and the lack of appropriate antibodies. Two dimensional electrophoresis analysis (Table 5.1) demonstrated these two proteins showed marked down-regulation (SDHA; -5 to -12-fold) or moderate up-regulation (Hsp25; +3-fold). Both proteins examined by western blotting showed the same pattern of expression as obtained from two dimensional electrophoresis analysis. That is, SDHA expression was significantly ($p < 0.001$) decreased, while Hsp25 expression was significantly ($p < 0.01$) increased in 9-week-old animals (Figure 5.4).

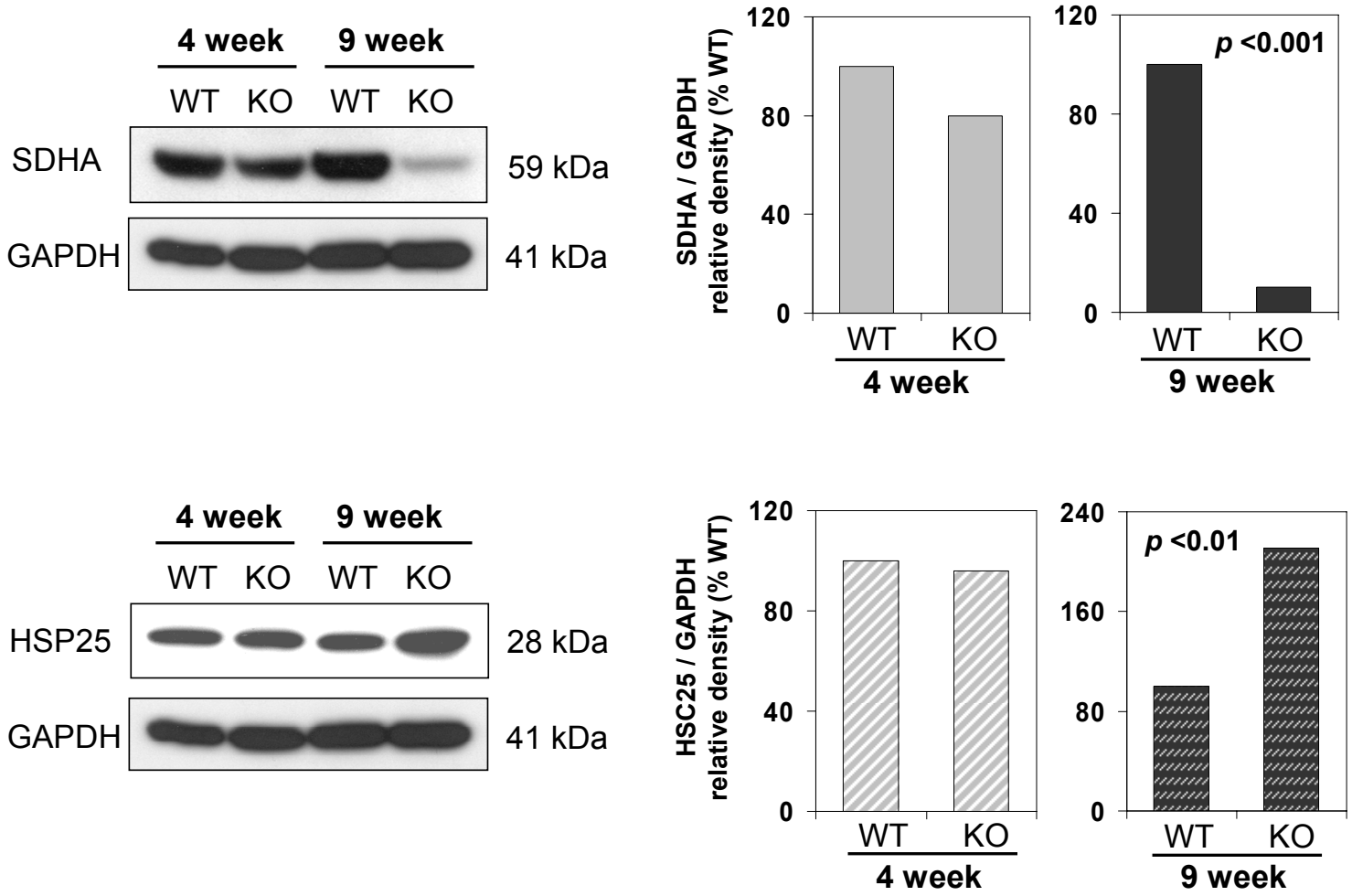

Figure 5.4 Western blot and densitometric analysis of succinate dehydrogenase subunit A (SDHA) and heat shock protein 25 (Hsp25) in wild type (WT) and knockout (KO) hearts from 4- and 9-week-old mice. Glyceraldehyde 3-phosphate dehydrogenase (GAPDH) was used as a control for equal loading of proteins. Representative experiment from 4 performed.

5.4 DISCUSSION

Despite many studies examining the role of frataxin in the pathogenesis of FA, surprisingly little is known about the function of this protein (Lodi et al., 2006). Moreover, the molecular alterations that occur during the cardiomyopathy observed in this disease are very poorly understood. In this study, we analysed changes in protein expression caused by deletion of frataxin in the hearts of MCK KO mice compared to their WT counterparts using two dimensional electrophoresis and proteomic analysis. A marked change in protein expression profile was observed in 9-week-old KO mice which developed severe cardiomyopathy (Puccio et al., 2001). The expression of 5 proteins that were markedly altered in 9-week-old KO mice were also significantly changed in 4-week-old KO mice (Table 5.1) that do not show any marked pathology (Puccio et al., 2001).

The proteins corresponding to the 51 spots showing significantly changed abundance in the KO mice can be divided into 4 groups: **(1)** enzymes of energy metabolism; **(2)** proteins involved in stress, protection and anti-oxidation; **(3)** cell structure & motility related proteins and **(4)** miscellaneous proteins with a variety of functions. An analysis of the roles of these proteins and their relevance to FA and the cardiomyopathy observed in the KO mouse is described below.

5.4.1 Proteins Involved in Energy Metabolism

The KO mice displayed a dramatic re-arrangement in mitochondrial energy metabolism (Figure 5.5). In 4-week-old KO mice, we observed a decrease in the expression of the components of complex I and II of oxidative phosphorylation chain and an increase in the components of pyruvate dehydrogenase complex and branched-

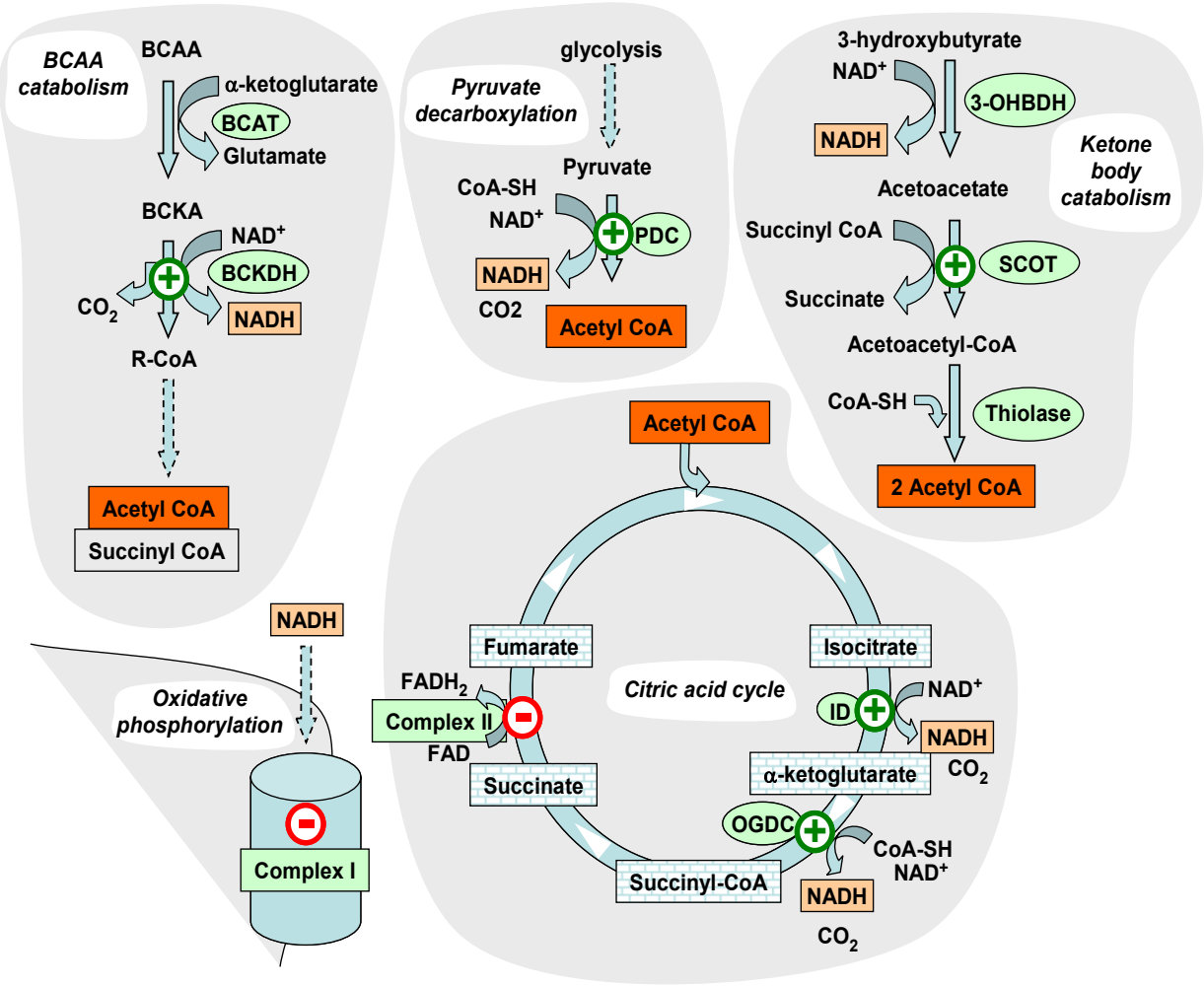

Figure 5.5 Schematic diagram illustrating the rearrangement of energy metabolism in the heart of MCK KO mice. Components of the oxidative phosphorylation complex I and II display decreased expression. Expression of enzymes participating in the citric acid cycle, the catabolism of branched-chain amino acids, ketone body utilisation and pyruvate decarboxylation are increased. Abbreviations: BCAA, branched-chain amino acids; BCAT, branched-chain amino acid aminotransferase; BCKDH, branched chain ketoacid dehydrogenase; CoA, Coenzyme A; PDC, pyruvate dehydrogenase complex; 3-OHBD, 3-hydroxybutyrate dehydrogenase; SCOT, succinyl-CoA:3-ketoacid-coenzyme A transferase; ID, isocitrate dehydrogenase; OGDH, oxoglutarate dehydrogenase.

chain ketoacid dehydrogenase. These changes were intensified in 9-week-old KO mice resulting in a 10-fold decrease in the expression of NADH dehydrogenase flavoprotein 2 and a 30-fold increase in the E2 component of pyruvate dehydrogenase complex. We hypothesise that in the heart of KO mice, failure to synthesise ISCs causes decreased expression of ISC-dependent complex I and II (Figure 5.6), the enzymatic activities of which are known to be significantly reduced in the MCK model (Puccio et al., 2001). These alterations in expression would result in decreased ATP production that leads to metabolic compensation from the activation of several energy metabolism pathways (Figure 5.6). These include the citric acid cycle, branched-chain amino acid catabolism pathways, ketone body utilisation and pyruvate decarboxylation. We observed increased expression of at least one component of each of these metabolic pathways (Figure 5.5).

Although we did not observe any change in the expression of the enzymes participating in β-oxidation (*i.e.*, fatty acid catabolism; Stryer, 1980), there was a significant increase in the expression of mitochondrial acyl-CoA thioesterase. This enzyme cleaves acyl-CoAs into fatty acids and coenzyme A and is thought to provide a means of removing excessive acyl-CoA from β-oxidation (Hunt and Alexson, 2002). Thus, we can hypothesise that the catabolism of fatty acids is probably also affected.

The current study also identified elevated expression of one of the subunits of the ATP synthase and a decrease in the expression of two enzymes involved in ATP homeostasis, namely creatine kinase and adenylate kinase. These changes probably reflect another response to the deficit in mitochondrial ATP production in cardiac muscle (Figure 5.6) that has been previously observed in skeletal muscle of FA patients (Lodi et al., 1999).

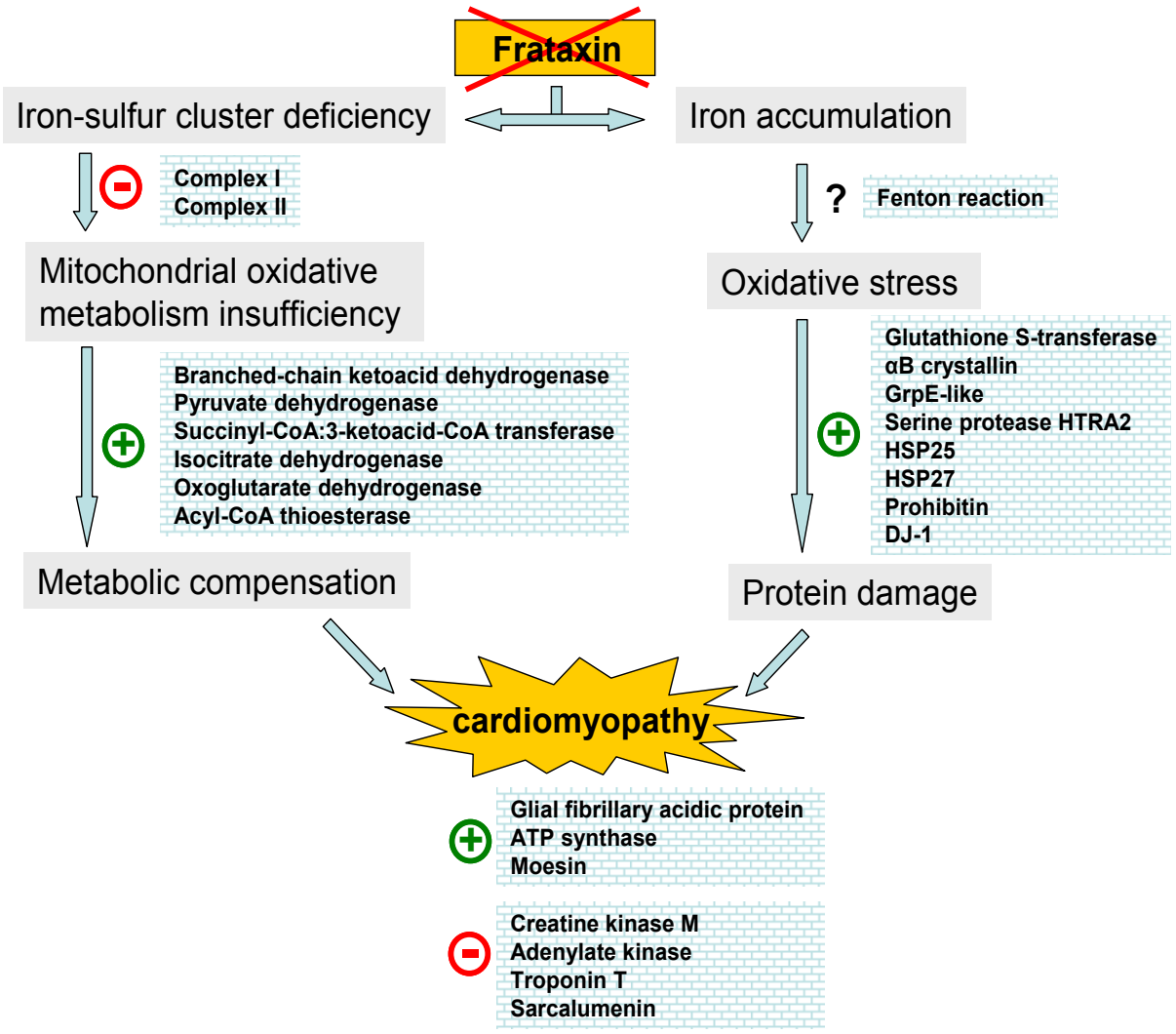

Figure 5.6 Schematic illustration of the proposed mechanism of the cardiomyopathy associated with FA. Impairment in the formation of ISC causes insufficient oxidative phosphorylation, resulting in metabolic compensation and the subsequent activation of different catabolic pathways (*e.g.,* pyruvate dehydrogenase *etc*). Oxidative stress that may be the result of the accumulation of mitochondrial iron or defects in the respiratory chain induce the expression of different proteins functioning in protection against oxidative stress (*e.g.*, glutathione-S-transferase, heat shock protein 27 *etc*). The resulting hypertrophy is associated with changed expression of proteins involved in ATP homeostasis and cell structure and motility.

Considering this, decreased adenylate kinase expression has also been identified as a new biomarker in the diseased diaphragm muscle from an X-linked muscular dystrophy animal model (Doran et al., 2006). In conjunction with creatine kinase, adenylate kinase provides a major nucleotide metabolizing pathway and the decrease of this key enzyme could lead to an abnormal regulation of nucleotide ratios. This appears to be a metabolic defect in dystrophinopathy (Doran et al., 2006) and also the heart of MCK KO mice.

It should be noted that disruption of respiratory chain complex activities (Puccio et al., 2001; Rotig et al., 1997; Wilson and Roof, 1997), decreased expression of succinate dehydrogenase (Tan et al., 2003) and abnormal tissue energy metabolism (Lodi et al., 1999; Lodi et al., 2001) have previously been documented in yeast and animal models of frataxin deficiency and also in FA patients. However, the current work is the first investigation to define the detailed molecular alterations in energy metabolism and metabolic compensation that occurs within the heart *in vivo* in frataxin KO mice.

5.4.2 Proteins Involved in Stress, Protection and Anti-Oxidation

It was demonstrated previously that frataxin deletion in cardiac tissue of KO mice leads to mitochondrial iron accumulation (Puccio et al., 2001). Considering the high potential of iron to participate in formation of reactive oxygen species, this could lead to oxidative stress (Eaton and Qian, 2002). Evidence of oxidative stress in FA patients includes elevated 8-hydroxy-2'-deoxyguanosine levels in urine as a marker of oxidative DNA damage (Schulz et al., 2000) and raised plasma malondialdehyde levels, suggesting increased lipid peroxidation (Emond et al., 2000). In the heart of KO mice, we observed a pronounced increase in expression of a battery of chaperones (Hsp27,

Hsp25, αB-crystallin), co-chaperones (GrpE) and other proteins involved in protection against cellular stress. Of these proteins, Hsp27 showed the greatest fold change (> 21-fold increase), with the functionally related proteins αB-crystallin, Hsp25 and mitochondrial GrpE, also being up-regulated (1.9- to 3.9-fold) in KO relative to WT mice (Table 5.1). These molecules enhance cellular survival upon exposure to noxious stimuli and play roles in protection against toxicity mediated by aberrantly folded proteins, myocardial ischaemia, oxidative stress and apoptosis (Arrigo, 2007; Arrigo et al., 2007; Borges et al., 2003; Jaattela, 1999). As an example of their crucial function, mutation of the human *αB-crystallin* gene causes a multi-system, protein aggregation disease that includes cardiomyopathy (Rajasekaran et al., 2007). Interestingly, response to stress *via* the up-regulation of heat shock proteins (*e.g.*, cvHsp) has also been identified as an important cellular mechanism in dystrophic muscle and has been suggested to be an exploitable approach to counteract muscle degeneration (Doran et al., 2006).

In addition to the molecular chaperones, the expression of a number of other protective molecules was also increased in the KO mice (Table 5.1). The more significant of these included: glutathione-S-transferase-Ω 1, that is known to protect against oxidative stress through its ability to conjugate glutathione to toxic metabolites (Hayes et al., 2005; Kolsch et al., 2004); DJ-1, which has a role in scavenging mitochondrial H_2O_2 (Andres-Mateos et al., 2007); and the serine protease, HTRA2, that is a survival enhancing protein induced by heat shock or toxins (Gray et al., 2000).

Collectively, the up-regulation of this armamentarium of molecular chaperones and protective molecules indicates that depletion of frataxin induces a marked stress

response (Figure 5.6). The origin of this response could be the oxidant stress that is known to exist in FA patients (Emond et al., 2000; Schulz et al., 2000). This may be mediated by the mitochondrial Fe-loading that occurs in the absence of frataxin and/or the disturbance in the respiratory chain due to dysfunctional ISC synthesis (Figure 5.6). Irrespective of the origin of the oxidant stress, the effectiveness of anti-oxidants such as idebenone, coenzyme Q and vitamin E (Di Prospero et al., 2007a; Di Prospero et al., 2007b; Hart et al., 2005) and the potential use of iron chelators in the treatment of FA (Richardson, 2003), can now be rationalized at the molecular level.

5.4.3 Proteins Involved in Cell Structure & Motility

The 9-week-old KO mice showed a severe cardiomyopathy that included marked cardiac hypertrophy (Puccio et al., 2001). Considering this, several proteins involved in cell structure and motility were differentially expressed in the hearts of this model. The most marked change in expression in this group of proteins was found for cardiac troponin T isoform A3b which was reduced 7.2-fold in KO mice relative to the WT. This class of molecules plays a role in modulating cardiac muscle contraction, in particular the sensitivity to Ca^{2+} and inhibition of force development (Gomes et al., 2002a; Gomes et al., 2002b). The importance of troponin T in cardiac contraction is demonstrated by the fact that mutations in this molecule are thought to be involved in the genesis of familial dilated cardiomyopathy (Martins et al., 2006). We also demonstrated a reduction in the expression of sarcalumenin, a calcium-binding protein contributing to calcium buffering within the longitudinal sarcoplasmic reticulum (Yoshida et al., 2005). Of interest, the decreased expression of sarcalumenin has been observed in the cardiomyopathy associated with Duchenne muscular dystrophy (Lohan and Ohlendieck, 2004).

Of the proteins in this group that demonstrated increased expression, moesin showed the greatest fold change (Table 5.1). Moesin is an important signal transducer during actin re-organization and plays roles in cell membrane organization, cell migration, phagocytosis and apoptosis (Niggli and Rossy, 2007; Tamma et al., 2007). Hence, moesin may be involved in marked cytoskeletal alterations that probably occur in the heart when frataxin is absent (Figure 5.6). Another protein that demonstrated increased expression was glial fibrillary acidic protein. This intermediate filament protein has been shown to be an indicator of stress in central nervous system astrocytes and radial glia of the retina (Hagemann et al., 2005; Lewis and Fisher, 2003).

5.4.4 Miscellaneous Proteins

Seven proteins with markedly different functions were identified to be differentially regulated in the hearts of KO mice compared to their WT counterparts (Table 5.1). Purine nucleoside phosphorylase was up-regulated in the KO mouse and plays a key role in the purine salvage pathway and is responsible for the dephosphorylation of purine ribonucleosides and 2'-deoxyribonucleosides (Silva et al., 2007). The increased expression of this enzyme indicates active DNA metabolism that could be necessary during the hypertrophy of the heart in the KO animal. Proteins that were down-regulated included: D-dopachrome decarboxylase, nitrilase family member 2, transthyretin and proteasome 28 subunit α that play roles in melanisation (Jiao et al., 2006), cell growth suppression (Lin et al., 2007), thyroid hormone/retinol binding protein transport (Hamilton and Benson, 2001) and proteasome function (Hanna and Finley, 2007), respectively. Of interest, a recent study has also demonstrated that there is a decrease in proteasome activity using the yeast model of Friedreich's ataxia

(Bulteau et al., 2007).

In summary, frataxin deficiency in the heart from MCK KO mice caused a marked rearrangement of energy metabolism, increased expression of proteins involved in protection against stress, differential expression of structural/motility proteins and alterations in the expression of proteins that play miscellaneous roles in metabolism (Figure 5.6). Our study indicates that changes in expression of proteins involved in these processes are involved in the development of the cardiomyopathy observed in this model. Hence, the current results deepen our understanding of the molecular mechanisms of the cardiomyopathy associated with FA. Moreover, proteins whose expression is affected in this disease may provide tools for monitoring FA prognosis and also the investigation of potential treatment strategies.

CHAPTER 6:

DISCUSSION

6.1 IRON CHELATION BY CLINICALLY RELEVANT ANTHRACYCLINES: ALTERATIONS IN EXPRESSION OF IRON REGULATED GENES AND ATYPICAL CHANGES IN INTRACELLULAR IRON DISTRIBUTION AND TRAFFICKING

6.1.1 *Summary of Principal Findings – Chapter 3*

It was previously demonstrated that anthracyclines altered cellular Fe metabolism and led to ^{59}Fe accumulation within ferritin (Kwok and Richardson, 2002, 2003 and 2004). Importantly, anthracyclines bind Fe and act as bidentate chelators (May et al., 1980). Thus, it is important to elucidate the molecular mechanism of anthracyclines on cellular Fe metabolism, especially their effect on the expression of iron regulated molecules, namely TfR1, Ndrg1 and ferritin.

We demonstrated that DOX, DAU and EPI could act like the well known chelator, DFO, increasing mRNA expression of the Fe-regulated genes, *TfR1* (Hentze and Kuhn, 1996) and *Ndrg1* (Le and Richardson, 2004). Indeed, the increased expression of *TfR1* and *Ndrg1* mRNA acted as a sensitive indice of intracellular Fe chelation and could be inhibited by pre-saturating the Fe-binding site of anthracyclines with Fe (Figure 3.4A). Therefore, the formation of the Fe complex prevented intracellular Fe chelation.

Our studies suggested up-regulation of *TfR1*, *Ndrg1* and *VEGF1* mRNA by DOX occurred *via* an HIF-1α-independent mechanism, as regulation was comparable in the presence or absence of this transcription factor. Collectively, the current work and previous studies (Helton et al., 2005; Le and Richardson, 2004) indicated functional redundancy in the control of HIF-1α target gene expression, with a HIF-1α-independent mechanism responding to Fe chelation.

Although anthracyclines could act like typical chelators such as DFO to bind Fe and induce up-regulation of Fe-responsive genes, the effect on cellular ^{59}Fe mobilisation and intracellular ^{59}Fe distribution were atypical compared to other ligands. For instance, DOX had no effect on ^{59}Fe release from cells or cellular lysates at the same concentrations that up-regulated *TfR1* and *Ndrg1* mRNA.

In contrast to its effect on *TfR1* and *Ndrg1* mRNA levels, DOX decreased TfR1 and Ndrg1 protein as a function of DOX concentration, which could be potentially explained by its role as a protein synthesis inhibitor. However, it was paradoxical that increasing DOX concentrations led to elevated ferritin protein expression, suggesting selective targeting of gene expression. This finding was surprising, but was in accordance with previous studies demonstrating the effect of DOX at differentially targeting the expression of other genes (Chen et al., 1999; Ito et al., 1990). This selective activity of DOX has not been reported for genes involved or modulated by Fe metabolism. At present, it remains uncertain what precise molecular mechanism leads to DOX inhibiting TfR1 and Ndrg1 protein expression and increasing ferritin protein synthesis. The apparent selectivity in altering gene expression could be important for understanding the complex pharmacological effects of DOX.

In summary, we demonstrate for the first time that anthracyclines act as atypical chelators, having a number of effects on Fe metabolism and the expression of Fe-regulated genes, probably due to their complicated chemical properties which leads to multiple mechanisms of action.

6.2 INVESTIGATION OF NOVEL FERRITIN PARTNER PROTEIN(S)

6.2.1 *Summary of Principal Findings – Chapter 4*

Ferritin degradation is probably important for Fe recycling, but the mechanisms by which Fe is released from ferritin for metabolic use are poorly understood (Kwok and Richardson, 2004). Previous and current studies showed that incubation of cells with anthracyclines or the protein synthesis inhibitor, CHX, leads to ^{59}Fe accumulation within ferritin in a similar manner (Kwok and Richardson, 2003, 2004; Xu et al., 2007). This was shown to be due to the effect of anthracyclines at preventing Fe release from this molecule, while the exact molecular mechanism was not clear (Kwok and Richardson, 2003).

It has been suggested that ferritin degradation within lysosomes is essential for Fe release (Persson et al., 2001; Radisky and Kaplan, 1998; Roberts and Bomford, 1988). Collectively, we hypothesised that DOX prevented Fe release from ferritin by inhibiting the expression of ferritin partner protein(s) which facilitate ferritin trafficking to lysosomes or ferritin-Fe release. Therefore, examination of novel ferritin partner protein(s) became important.

We first identified that treatment with DOX or CHX altered the cellular protein profile using anion exchange chromatography *via* the FPLC technique (Figure 4.1A). After anion-exchange chromatography and native-gradient PAGE, a number of proteins were commonly identified by LC-MS in control, DOX and CHX treated samples, including elongation factor 1, vesicle amine transporter protein 1 and heat shock protein 60. However, assessment of the literature demonstrated no correlation between these proteins and cellular Fe metabolism.

To verify the presence of the potential ferritin partner proteins, an improved purification protocol was employed by using ultra-centrifugation, anion-exchange FPLC, size exclusion FPLC and native-gradient PAGE (see Section 4.3.2). Using normal mouse liver, four potential ferritin partner proteins were consistently identified over 3 separate experiments, including ALDH1L1, UDP-glucose pyrophosphorylase 2, glutamine synthetase and aspartyl aminopeptidase. The latter three proteins have not yet been shown to correlate with cellular Fe metabolism.

ALDH1L1 catalyses the NADP-dependent oxidation of 10THF to THF (Oppenheim et al., 2001). It has been reported that increased ferritin H-subunits induced the expression of the folate-dependent enzyme, cSHMT, which is involved in 10FTHF/THF circulation (Oppenheim et al., 2001). The precise molecular mechanism of Fe altered folate metabolism needs to be further clarified. However, considering the significance of ALDH1L1 in folate metabolism, it is possible to speculate upon some association between this molecule and ferritin where formation of a high molecular weight complex could be beneficial in the efficient coupling of metabolic intermediates.

It should be noted that the three potential ferritin partner proteins described above from mouse liver were not observed in initial studies using human SK-Mel-28 melanoma cells where we identified elongation factor 1, vesicle amine transporter protein 1 and heat shock protein 60 as potential ferritin partners. This could be explained by the fact that different cell types were used and the separation procedure was also different.

In conclusion, ferritin was purified along with several high molecular weight proteins. Among the possible ferritin partner proteins identified, ALDH1L1 was considered as the most likely candidate for further study considering its involvement in the 10FTHF/THF cycle, which could be regulated by the ferritin H-subunit. Further studies need to be performed to clarify the correlation of this protein with cellular Fe metabolism.

6.3 PROTEOMIC ANALYSIS OF HEARTS FROM FRATAXIN KNOCKOUT MICE: MARKED REARRANGEMENT OF ENERGY METABOLISM, A RESPONSE TO CELLULAR STRESS AND ALTERED EXPRESSION OF PROTEINS INVOLVED IN CELL STRUCTURE, MOTILITY AND METABOLISM

6.3.1 *Summary of Principal Findings – Chapter 5*

Friedriech's ataxia (FA) is an autosomal recessive disease, featuring markedly decreased frataxin protein expression in patients (Campuzano et al., 1997; Koutnikova et al., 1997). It has been shown that decreased frataxin expression led to increased mitochondrial iron, decreased respiratory chain activity and oxidative damage (Pandolfo, 2006). Despite many studies examining the role of frataxin in the pathogenesis of FA, little is known about the function of this protein (Lodi et al., 2006). Moreover, the molecular alterations that occur during the cardiomyopathy observed in this disease are very poorly understood.

In this study, we discovered marked alterations in protein expression caused by the deletion of frataxin in the hearts of 9-week-old MCK KO mice compared to their WT counterparts, using two dimensional electrophoresis and proteomic analysis (Table 5.1). A total of 51 proteins were identified as showing significant changes in the KO mice, and can be divided into 4 groups: **(1)** enzymes of energy metabolism; **(2)** proteins involved in stress, protection and anti-oxidation; **(3)** cell structure & motility related proteins and **(4)** miscellaneous proteins with a variety of functions.

These results suggested that in the heart of KO mice, failure to synthesise iron-sulfur clusters (ISCs) causes decreased expression of ISC-dependent complex I and II (Figure

5.6), resulting in decreased ATP production that leads to metabolic compensation from the activation of several energy metabolism pathways (Figure 5.6). The current work is the first investigation to define the detailed molecular alterations in energy metabolism and metabolic compensation that occurs within the heart *in vivo* in frataxin KO mice.

A number of molecular chaperones, *e.g.* Hsp27, and protective molecules *e.g.* glutathione-S-transferase-Ω 1 were up-regulated to protect against oxidative stress (Hayes et al., 2005; Kolsch et al., 2004), suggesting that the depletion of frataxin induces a marked stress response (Figure 5.6). Therefore, the effectiveness of anti-oxidants such as idebenone, coenzyme Q and vitamin E (Di Prospero et al., 2007a; Di Prospero et al., 2007b; Hart et al., 2005) and the potential use of iron chelators in the treatment of FA (Richardson, 2003), can now be rationalised at the molecular level.

In conclusion, frataxin deficiency in the hearts of MCK KO mice caused a marked rearrangement of energy metabolism, increased expression of proteins involved in protection against stress, differential expression of structural/motility proteins and alterations in the expression of proteins that play miscellaneous roles in metabolism (Figure 5.6). Our study indicates that changes in the expression of proteins involved in these processes are involved in the development of the cardiomyopathy observed in this model. Hence, the current results deepen our understanding of the molecular mechanisms of the cardiomyopathy associated with FA. Moreover, proteins whose expression is affected in this disease may provide tools for monitoring FA prognosis and also the investigation of potential treatment strategies.

6.4 FUTURE DIRECTIONS

6.4.1 The Molecular Mechanisms of Anthraclines on Altered Fe Metabolism

We are the first to demonstrate that anthracyclines act as atypical chelators up-regulating the mRNA expression of the Fe-regulated genes, *TfR1* and *Ndrg1* by their chelation of intracellular Fe. However, this complexation of Fe did not lead to increased TfR1 or Ndrg1 protein levels, nor did DOX induce cellular Fe mobilisation. Although anthracyclines mediated a dose-dependent reduction of TfR1 and Ndrg1 protein expression, it paradoxically increased ferritin protein expression and led to ferritin Fe accumulation. Hence, the effect of anthracyclines on Fe metabolism was multi-faceted, probably due to their complicated chemical properties which leads to multiple mechanisms of action. The cardiotoxic effects induced by anthracyclines are still unclear. Therefore, it is necessary to extend our research by using novel Fe chelators, which could be a solution for the treatment of anthracycline-mediated cardiotoxicity. Furthermore, animal models will be used, which will help us to understand the mechanisms of anthracycline-mediated toxicity.

6.4.1.1 Novel Fe Chelators

Previous studies showed that Fe potentiates anthracycline toxicity and the Fe chelator DFO, which is used to treat Fe overload disease, has been shown to reduce the cardiotoxic effect of DOX in Fe-loaded myocardial cells (Hershko et al., 1993) and *in vivo* animal models (Saad et al., 2001). Therefore, to test the ability of chelators to inhibit anthracycline mediated alterations of Fe-regulated genes maybe a potential key to treat anthracycline-mediated cardiotoxicity.

Previous results in our laboratory showed that DFO is effective at inhibiting DOX-

mediated ferritin-Fe accumulation in cardiomyocytes (Kwok and Richardson, 2003). Thus, it would be interesting to test the effect of DFO at preventing DOX-induced changes in Fe regulated genes, such as TfR1, Ndrg1 and ferritin. However, the low membrane permeability of DFO and its short plasma half-life (Chaston and Richardson, 2003) limit its ability to inhibit anthracycline-mediated cardiotoxicity. Another Fe chelator known as dexrazoxane (ICRF-187) is used clinically to reduce the anthracycline-induced toxcicity. However, this agent does not confer abosolute cardioprotection (Kwok and Richardson, 2000; Swain et al., 1997b). Hence, there is a need for the development of novel cardioprotective agents, such as membrane-permeable chelators. As a result, a novel group of orally effective and highly membrane permeable Fe chelators were developed, called the 2-pyridylcarboxaldehyde isonicotinoyl hydrazone (PCIH) analogues (Becker and Richardson, 1999; Wong et al., 2004). These properties overcome the disadvantages of the clinically used chelator, DFO, that requires long sc infusion (12-24 h/day, 5-6 days/week), is orally inactive and suffers from poor patient compliance (Chaston and Richardson, 2003). It has been demonstrated that PCIH inhibits DOX-mediated ferritin-Fe accumulation and does not interfere with the anti-tumour activity of DOX (Kwok and Richardson, 2003; Wong et al., 2004). Our laboratory demonstrated that the PCIH analogue, PCTH (2-pyridylcarboxaldehyde 2-thiophenecarboxyl hydrazone), is effective at inducing Fe mobilisation *in vivo* and is well tolerated (Wong et al., 2004).

Furthermore, a novel Fe chelator with high membrane-permability, known as di-2-pyridylketone-4,4-dimethyl-3-thiosemicarbazone (Dp44mT), has been synthesised and discovered to be a highly effective anti-cancer agent (Whitnall et al., 2006). A group of novel chelators, 2-benzoylpyridine thiosemicarbazone series, has also been synthesised

and characterised by our group and has prominent anti-tumour effects (Kalinowski et al., 2007).

A well known chelator, namely pyridoxal isonicotinoyl hydrazone (PIH) has shown to prevent anthracycline-mediated cardiotoxicity in rabbits (Simunek et al., 2005). However, this agent is not protected by an international patent and would not be of interest for pharmaceutical development. In contrast, our PCIH chelators are protected by world wide patents. Furthermore, since our PCIH chelators are highly membrane-permeable (Becker and Richardson, 1999; Wong et al., 2004) and inhibit anthracycline-mediated ferritin-Fe accumulation (Kwok and Richardson, 2003), their effect at preventing anthracycline-mediated cardiotoxicity needs to be assessed.

6.4.2 Assessment of the Ability of Fe Chelators to Prevent Anthracycline-Mediated Cardiotoxicity *In Vivo*

6.4.2.1 Investigate the Effect of Anthracyclines at Inducing Ferritin-Fe Accumulation *In Vivo* & the Ability of Chelators to Prevent Cardiotoxicity

Anthracyclines induce ferritin-Fe accumulation in cardiomyocytes, which could be a potential reason for their cardiotoxicity (Kwok and Richardson, 2003). Therefore, it is important to examine the effect of these agents *in vivo*. More importantly, we need to assess whether our novel chelators can prevent cardiotoxicity *in vivo*.

The only widely used chelator for anthracycline-mediated toxicitiy is ICRF-187 (Kwok and Richardson, 2000). However, this agent does not confer absolute cardioprotection (Swain et al., 1997b) and causes myelosuppression (Curran et al., 1991). Thus, novel cardioprotective agents are required. It has been shown that DFO inhibits DOX-

mediated cardiotoxicity (Hershko et al., 1993) but is required to be at very high levels (Saad et al., 2001) due to its low membrane permeability (Chaston and Richardson, 2003; Richardson et al., 1994). Future experiments will use highly permeable and orally effective chelators such as PCIH ligands (Wong et al., 2004). These chelators will be used as cardioprotective agents and given prior to DOX. The aim is to prevent cardiotoxicity by limited Fe chelation rather than whole body Fe depletion.

6.4.2.2 *In Vivo* Studies – Single Bolus Administration to Mimic Acute DOX Cardioxtocicity

In "acute" bolus studies, a vehicle control (saline) or saline plus DOX (25 mg/kg; Chaston and Richardson, 2003) will be examined. This DOX dose results in cardiotoxicity as shown by histopathology using H&E staining and increased serum levels of creatine kinase isoenzyme (CK-MB), troponin I, lactate dehydrogenase (LDH), creatinine, urea and transaminases (ALT & AST; Wong et al., 2004). Mice will be given 1 bolus i.v. injection of DOX (25 mg/kg) or the vehicle (saline) during a 48 h period (Chaston and Richardson, 2003). Twenty four hours prior to euthanasia, mice will be injected with saline or 6 uCi of ^{59}Fe-Tf *via* the tail vein which results in physiolological labelling of ^{59}Fe in organs (Wong et al., 2004).

In studies on the effects of chelators in inhibiting ferritin-^{59}Fe loading, mice will be injected i.v. with chelator or vehicle 30 min prior to injection of DOX, as performed by Saad (Saad et al., 2001) using DFO. We will compare DFO and ICRF-187 to our chelator, PCTH, that shows high Fe chelation efficacy *in vitro* & *in vivo* (Bernhardt et al., 2001; Wong et al., 2004). The dose of chelators will be equal to 5-10-times that of DOX (*i.e.* 25, 125 & 250 mg/kg), as DFO doses in excess of that found for DOX are

protective against cardiotoxicity (Saad et al., 2001). The efficacy of PCTH administed i.v. or orally at inhibiting DOX-medicated cardiotoxicity will be examined.

At the end of the experiment, mice will be sacrificed and blood collected by cardiac puncture. The kidney, liver, heart and skeletal muscle will be collected for histopathology and determination of total ^{59}Fe activity. To confirm acute DOX toxicity, tissues will be harvested, fixed and stained with H&E. DOX-induced heart toxicity will be qualitatively assessed by examining histopathological changes *e.g.*, myocardial fiber swelling, interstitial oedema and necrosis of myofibers (Saad et al., 2001). Markers of cardiac damage will be assessed including creatine kinase isoenzyme (CK-MB) relative to total CK and tropinin I. Moreover, the level of LDH, creatinine, urea, AST and ALT will be assessed.

6.4.2.3 *In Vivo* Studies – Repeated Administration to Simulate Chronic DOX Toxicity

In this study, the vehicle control (saline) or DOX (2 mg/kg) will be given to mice by tail vein once every 3 days for 10 weeks (Nakamura et al., 2000). As in 7.5.2.2, 24 h prior to euthanasia, mice will be injected with saline or 6 uCi of ^{59}Fe-Tf *via* the tail vein. PCTH (2, 10 and 20 mg/kg) will be administered i.v. or orally 30 min before each dose of DOX. Before therapy starts and every 3 weeks thereafter, heart functions will be assessed using echocardiography to measure heart wall thickness and percentage fractional shortening of the left ventricle as an indicator of systolic function (Nakamura et al., 2000). At the end of the study, mice will be euthanased, then blood and organs will be collected for biochemistry, histopathology and native PAGE ^{59}Fe-autoradiography. Animal weight will be recorded as a function of time twice weekly

and prior to euthanasia. The heart will be weighed to calculate organ:body weight ratios to help identify the hypertrophy that occurs after chronic DOX treatment (Nakamura et al., 2000).

6.4.3 Further Investigations on Ferritin Partner Proteins and the Effect of DOX on Ferritin-Fe Accumulation

6.4.3.1 Confirm the Involvement of ALDH1L1 in Ferritin Metabolism

Anthracyclines induced marked ^{59}Fe accumulation within ferritin and prevented Fe release from this molecule (Kwok and Richardson, 2003), which could play an important role in anthracycline-mediated cardiotoxicity. We hypothesised that DOX prevented Fe release from ferritin by inhibiting the expression of ferritin partner protein(s) which facilitate ferritin trafficking to lysosomes or ferritin-Fe release. Therefore, examination of novel ferritin partner protein(s) is important.

Our study demonstrated that ALDH1L1 co-migrated with ferritin utilising a combination of native separation techniques, including ultra-centrifugation, size exclusion FPLC, native gradient PAGE and LC-MS. Although ALDH1L1 shows indirect correlations with the ferritin H-subunit (Oppenheim et al., 2001), it is necessary to confirm the association of ALDH1L1 with ferritin.

In this study, nine-week-old mice will be sacrificed to isolate the liver. The livers will be homogenised and cellular proteins extracted as described in Section 4.2.1.1. Protein A/G (Pierce, Rockford, IL) gel will be used for immunoprecipitation. In an eppendorf tube, 1mL of protein extracts will be added to an optimised amount of anti-ferritin antibody (In-Vitro Technologies, Australia). The reaction will then be incubated

overnight at 4ºC. Protein A/G slurry (100uL) will be added to the antigen-antibody complex and incubated for 2 hours at room temperature with gentle mixing. Immunoprecipitation (IP) buffer (0.5 mL; 25 mM Tris, 150 mM NaCl, pH7.2) will be added and the tube will be centrifuged for 1-3 minutes at 2,500 x*g*. The supernatant will be discarded and this step will be repeated several times. To elute the immune complex, electrophoresis loading buffer will be added to the complex-bound gel and incubated for 5 min at 95ºC. The gel mixture will be centrifuged at 2500 x*g*, the supernatant will be collected and evaluated by SDS-PAGE. Anti-ALDH1L1 antibody (Abcam, Cambridge, MA) and anti-ferritin antibody (In-Vitro Technologies, VIC, Australia) will be used to detect the co-existence of these two proteins. If both of these proteins are detected, ALDH1L1 will be confirmed to be a ferritin associated protein.

To further elucidate the role of ALDH1L1 in Fe metabolism, SK-Mel-28 cells will be used and RNA interference studies will be performed. In brief, Adenovirus will be purchased from Sigma-Aldrich that expresses small interfering RNA strands (siRNA), which contain complementary nucleotide sequences to the ALDH1L1 mRNA. SK-Mel-28 cells will be transfected with this adenovirus and the translation of ALDH1L1 will be markedly decreased (ALDH1L1 knockout cell line). The ferritin protein level in this knockout cell line will be examined using Western Blot and compared to the control. Theoretically, the down-regulation of ALDH1L1 will impair ferritin-Fe metabolism and then alter the expression of ferritin levels. Moreover, ^{59}Fe uptake and efflux experiments will be performed using both the control and knockout cell lines (Section 2.6). If the ^{59}Fe-uptake and efflux levels are changed in the knockout cell line, ALDH1L1 will be assured to be a ferritin associated protein.

6.4.3.2 Examine the Effect of DOX on ALDH1L1

If ALDH1L1 is confirmed to be a ferritin associated protein, it is necessary to examine the effect of DOX on this protein. Previous studies showed that DOX mediated ^{59}Fe accumulation within ferritin and prevented Fe release from this molecule (Kwok and Richardson, 2003). The detailed molecular mechanism of DOX on ferritin-Fe accumulation is unclear. However, the role of DOX as a protein synthesis inhibitor could be a key answer to this effect. For instance, DOX could inhibit the expression of one/several ferritin associated proteins, which may be involved in ferritin-Fe release.

To examine the effect of DOX on ALDH1L1 levels *in vivo*, mice will be treated with 1 bolus i.v. injection of DOX (25 mg/kg) or the vehicle (saline) for 48 h. In parallel experiments, SK-Mel-28 cells will be treated with DOX (5 μM) for 24 h. Protein from mouse liver tissue and human SK-Mel-28 cells will be extracted and the expression of ALDH1L1 protein will be examined by Western blot.

6.4.3.3 Investigate the Effect of DOX on Lysosomes

Intriguingly, anthracyclines accumulate in lysosomes (Hurwitz et al., 1997) and this organelle has been implicated in Fe release from ferritin (Radisky and Kaplan, 1998). Previous studies have shown that inhibitors of lysosomal protease and lysosomotropic agents induce ferritin Fe-loading in a similar way as that found with DOX (Kwok and Richardson, 2004). If lysosomes are involved in ferritin degradation and Fe release, it would be expected that lysosomes and ferritin would co-localise.

Therefore, it is important to examine the (1) effect of DOX on lysosomes; (2) the accumulation and (3) trafficking of ferritin after incubation with DOX. For this study,

electron microscopy (EM) coupled to immunogold labelling will be utilised. This work will be carried out by Ms Jennifer Norman (Microscopy Unit, UNSW). In brief, cardiomyocytes will be incubated in the presence or absence of 5 μM DOX for 24 h. Samples will be fixed and processed as described previously (Miyazaki et al., 2002). Ultra-thin sections will be incubated with anti-ferritin antibody and incubated with goat anti-sheep IgG coupled with colloidal gold particles (10 nm diameter; Proscitech). The sections will be washed, dried, counterstained with lead and examined using EM. Controls will be used including (1) sections incubated without the primary ferritin antibody and (2) the use of antibodies against the lysosome-associated membrane proteins 1 and 2 (LAMPS 1 and 2; Santa Cruz) that make up 50% of lysosomal membrane proteins (Pillay et al., 2002) and will be critical for positively identifying lysosomes. These EM studies will examine if DOX induces alterations in ferritin trafficking and its accumulation within the lysosome.

6.4.4 Examine the Effect of Novel Fe Chelators on Cellular Protein Profiles using Two Dimensional Electrophoresis

The current study has identified seven proteins which are differentially regulated by DFO (Chapter 6). These proteins are involved in DNA damage repair, oxidative stress and cell migration, etc. However, the effectiveness of desferrioxamine is greatly hindered by a range of disadvantages, including a short plasma half-life, poor membrane permeability, and the requirement for long s.c. infusion (Lovejoy and Richardson, 2003). Therefore, our laboratory has designed two novel chelators, PCIH and PCTH (Section 7.5.1.1), which are orally effective and highly membrane permeable (Becker and Richardson, 1999; Wong et al., 2004). These chelators are highly effective anti-cancer agents as they overcome the disadvantages of DFO. Hence,

it is necessary to investigate the molecular targets of these chelators.

In this study, human SK-Mel-28 melanoma cells will be treated with control media, PCIH (50 μM) or PCTH (50 μM) for 24 h. Cellular proteins will be extracted and two dimensional electrophoresis performed as described in Section 2.9. The altered protein expression profiles from these two agents will be compared to DFO. If any common protein is found to be altered by all three chelators, this protein could play an important role in the chelator-mediated anti-cancer effect.

Conclusion Remarks

In summary, this project has contributed significant new data relating to the molecular mechanisms of Fe metabolism in both normal and neoplastic cells. This information is crucial for further understanding of the anti-tumour activities of anthracyclines and Fe chelators. This is a vital step in the development of novel treatment regimens with improved anti-cancer efficacy. Furthermore, this project demonstrated the marked alterations of protein expression in the MCK KO mouse model, which provides critical information for designing novel treatments for FA patients.

CHAPTER 7:

REFERENCES

Aouad F, Florence A, Zhang Y, Collins F, Henry C, Ward RJ, and Crichton RR (2002) Evaluation of new iron chelators and their therapeutic potential. *Inorg Chim Acta* **339**:470-480.

Aisen P and Listowsky I (1980) Iron transport and storage proteins. *Annu Rev Biochem* **49**:357-93.

Aksamit RR and Ebner KE (1972) Purification, properties and kinetic analysis of UDP-glucose pyrophosphorylase from bovine mammary tissue. *Biochim Biophys Acta* **268**:102-12.

Alpert E (1975) Characterization and subunit analysis of ferritin isolated from normal and malignant human liver. *Cancer Res* **35**:1505-9.

Andres-Mateos E, Perier C, Zhang L, Blanchard-Fillion B, Greco TM, Thomas B, Ko HS, Sasaki M, Ischiropoulos H, Przedborski S, Dawson TM and Dawson VL (2007) DJ-1 gene deletion reveals that DJ-1 is an atypical peroxiredoxin-like peroxidase. *Proc Natl Acad Sci U S A* **104**:14807-12.

Anguera MC, Field MS, Perry C, Ghandour H, Chiang EP, Selhub J, Shane B and Stover PJ (2006) Regulation of folate-mediated one-carbon metabolism by 10-formyltetrahydrofolate dehydrogenase. *J Biol Chem* **281**:18335-42.

Arosio P, Adelman TG and Drysdale JW (1978) On ferritin heterogeneity. Further evidence for heteropolymers. *J Biol Chem* **253**:4451-8.

Arrigo AP (2007) The cellular "networking" of mammalian Hsp27 and its functions in the control of protein folding, redox state and apoptosis. *Adv Exp Med Biol* **594**:14-26.

Arrigo AP, Simon S, Gibert B, Kretz-Remy C, Nivon M, Czekalla A, Guillet D, Moulin M, Diaz-Latoud C and Vicart P (2007) Hsp27 (HspB1) and alphaB-crystallin (HspB5) as therapeutic targets. *FEBS Lett* **581**:3665-74.

Babcock M, de Silva D, Oaks R, Davis-Kaplan S, Jiralerspong S, Montermini L, Pandolfo M and Kaplan J (1997) Regulation of mitochondrial iron accumulation by Yfh1p, a putative homolog of frataxin. *Science* **276**:1709-12.

Babusiak M, Man P, Sutak R, Petrak J and Vyoral D (2005) Identification of heme binding protein complexes in murine erythroleukemic cells: study by a novel two dimensional native separation -- liquid chromatography and electrophoresis. *Proteomics* **5**:340-50.

Becker E and Richardson DR (1999) Development of novel aroylhydrazone ligands for iron chelation therapy: 2-pyridylcarboxaldehyde isonicotinoyl hydrazone analogs.

J Lab Clin Med **134**:510-21.

Becker EM, Greer JM, Ponka P and Richardson DR (2002) Erythroid differentiation and protoporphyrin IX down-regulate frataxin expression in Friend cells: characterization of frataxin expression compared to molecules involved in iron metabolism and hemoglobinization. *Blood* **99**:3813-22.

Beerepoot LV, Shima DT, Kuroki M, Yeo KT and Voest EE (1996) Up-regulation of vascular endothelial growth factor production by iron chelators. *Cancer Res* **56**:3747-51.

Beraldo H, Garnier-Suillerot A, Tosi L and Lavelle F (1985) Iron(III)-adriamycin and Iron(III)-daunorubicin complexes: physicochemical characteristics, interaction with DNA, and antitumor activity. *Biochemistry* **24**:284-9.

Bernhardt PV, Chin P and Richardson DR (2001) Unprecedented oxidation of a biologically active aroylhydrazone chelator catalysed by iron(III): serendipitous identification of diacylhydrazine ligands with high iron chelation efficacy. *J Biol Inorg Chem* **6**:801-9.

Bianchi L, Tacchini L and Cairo G (1999) HIF-1-mediated activation of transferrin receptor gene transcription by iron chelation. *Nucleic Acids Res* **27**:4223-7.

Blanco F, Alana A, Llama MJ and Serra JL (1989) Purification and properties of glutamine synthetase from the non-N2-fixing cyanobacterium Phormidium laminosum. *J Bacteriol* **171**:1158-65.

Borges JC, Fischer H, Craievich AF, Hansen LD and Ramos CH (2003) Free human mitochondrial GrpE is a symmetric dimer in solution. *J Biol Chem* **278**:35337-44.

Brazzolotto X, Andriollo M, Guiraud P, Favier A and Moulis JM (2003) Interactions between doxorubicin and the human iron regulatory system. *Biochim Biophys Acta* **1593**:209-18.

Brittenham GM (1990) Pyridoxal isonicotinoyl hydrazone: an effective iron-chelator after oral administration. *Semin Hematol* **27**:112-6.

Bruick RK (2000) Expression of the gene encoding the proapoptotic Nip3 protein is induced by hypoxia. *Proc Natl Acad Sci U S A* **97**:9082-7.

Bulteau AL, Dancis A, Gareil M, Montagne JJ, Camadro JM and Lesuisse E (2007) Oxidative stress and protease dysfunction in the yeast model of Friedreich ataxia. *Free Radic Biol Med* **42**:1561-70.

Cairo G, Recalcati S, Pietrangelo A and Minotti G (2002) The iron regulatory proteins: targets and modulators of free radical reactions and oxidative damage. *Free*

Radic Biol Med **32**:1237-43.

Calabrese V, Lodi R, Tonon C, D'Agata V, Sapienza M, Scapagnini G, Mangiameli A, Pennisi G, Stella AM and Butterfield DA (2005) Oxidative stress, mitochondrial dysfunction and cellular stress response in Friedreich's ataxia. *J Neurol Sci* **233**:145-62.

Camaschella C, Roetto A, Cali A, De Gobbi M, Garozzo G, Carella M, Majorano N, Totaro A and Gasparini P (2000) The gene TFR2 is mutated in a new type of haemochromatosis mapping to 7q22. *Nat Genet* **25**:14-5.

Campuzano V, Montermini L, Lutz Y, Cova L, Hindelang C, Jiralerspong S, Trottier Y, Kish SJ, Faucheux B, Trouillas P, Authier FJ, Durr A, Mandel JL, Vescovi A, Pandolfo M and Koenig M (1997) Frataxin is reduced in Friedreich ataxia patients and is associated with mitochondrial membranes. *Hum Mol Genet* **6**:1771-80.

Campuzano V, Montermini L, Molto MD, Pianese L, Cossee M, Cavalcanti F, Monros E, Rodius F, Duclos F, Monticelli A, Zara F, Canizares J, Koutnikova H, Bidichandani SI, Gellera C, Brice A, Trouillas P, De Michele G, Filla A, De Frutos R, Palau F, Patel PI, Di Donato S, Mandel JL, Cocozza S, Koenig M and Pandolfo M (1996) Friedreich's ataxia: autosomal recessive disease caused by an intronic GAA triplet repeat expansion. *Science* **271**:1423-7.

Cavadini P, O'Neill HA, Benada O and Isaya G (2002) Assembly and iron-binding properties of human frataxin, the protein deficient in Friedreich ataxia. *Hum Mol Genet* **11**:217-27.

Chaston TB, Lovejoy DB, Watts RN and Richardson DR (2003) Examination of the antiproliferative activity of iron chelators: multiple cellular targets and the different mechanism of action of triapine compared with desferrioxamine and the potent pyridoxal isonicotinoyl hydrazone analogue 311. *Clin Cancer Res* **9**:402-14.

Chaston TB and Richardson DR (2003) Iron chelators for the treatment of iron overload disease: relationship between structure, redox activity, and toxicity. *Am J Hematol* **73**:200-10.

Chen S, Garami M and Gardner DG (1999) Doxorubicin selectively inhibits brain versus atrial natriuretic peptide gene expression in cultured neonatal rat myocytes. *Hypertension* **34**:1223-31.

Cheng Y, Zak O, Aisen P, Harrison SC and Walz T (2004) Structure of the human

transferrin receptor-transferrin complex. *Cell* **116**:565-76.

Corna G, Santambrogio P, Minotti G and Cairo G (2004) Doxorubicin paradoxically protects cardiomyocytes against iron-mediated toxicity: role of reactive oxygen species and ferritin. *J Biol Chem* **279**:13738-45.

Crichton RR and Ward RJ (1992) Iron metabolism--new perspectives in view. *Biochemistry* **31**:11255-64.

Curran CF, Narang PK and Reynolds RD (1991) Toxicity profile of dexrazoxane (Zinecard, ICRF-187, ADR-529, NSC-169780), a modulator of doxorubicin cardiotoxicity. *Cancer Treat Rev* **18**:241-52.

De Domenico I, Vaughn MB, Li L, Bagley D, Musci G, Ward DM and Kaplan J (2006) Ferroportin-mediated mobilization of ferritin iron precedes ferritin degradation by the proteasome. *Embo J* **25**:5396-404.

Di Prospero NA, Baker A, Jeffries N and Fischbeck KH (2007a) Neurological effects of high-dose idebenone in patients with Friedreich's ataxia: a randomised, placebo-controlled trial. *Lancet Neurol* **6**:878-86.

Di Prospero NA, Sumner CJ, Penzak SR, Ravina B, Fischbeck KH and Taylor JP (2007b) Safety, tolerability, and pharmacokinetics of high-dose idebenone in patients with Friedreich ataxia. *Arch Neurol* **64**:803-8.

Donovan A, Brownlie A, Zhou Y, Shepard J, Pratt SJ, Moynihan J, Paw BH, Drejer A, Barut B, Zapata A, Law TC, Brugnara C, Lux SE, Pinkus GS, Pinkus JL, Kingsley PD, Palis J, Fleming MD, Andrews NC and Zon LI (2000) Positional cloning of zebrafish ferroportin1 identifies a conserved vertebrate iron exporter. *Nature* **403**:776-81.

Doran P, Martin G, Dowling P, Jockusch H and Ohlendieck K (2006) Proteome analysis of the dystrophin-deficient MDX diaphragm reveals a drastic increase in the heat shock protein cvHSP. *Proteomics* **6**:4610-21.

Doroshow JH (1983) Anthracycline antibiotic-stimulated superoxide, hydrogen peroxide, and hydroxyl radical production by NADH dehydrogenase. *Cancer Res* **43**:4543-51.

Drysdale JW and Munro HN (1966) Regulation of synthesis and turnover of ferritin in rat liver. *J Biol Chem* **241**:3630-7.

Durr A, Cossee M, Agid Y, Campuzano V, Mignard C, Penet C, Mandel JL, Brice A and Koenig M (1996) Clinical and genetic abnormalities in patients with Friedreich's ataxia. *N Engl J Med* **335**:1169-75.

Eaton JW and Qian M (2002) Molecular bases of cellular iron toxicity. *Free Radic Biol Med* **32**:833-40.

Emond M, Lepage G, Vanasse M and Pandolfo M (2000) Increased levels of plasma malondialdehyde in Friedreich ataxia. *Neurology* **55**:1752-3.

Esposito BP, Epsztejn S, Breuer W and Cabantchik ZI (2002) A review of fluorescence methods for assessing labile iron in cells and biological fluids. *Anal Biochem* **304**:1-18.

Feder JN, Gnirke A, Thomas W, Tsuchihashi Z, Ruddy DA, Basava A, Dormishian F, Domingo R, Jr., Ellis MC, Fullan A, Hinton LM, Jones NL, Kimmel BE, Kronmal GS, Lauer P, Lee VK, Loeb DB, Mapa FA, McClelland E, Meyer NC, Mintier GA, Moeller N, Moore T, Morikang E, Wolff RK and et al. (1996) A novel MHC class I-like gene is mutated in patients with hereditary haemochromatosis. *Nat Genet* **13**:399-408.

Foury F and Cazzalini O (1997) Deletion of the yeast homologue of the human gene associated with Friedreich's ataxia elicits iron accumulation in mitochondria. *FEBS Lett* **411**:373-7.

Gakh O, Park S, Liu G, Macomber L, Imlay JA, Ferreira GC and Isaya G (2006) Mitochondrial iron detoxification is a primary function of frataxin that limits oxidative damage and preserves cell longevity. *Hum Mol Genet* **15**:467-79.

Ganz T (2003) Hepcidin, a key regulator of iron metabolism and mediator of anemia of inflammation. *Blood* **102**:783-8.

Garnier-Suillerot A and Gattegno L (1988) Interaction of adriamycin with human erythrocyte membranes. Role of the negatively charged phospholipids. *Biochim Biophys Acta* **936**:50-60.

Gatlin CL, Kleemann GR, Hays LG, Link AJ and Yates JR, 3rd (1998) Protein identification at the low femtomole level from silver-stained gels using a new fritless electrospray interface for liquid chromatography-microspray and nanospray mass spectrometry. *Anal Biochem* **263**:93-101.

Gewirtz DA (1999) A critical evaluation of the mechanisms of action proposed for the antitumor effects of the anthracycline antibiotics adriamycin and daunorubicin. *Biochem Pharmacol* **57**:727-41.

Gianni L and Myers C (1992) The role of free radical formation in the cardiotoxicity of anthracyclines, in *Cancer Treatment and the Heart* (FM M, MD G and JL S eds) pp 9-46, Johns Hopkins University Press, Baltimore.

Gianni L, Zweier JL, Levy A and Myers CE (1985) Characterization of the cycle of iron-mediated electron transfer from Adriamycin to molecular oxygen. *J Biol Chem* **260**:6820-6.

Gomes AV, Guzman G, Zhao J and Potter JD (2002a) Cardiac troponin T isoforms affect the Ca2+ sensitivity and inhibition of force development. Insights into the role of troponin T isoforms in the heart. *J Biol Chem* **277**:35341-9.

Gomes AV, Potter JD and Szczesna-Cordary D (2002b) The role of troponins in muscle contraction. *IUBMB Life* **54**:323-33.

Graham MA, Newell DR, Butler J, Hoey B and Patterson LH (1987) The effect of the anthrapyrazole antitumour agent CI941 on rat liver microsome and cytochrome P-450 reductase mediated free radical processes. Inhibition of doxorubicin activation in vitro. *Biochem Pharmacol* **36**:3345-51.

Gray CW, Ward RV, Karran E, Turconi S, Rowles A, Viglienghi D, Southan C, Barton A, Fantom KG, West A, Savopoulos J, Hassan NJ, Clinkenbeard H, Hanning C, Amegadzie B, Davis JB, Dingwall C, Livi GP and Creasy CL (2000) Characterization of human HtrA2, a novel serine protease involved in the mammalian cellular stress response. *Eur J Biochem* **267**:5699-710.

Gu YZ, Moran SM, Hogenesch JB, Wartman L and Bradfield CA (1998) Molecular characterization and chromosomal localization of a third alpha-class hypoxia inducible factor subunit, HIF3alpha. *Gene Expr* **7**:205-13.

Guo B, Brown FM, Phillips JD, Yu Y and Leibold EA (1995) Characterization and expression of iron regulatory protein 2 (IRP2). Presence of multiple IRP2 transcripts regulated by intracellular iron levels. *J Biol Chem* **270**:16529-35.

Gurgueira SA and Meneghini R (1996) An ATP-dependent iron transport system in isolated rat liver nuclei. *J Biol Chem* **271**:13616-20.

Hagemann TL, Gaeta SA, Smith MA, Johnson DA, Johnson JA and Messing A (2005) Gene expression analysis in mice with elevated glial fibrillary acidic protein and Rosenthal fibers reveals a stress response followed by glial activation and neuronal dysfunction. *Hum Mol Genet* **14**:2443-58.

Hamilton JA and Benson MD (2001) Transthyretin: a review from a structural perspective. *Cell Mol Life Sci* **58**:1491-521.

Hanna J and Finley D (2007) A proteasome for all occasions. *FEBS Lett* **581**:2854-61.

Harrison PM and Arosio P (1996) The ferritins: molecular properties, iron storage function and cellular regulation. *Biochim Biophys Acta* **1275**:161-203.

Hart PE, Lodi R, Rajagopalan B, Bradley JL, Crilley JG, Turner C, Blamire AM, Manners D, Styles P, Schapira AH and Cooper JM (2005) Antioxidant treatment of patients with Friedreich ataxia: four-year follow-up. *Arch Neurol* **62**:621-6.

Hasinoff BB (1998) Chemistry of dexrazoxane and analogues. *Semin Oncol* **25**:3-9.

Hasinoff BB, Patel D and Wu X (2003) The oral iron chelator ICL670A (deferasirox) does not protect myocytes against doxorubicin. *Free Radic Biol Med* **35**:1469-79.

Hayes JD, Flanagan JU and Jowsey IR (2005) Glutathione transferases. *Annu Rev Pharmacol Toxicol* **45**:51-88.

Helton R, Cui J, Scheel JR, Ellison JA, Ames C, Gibson C, Blouw B, Ouyang L, Dragatsis I, Zeitlin S, Johnson RS, Lipton SA and Barlow C (2005) Brain-specific knock-out of hypoxia-inducible factor-1alpha reduces rather than increases hypoxic-ischemic damage. *J Neurosci* **25**:4099-107.

Hensley ML, Schuchter LM, Lindley C, Meropol NJ, Cohen GI, Broder G, Gradishar WJ, Green DM, Langdon RJ, Jr., Mitchell RB, Negrin R, Szatrowski TP, Thigpen JT, Von Hoff D, Wasserman TH, Winer EP and Pfister DG (1999) American Society of Clinical Oncology clinical practice guidelines for the use of chemotherapy and radiotherapy protectants. *J Clin Oncol* **17**:3333-55.

Hentze MW and Kuhn LC (1996) Molecular control of vertebrate iron metabolism: mRNA-based regulatory circuits operated by iron, nitric oxide, and oxidative stress. *Proc Natl Acad Sci U S A* **93**:8175-82.

Hentze MW, Rouault TA, Caughman SW, Dancis A, Harford JB and Klausner RD (1987) A cis-acting element is necessary and sufficient for translational regulation of human ferritin expression in response to iron. *Proc Natl Acad Sci U S A* **84**:6730-4.

Herman EH and Ferrans VJ (1990) Examination of the potential long-lasting protective effect of ICRF-187 against anthracycline-induced chronic cardiomyopathy. *Cancer Treat Rev* **17**:155-60.

Herman EH, Ferrans VJ and Sanchez J (1992) Methods of reducing the cardiotoxicity of anthracycline., in *Cancer Treatment and the Heart, Baltimore* (Muggia FM, Green MD and JL. S eds) pp 114-169., Johns Hopkins University Press, Baltimore.

Herman EH, Ferrans VJ, Young RS and Hamlin RL (1988) Effect of pretreatment with ICRF-187 on the total cumulative dose of doxorubicin tolerated by beagle dogs. *Cancer Res* **48**:6918-25.

Hershko C (1994) Control of disease by selective iron depletion: a novel therapeutic strategy utilizing iron chelators. *Baillieres Clin Haematol* **7**:965-1000.

Hershko C, Avramovici-Grisaru S, Link G, Gelfand L and Sarel S (1981) Mechanism of in vivo iron chelation by pyridoxal isonicotinoyl hydrazone and other imino derivatives of pyridoxal. *J Lab Clin Med* **98**:99-108.

Hershko C, Konijn AM, Nick HP, Breuer W, Cabantchik ZI and Link G (2001) ICL670A: a new synthetic oral chelator: evaluation in hypertransfused rats with selective radioiron probes of hepatocellular and reticuloendothelial iron stores and in iron-loaded rat heart cells in culture. *Blood* **97**:1115-22.

Hershko C, Link G, Tzahor M, Kaltwasser JP, Athias P, Grynberg A and Pinson A (1993) Anthracycline toxicity is potentiated by iron and inhibited by desferoxamine: studies in rat heart cells in culture. *J. Lab. Clin. Med.* **122**:245-251.

Holden HM, Rayment I and Thoden JB (2003) Structure and function of enzymes of the Leloir pathway for galactose metabolism. *J Biol Chem* **278**:43885-8.

Hoy T, Humphrys J, Jacobs A, Williams A and Ponka P (1979) Effective iron chelation following oral administration of an isoniazid-pyridoxal hydrazone. *Br J Haematol* **43**:443-9.

Hu CJ, Wang LY, Chodosh LA, Keith B and Simon MC (2003) Differential roles of hypoxia-inducible factor 1alpha (HIF-1alpha) and HIF-2alpha in hypoxic gene regulation. *Mol Cell Biol* **23**:9361-74.

Hunt MC and Alexson SE (2002) The role Acyl-CoA thioesterases play in mediating intracellular lipid metabolism. *Prog Lipid Res* **41**:99-130.

Hurwitz SJ, Terashima M, Mizunuma N and Slapak CA (1997) Vesicular anthracycline accumulation in doxorubicin-selected U-937 cells: participation of lysosomes. *Blood* **89**:3745-54.

Imondi AR, Della Torre P, Mazue G, Sullivan TM, Robbins TL, Hagerman LM, Podesta A and Pinciroli G (1996) Dose-response relationship of dexrazoxane for prevention of doxorubicin-induced cardiotoxicity in mice, rats, and dogs. *Cancer Res* **56**:4200-4.

Ito H, Miller SC, Billingham ME, Akimoto H, Torti SV, Wade R, Gahlmann R, Lyons G, Kedes L and Torti FM (1990) Doxorubicin selectively inhibits muscle gene expression in cardiac muscle cells in vivo and in vitro. *Proc Natl Acad Sci U S A* **87**:4275-9.

Jaattela M (1999) Heat shock proteins as cellular lifeguards. *Ann Med* **31**:261-71.

Jiao Z, Zhang ZG, Hornyak TJ, Hozeska A, Zhang RL, Wang Y, Wang L, Roberts C, Strickland FM and Chopp M (2006) Dopachrome tautomerase (Dct) regulates neural progenitor cell proliferation. *Dev Biol* **296**:396-408.

Jung K and Reszka R (2001) Mitochondria as subcellular targets for clinically useful anthracyclines. *Advanced Drug Delivery Reviews.* **49.**:87-105.

Kaiserova H, Simunek T, Sterba M, den Hartog GJ, Schroterova L, Popelova O, Gersl V, Kvasnickova E and Bast A (2007) New iron chelators in anthracycline-induced cardiotoxicity. *Cardiovasc Toxicol* **7**:145-50.

Kalinowski D and Richardson DR (2005) Evolution of iron chelators for the treatment of iron overload disease and cancer. *Pharmacol. Rev.* **57**:1-37.

Kalinowski DS, Yu Y, Sharpe PC, Islam M, Liao YT, Lovejoy DB, Kumar N, Bernhardt PV and Richardson DR (2007) Design, synthesis, and characterization of novel iron chelators: structure-activity relationships of the 2-benzoylpyridine thiosemicarbazone series and their 3-nitrobenzoyl analogues as potent antitumor agents. *J Med Chem* **50**:3716-29.

Kashem MA, James G, Harper C, Wilce P and Matsumoto I (2007) Differential protein expression in the corpus callosum (splenium) of human alcoholics: a proteomics study. *Neurochem Int* **50**:450-9.

Kawabata H, Germain RS, Ikezoe T, Tong X, Green EM, Gombart AF and Koeffler HP (2001) Regulation of expression of murine transferrin receptor 2. *Blood* **98**:1949-54.

Kawabata H, Yang R, Hirama T, Vuong PT, Kawano S, Gombart AF and Koeffler HP (1999) Molecular cloning of transferrin receptor 2. A new member of the transferrin receptor-like family. *J Biol Chem* **274**:20826-32.

Keizer HG, Pinedo HM, Schuurhuis GJ and Joenje H (1990) Doxorubicin (adriamycin): a critical review of free radical-dependent mechanisms of cytotoxicity. *Pharmacol Ther* **47**:219-31.

Kelly JA, Neidle EL and Neidle A (1983) An aminopeptidase from mouse brain cytosol that cleaves N-terminal acidic amino acid residues. *J Neurochem* **40**:1727-34.

Kidane TZ, Sauble E and Linder MC (2006) Release of iron from ferritin requires lysosomal activity. *Am J Physiol Cell Physiol* **291**:C445-55.

Kim HY, Klausner RD and Rouault TA (1995) Translational repressor activity is equivalent and is quantitatively predicted by in vitro RNA binding for two iron-

responsive element-binding proteins, IRP1 and IRP2. *J Biol Chem* **270**:4983-6.

Kisliuk R (1999) *Folate biochemistry in relation to antifolate selectivity*. Humana Press Inc., Totowa, NJ.

Kolsch H, Linnebank M, Lutjohann D, Jessen F, Wullner U, Harbrecht U, Thelen KM, Kreis M, Hentschel F, Schulz A, von Bergmann K, Maier W and Heun R (2004) Polymorphisms in glutathione S-transferase omega-1 and AD, vascular dementia, and stroke. *Neurology* **63**:2255-60.

Kostoryz EL and Yourtee DM (2001) Oxidative mutagenesis of doxorubicin-Fe(III) complex. *Mutat Res* **490**:131-9.

Kotamraju S, Chitambar CR, Kalivendi SV, Joseph J and Kalyanaraman B (2002) Transferrin receptor-dependent iron uptake is responsible for doxorubicin-mediated apoptosis in endothelial cells: role of oxidant-induced iron signaling in apoptosis. *J Biol Chem* **277**:17179-87.

Koutnikova H, Campuzano V, Foury F, Dolle P, Cazzalini O and Koenig M (1997) Studies of human, mouse and yeast homologues indicate a mitochondrial function for frataxin. *Nat Genet* **16**:345-51.

Kovacevic Z and Richardson DR (2006) The metastasis suppressor, Ndrg-1: A new ally in the fight against cancer. *Carcinogenesis* **27**:2355-2366.

Krupenko SA and Oleinik NV (2002) 10-formyltetrahydrofolate dehydrogenase, one of the major folate enzymes, is down-regulated in tumor tissues and possesses suppressor effects on cancer cells. *Cell Growth Differ* **13**:227-36.

Krupenko SA and Wagner C (1999) Aspartate 142 is involved in both hydrolase and dehydrogenase catalytic centers of 10-formyltetrahydrofolate dehydrogenase. *J Biol Chem* **274**:35777-84.

Kuhar SG, Feng L, Vidan S, Ross ME, Hatten ME and Heintz N (1993) Changing patterns of gene expression define four stages of cerebellar granule neuron differentiation. *Development* **117**:97-104.

Kuhn LC and Hentze MW (1992) Coordination of cellular iron metabolism by post-transcriptional gene regulation. *J Inorg Biochem* **47**:183-95.

Kwok JC and Richardson DR (2000) The cardioprotective effect of the iron chelator dexrazoxane (ICRF-187) on anthracycline-mediated cardiotoxicity. *Redox Rep* **5**:317-24.

Kwok JC and Richardson DR (2002) Unexpected anthracycline-mediated alterations in iron-regulatory protein-RNA-binding activity: the iron and copper complexes of

anthracyclines decrease RNA-binding activity. *Mol Pharmacol* **62**:888-900.

Kwok JC and Richardson DR (2003) Anthracyclines induce accumulation of iron in ferritin in myocardial and neoplastic cells: inhibition of the ferritin iron mobilization pathway. *Mol Pharmacol* **63**:849-61.

Kwok JC and Richardson DR (2004) Examination of the mechanism(s) involved in doxorubicin-mediated iron accumulation in ferritin: studies using metabolic inhibitors, protein synthesis inhibitors, and lysosomotropic agents. *Mol Pharmacol* **65**:181-95.

LaVaute T, Smith S, Cooperman S, Iwai K, Land W, Meyron-Holtz E, Drake SK, Miller G, Abu-Asab M, Tsokos M, Switzer R, 3rd, Grinberg A, Love P, Tresser N and Rouault TA (2001) Targeted deletion of the gene encoding iron regulatory protein-2 causes misregulation of iron metabolism and neurodegenerative disease in mice. *Nat Genet* **27**:209-14.

Le NT and Richardson DR (2004) Iron chelators with high antiproliferative activity up-regulate the expression of a growth inhibitory and metastasis suppressor gene: a link between iron metabolism and proliferation. *Blood* **104**:2967-75.

Lebron JA, West AP, Jr. and Bjorkman PJ (1999) The hemochromatosis protein HFE competes with transferrin for binding to the transferrin receptor. *J Mol Biol* **294**:239-45.

Lesuisse E, Santos R, Matzanke BF, Knight SA, Camadro JM and Dancis A (2003) Iron use for haeme synthesis is under control of the yeast frataxin homologue (Yfh1). *Hum Mol Genet* **12**:879-89.

Levi S, Yewdall SJ, Harrison PM, Santambrogio P, Cozzi A, Rovida E, Albertini A and Arosio P (1992) Evidence of H- and L-chains have co-operative roles in the iron-uptake mechanism of human ferritin. *Biochem J* **288 (Pt 2)**:591-6.

Lewis GP and Fisher SK (2003) Up-regulation of glial fibrillary acidic protein in response to retinal injury: its potential role in glial remodeling and a comparison to vimentin expression. *Int Rev Cytol* **230**:263-90.

Lin CH, Chung MY, Chen WB and Chien CH (2007) Growth inhibitory effect of the human NIT2 gene and its allelic imbalance in cancers. *Febs J* **274**:2946-56.

Link G, Tirosh R, Pinson A and Hershko C (1996) Role of iron in the potentiation of anthracycline cardiotoxicity: identification of heart cell mitochondria as a major site of iron-anthracycline-iron complex. *J. Lab. Clin. Med.* **127.**:272-278.

Lodi R, Cooper JM, Bradley JL, Manners D, Styles P, Taylor DJ and Schapira AH

(1999) Deficit of in vivo mitochondrial ATP production in patients with Friedreich ataxia. *Proc Natl Acad Sci U S A* **96**:11492-5.

Lodi R, Rajagopalan B, Blamire AM, Cooper JM, Davies CH, Bradley JL, Styles P and Schapira AH (2001) Cardiac energetics are abnormal in Friedreich ataxia patients in the absence of cardiac dysfunction and hypertrophy: an in vivo 31P magnetic resonance spectroscopy study. *Cardiovasc Res* **52**:111-9.

Lodi R, Tonon C, Calabrese V and Schapira AH (2006) Friedreich's ataxia: from disease mechanisms to therapeutic interventions. *Antioxid Redox Signal* **8**:438-43.

Lohan J and Ohlendieck K (2004) Drastic reduction in the luminal Ca2+ -binding proteins calsequestrin and sarcalumenin in dystrophin-deficient cardiac muscle. *Biochim Biophys Acta* **1689**:252-8.

Lok CN and Ponka P (1999) Identification of a hypoxia response element in the transferrin receptor gene. *J Biol Chem* **274**:24147-52.

Lovejoy DB and Richardson DR (2003) Iron chelators as anti-neoplastic agents: current developments and promise of the PIH class of chelators. *Curr Med Chem* **10**:1035-49.

Lombardo T, Ferro G, Frontini V and Percolla S (1996) High-dose intravenous desferrioxamine (DFO) delivery in four thalassemic patients allergic to subcutaneous DFO administration. *Am J Hematol* **51**:90-2.

Martins E, Silva-Cardoso J, Alves C, Pereira H, Soares B, Damasceno A, Abreu-Lima C, Amorim A and Rocha-Goncalves F (2006) Familial dilated cardiomyopathy with troponin T K210del mutation. *Rev Port Cardiol* **25**:295-300.

May PM, Williams GK and Williams DR (1980) Solution chemistry studies of adriamycin--iron complexes present in vivo. *Eur J Cancer* **16**:1275-6.

Meyron-Holtz EG, Ghosh MC, Iwai K, LaVaute T, Brazzolotto X, Berger UV, Land W, Ollivierre-Wilson H, Grinberg A, Love P and Rouault TA (2004) Genetic ablations of iron regulatory proteins 1 and 2 reveal why iron regulatory protein 2 dominates iron homeostasis. *Embo J* **23**:386-95.

Minotti G, Cavaliere AF, Mordente A, Rossi M, Schiavello R, Zamparelli R and Possati G (1995) Secondary alcohol metabolites mediate iron delocalization in cytosolic fractions of myocardial biopsies exposed to anticancer anthracyclines. Novel linkage between anthracycline metabolism and iron-induced cardiotoxicity. *J Clin Invest* **95**:1595-605.

Minotti G, Menna P, Salvatorelli E, Cairo G and Gianni L (2004a) Anthracyclines:

molecular advances and pharmacologic developments in antitumor activity and cardiotoxicity. *Pharmacol Rev* **56**:185-229.

Minotti G, Recalcati S, Menna P, Salvatorelli E, Corna G and Cairo G (2004b) Doxorubicin cardiotoxicity and the control of iron metabolism: quinone-dependent and independent mechanisms. *Methods Enzymol* **378**:340-61.

Minotti G, Recalcati S, Mordente A, Liberi G, Calafiore AM, Mancuso C, Preziosi P and Cairo G (1998) The secondary alcohol metabolite of doxorubicin irreversibly inactivates aconitase/iron regulatory protein-1 in cytosolic fractions from human myocardium. *Faseb J* **12**:541-52.

Minotti G, Ronchi R, Salvatorelli E, Menna P and Cairo G (2001) Doxorubicin irreversibly inactivates iron regulatory proteins 1 and 2 in cardiomyocytes: evidence for distinct metabolic pathways and implications for iron-mediated cardiotoxicity of antitumor therapy. *Cancer Res* **61**:8422-8.

Miranda CJ, Makui H, Soares RJ, Bilodeau M, Mui J, Vali H, Bertrand R, Andrews NC and Santos MM (2003) Hfe deficiency increases susceptibility to cardiotoxicity and exacerbates changes in iron metabolism induced by doxorubicin. *Blood* **102**:2574-80.

Miura T, Muraoka S and Ogiso T (1991) Lipid peroxidation of rat erythrocyte membrane induced by adriamycin-Fe3+. *Pharmacol Toxicol* **69**:296-300.

Miyazaki E, Kato J, Kobune M, Okumura K, Sasaki K, Shintani N, Arosio P and Niitsu Y (2002) Denatured H-ferritin subunit is a major constituent of haemosiderin in the liver of patients with iron overload. *Gut* **50**:413-9.

Mizutani H, Tada-Oikawa S, Hiraku Y, Kojima M and Kawanishi S (2005) Mechanism of apoptosis induced by doxorubicin through the generation of hydrogen peroxide. *Life Sci* **76**:1439-53.

Muhlenhoff U, Richhardt N, Ristow M, Kispal G and Lill R (2002) The yeast frataxin homolog Yfh1p plays a specific role in the maturation of cellular Fe/S proteins. *Hum Mol Genet* **11**:2025-36.

Myers C (1998) The role of iron in doxorubicin-induced cardiomyopathy. *Semin Oncol* **25**:10-4.

Nakamura T, Ueda Y, Juan Y, Katsuda S, Takahashi H and Koh E (2000) Fas-mediated apoptosis in adriamycin-induced cardiomyopathy in rats: In vivo study. *Circulation* **102**:572-8.

Napier I, Ponka P and Richardson DR (2005) Iron trafficking in the mitochondrion:

novel pathways revealed by disease. *Blood* **105**:1867-74.

Nemeth E, Tuttle MS, Powelson J, Vaughn MB, Donovan A, Ward DM, Ganz T and Kaplan J (2004) Hepcidin regulates cellular iron efflux by binding to ferroportin and inducing its internalization. *Science* **306**:2090-3.

Nie G, Chen G, Sheftel AD, Pantopoulos K and Ponka P (2006) In vivo tumor growth is inhibited by cytosolic iron deprivation caused by the expression of mitochondrial ferritin. *Blood* **108**:2428-34.

Niggli V and Rossy J (2007) Ezrin/radixin/moesin: Versatile controllers of signaling molecules and of the cortical cytoskeleton. *Int J Biochem Cell Biol*.

Nisbet-Brown E, Olivieri NF, Giardina PJ, Grady RW, Neufeld EJ, Sechaud R, Krebs-Brown AJ, Anderson JR, Alberti D, Sizer KC and Nathan DG (2003) Effectiveness and safety of ICL670 in iron-loaded patients with thalassaemia: a randomised, double-blind, placebo-controlled, dose-escalation trial. *Lancet* **361**:1597-602.

Oleinik NV and Krupenko SA (2003) Ectopic expression of 10-formyltetrahydrofolate dehydrogenase in A549 cells induces G1 cell cycle arrest and apoptosis. *Mol Cancer Res* **1**:577-88.

Oppenheim EW, Adelman C, Liu X and Stover PJ (2001) Heavy chain ferritin enhances serine hydroxymethyltransferase expression and de novo thymidine biosynthesis. *J Biol Chem* **276**:19855-61.

Oppenheim EW, Nasrallah IM, Mastri MG and Stover PJ (2000) Mimosine is a cell-specific antagonist of folate metabolism. *J Biol Chem* **275**:19268-74.

Pandolfo M (2006) Iron and Friedreich ataxia. *J Neural Transm Suppl*:143-6.

Pantopoulos K and Hentze MW (1995) Rapid responses to oxidative stress mediated by iron regulatory protein. *EMBO J* **14**:2917-24.

Park S, Gakh O, O'Neill HA, Mangravita A, Nichol H, Ferreira GC and Isaya G (2003) Yeast frataxin sequentially chaperones and stores iron by coupling protein assembly with iron oxidation. *J Biol Chem* **278**:31340-51.

Persson HL, Nilsson KJ and Brunk UT (2001) Novel cellular defenses against iron and oxidation: ferritin and autophagocytosis preserve lysosomal stability in airway epithelium. *Redox Rep* **6**:57-63.

Petrak JV and Vyoral D (2001) Detection of iron-containing proteins contributing to the cellular labile iron pool by a native electrophoresis metal blotting technique. *J Inorg Biochem* **86**:669-75.

Petrat F, de Groot H and Rauen U (2001) Subcellular distribution of chelatable iron: a laser scanning microscopic study in isolated hepatocytes and liver endothelial cells. *Biochem J* **356**:61-9.

Philpott CC, Haile D, Rouault TA and Klausner RD (1993) Modification of a free Fe-S cluster cysteine residue in the active iron-responsive element-binding protein prevents RNA binding. *J Biol Chem* **268**:17655-8.

Pietrangelo A (2002) Physiology of iron transport and the hemochromatosis gene. *Am J Physiol Gastrointest Liver Physiol* **282**:G403-14.

Pigeon C, Ilyin G, Courselaud B, Leroyer P, Turlin B, Brissot P and Loreal O (2001) A new mouse liver-specific gene, encoding a protein homologous to human antimicrobial peptide hepcidin, is overexpressed during iron overload. *J Biol Chem* **276**:7811-9.

Pillay CS, Elliott E and Dennison C (2002) Endolysosomal proteolysis and its regulation. *Biochem J* **363**:417-29.

Ponka P (1997) Tissue-specific regulation of iron metabolism and heme synthesis: distinct control mechanisms in erythroid cells. *Blood* **89**:1-25.

Ponka P, Borova J, Neuwirt J and Fuchs O (1979a) Mobilization of iron from reticulocytes. Identification of pyridoxal isonicotinoyl hydrazone as a new iron chelating agent. *FEBS Lett* **97**:317-21.

Ponka P, Borova J, Neuwirt J, Fuchs O and Necas E (1979b) A study of intracellular iron metabolism using pyridoxal isonicotinoyl hydrazone and other synthetic chelating agents. *Biochim Biophys Acta* **586**:278-97.

Puccio H, Simon D, Cossee M, Criqui-Filipe P, Tiziano F, Melki J, Hindelang C, Matyas R, Rustin P and Koenig M (2001) Mouse models for Friedreich ataxia exhibit cardiomyopathy, sensory nerve defect and Fe-S enzyme deficiency followed by intramitochondrial iron deposits. *Nat Genet* **27**:181-6.

Radisky DC and Kaplan J (1998) Iron in cytosolic ferritin can be recycled through lysosomal degradation in human fibroblasts. *Biochem J* **336 (Pt 1)**:201-5.

Rajasekaran NS, Connell P, Christians ES, Yan LJ, Taylor RP, Orosz A, Zhang XQ, Stevenson TJ, Peshock RM, Leopold JA, Barry WH, Loscalzo J, Odelberg SJ and Benjamin IJ (2007) Human alpha B-crystallin mutation causes oxido-reductive stress and protein aggregation cardiomyopathy in mice. *Cell* **130**:427-39.

Richardson D, Ponka P and Baker E (1994) The effect of the iron(III) chelator, desferrioxamine, on iron and transferrin uptake by the human malignant

melanoma cell. *Cancer Res* **54**:685-9.

Richardson DR (2003) Friedreich's ataxia: Iron chelation as a therapeutic strategy ? *Exp. Opin. Invest. Drugs.* **12**:235-245.

Richardson DR and Milnes K (1997) The potential of iron chelators of the pyridoxal isonicotinoyl hydrazone class as effective antiproliferative agents II: the mechanism of action of ligands derived from salicylaldehyde benzoyl hydrazone and 2-hydroxy-1-naphthylaldehyde benzoyl hydrazone. *Blood* **89**:3025-38.

Richardson DR and Ponka P (1997) The molecular mechanisms of the metabolism and transport of iron in normal and neoplastic cells. *Biochim Biophys Acta* **1331**:1-40.

Richardson DR and Ponka P (1998) Pyridoxal isonicotinoyl hydrazone and its analogs: potential orally effective iron-chelating agents for the treatment of iron overload disease. *J Lab Clin Med* **131**:306-15.

Richardson DR, Tran EH and Ponka P (1995) The potential of iron chelators of the pyridoxal isonicotinoyl hydrazone class as effective antiproliferative agents. *Blood* **86**:4295-306.

Rickwood D and Patel D (1995) *Fractionation and analytical methods*. chichester, New York.

Roberts S and Bomford A (1988) Ferritin iron kinetics and protein turnover in K562 cells. *J Biol Chem* **263**:19181-7.

Rotig A, de Lonlay P, Chretien D, Foury F, Koenig M, Sidi D, Munnich A and Rustin P (1997) Aconitase and mitochondrial iron-sulphur protein deficiency in Friedreich ataxia. *Nat Genet* **17**:215-7.

Rouault TA, Tang CK KS, Burgess WH, Haile DJ, Samaniego F, McBride OW, JB H and RD. K (1990) Cloning of the cDNA encoding an RNA regulatory protein--the human iron-responsive element-binding protein. *Proc Natl Acad Sci U S A* **87.**:7958-62.

Ryan HE PM, McNulty W, Elson D, Gassmann M, Arbeit JM, Johnson RS. (2000) Hypoxia-inducible factor-1alpha is a positive factor in solid tumor growth. *Cancer Res.* **60**:4010-4015.

Saad SY, Najjar TA and Al-Rikabi AC (2001) The preventive role of deferoxamine against acute doxorubicin-induced cardiac, renal and hepatic toxicity in rats. *Pharmacol Res* **43**:211-8.

Sambrook J, Fritsch EF and Maniatis T (1989) *Molecular Cloning: A Laboratory Manual*. Cold Spring Harbour Laboratory Press, USA.

Schirch D, Villar E, Maras B, Barra D and Schirch V (1994) Domain structure and function of 10-formyltetrahydrofolate dehydrogenase. *J Biol Chem* **269**:24728-35.

Schroterova L, Kaiserova H, Baliharova V, Velik J, Gersl V and Kvasnickova E (2004) The effect of new lipophilic chelators on the activities of cytosolic reductases and P450 cytochromes involved in the metabolism of anthracycline antibiotics: studies in vitro. *Physiol Res* **53**:683-91.

Schulz JB, Dehmer T, Schols L, Mende H, Hardt C, Vorgerd M, Burk K, Matson W, Dichgans J, Beal MF and Bogdanov MB (2000) Oxidative stress in patients with Friedreich ataxia. *Neurology* **55**:1719-21.

Shan Y, Napoli E and Cortopassi G (2007) Mitochondrial frataxin interacts with ISD11 of the NFS1/ISCU complex and multiple mitochondrial chaperones. *Hum Mol Genet* **16**:929-41.

Sibille JC, Ciriolo M, Kondo H, Crichton RR and Aisen P (1989) Subcellular localization of ferritin and iron taken up by rat hepatocytes. *Biochem J* **262**:685-8.

Silva RG, Nunes JE, Canduri F, Borges JC, Gava LM, Moreno FB, Basso LA and Santos DS (2007) Purine nucleoside phosphorylase: a potential target for the development of drugs to treat T-cell- and apicomplexan parasite-mediated diseases. *Curr Drug Targets* **8**:413-22.

Simunek T, Klimtova I, Kaplanova J, Sterba M, Mazurova Y, Adamcova M, Hrdina R, Gersl V and Ponka P (2005) Study of daunorubicin cardiotoxicity prevention with pyridoxal isonicotinoyl hydrazone in rabbits. *Pharmacol Res* **51**:223-31.

Singal PK, Iliskovic N, Li T and Kumar D (1997) Adriamycin cardiomyopathy: pathophysiology and prevention. *Faseb J* **11**:931-6.

Stryer L (1980) Biochemistry, WH Freedman Publishers, San Francisco, CA.

Suryakala S and Deshpande V (1999) Purification and characterization of liver ferritins from different animal species. *Vet Res Commun* **23**:165-81.

Swain SM, Whaley FS, Gerber MC, Ewer MS, Bianchine JR and Gams RA (1997a) Delayed administration of dexrazoxane provides cardioprotection for patients with advanced breast cancer treated with doxorubicin-containing therapy. *J Clin Oncol* **15**:1333-40.

Swain SM, Whaley FS, Gerber MC, Weisberg S, York M, Spicer D, Jones SE, Wadler S, Desai A, Vogel C, Speyer J, Mittelman A, Reddy S, Pendergrass K, Velez-Garcia E, Ewer MS, Bianchine JR and Gams RA (1997b) Cardioprotection with dexrazoxane for doxorubicin-containing therapy in advanced breast cancer. *J*

Clin Oncol **15**:1318-32.

Tamma G, Procino G, Svelto M and Valenti G (2007) Hypotonicity causes actin reorganization and recruitment of the actin-binding ERM protein moesin in membrane protrusions in collecting duct principal cells. *Am J Physiol Cell Physiol* **292**:C1476-84.

Tan G, Napoli E, Taroni F and Cortopassi G (2003) Decreased expression of genes involved in sulfur amino acid metabolism in frataxin-deficient cells. *Hum Mol Genet* **12**:1699-711.

Tarr M and van Helden PD (1990) Inhibition of transcription by adriamycin is a consequence of the loss of negative superhelicity in DNA mediated by topoisomerase II. *Mol Cell Biochem* **93**:141-6.

Tephly TR (1991) The toxicity of methanol. *Life Sci* **48**:1031-41.

Tewey KM, Chen GL, Nelson EM and Liu LF (1984a) Intercalative antitumor drugs interfere with the breakage-reunion reaction of mammalian DNA topoisomerase II. *J Biol Chem* **259**:9182-7.

Tewey KM, Rowe TC, Yang L, Halligan BD and Liu LF (1984b) Adriamycin-induced DNA damage mediated by mammalian DNA topoisomerase II. *Science* **226**:466-8.

Theil EC (2003) Ferritin: at the crossroads of iron and oxygen metabolism. *J Nutr* **133**:1549S-53S.

Theil EC and Eisenstein RS (2000) Combinatorial mRNA regulation: Iron regulatory proteins and iso-iron-responsive elements (Iso-IREs). *The Journal of Biological Chemistry* **275**:40659-40662.

Thoden JB and Holden HM (2007) The molecular architecture of glucose-1-phosphate uridylyltransferase. *Protein Sci* **16**:432-40.

Thomas CE and Aust SD (1986) Reductive release of iron from ferritin by cation free radicals of paraquat and other bipyridyls. *J Biol Chem* **261**:13064-70.

Turnquist RL, Turnquist MM, Bachmann RC and Hansen RG (1974) Uridine diphosphate glucose pyrophosphorylase: differential heat inactivation and further characterization of human liver enzyme. *Biochim Biophys Acta* **364**:59-67.

Vasiliou V, Pappa A and Petersen DR (2000) Role of aldehyde dehydrogenases in endogenous and xenobiotic metabolism. *Chem Biol Interact* **129**:1-19.

Voest EE, van Acker SA, van der Vijgh WJ, van Asbeck BS and Bast A (1994) Comparison of different iron chelators as protective agents against acute

doxorubicin-induced cardiotoxicity. *J Mol Cell Cardiol* **26**:1179-85.

Vogt TM, Blackwell AD, Giannetti AM, Bjorkman PJ and Enns CA (2003) Heterotypic interactions between transferrin receptor and transferrin receptor 2. *Blood* **101**:2008-14.

Vulpe CD, Kuo YM, Murphy TL, Cowley L, Askwith C, Libina N, Gitschier J and Anderson GJ (1999) Hephaestin, a ceruloplasmin homologue implicated in intestinal iron transport, is defective in the sla mouse. *Nat Genet* **21**:195-9.

Vyoral D and Petrak J (1998) Iron transport in K562 cells: a kinetic study using native gel electrophoresis and 59Fe autoradiography. *Biochim Biophys Acta* **1403**:179-88.

Vyoral D, Petrak J and Hradilek A (1998) Separation of cellular iron containing compounds by electrophoresis. *Biol Trace Elem Res* **61**:263-75.

Wade VJ, Levi S, Arosio P, Treffry A, Harrison PM and Mann S (1991) Influence of site-directed modifications on the formation of iron cores in ferritin. *J. Mol. Biol.* **221**:1443-1452.

Watts RN and Richardson DR (2002) The mechanism of nitrogen monoxide (NO)-mediated iron mobilization from cells. NO intercepts iron before incorporation into ferritin and indirectly mobilizes iron from ferritin in a glutathione-dependent manner. *Eur J Biochem* **269**:3383-92.

Wexler LH (1998) Ameliorating anthracycline cardiotoxicity in children with cancer: clinical trials with dexrazoxane. *Semin Oncol* **25**:86-92.

Whitnall M, Howard J, Ponka P and Richardson DR (2006) A class of iron chelators with a wide spectrum of potent antitumor activity that overcomes resistance to chemotherapeutics. *Proc Natl Acad Sci U S A* **103**:14901-6.

Wilk S, Wilk E and Magnusson RP (1998) Purification, characterization, and cloning of a cytosolic aspartyl aminopeptidase. *J Biol Chem* **273**:15961-70.

Wilson RB (2006) Iron dysregulation in Friedreich ataxia. *Semin Pediatr Neurol* **13**:166-75.

Wilson RB and Roof DM (1997) Respiratory deficiency due to loss of mitochondrial DNA in yeast lacking the frataxin homologue. *Nat Genet* **16**:352-7.

Winzerling JJ, Nez P, Porath J and Law JH (1995) Rapid and efficient isolation of transferrin and ferritin from Manduca sexta. *Insect Biochem Mol Biol* **25**:217-24.

Wong CS, Kwok JC and Richardson DR (2004) PCTH: a novel orally active chelator of the aroylhydrazone class that induces iron excretion from mice. *Biochim*

Biophys Acta **1739**:70-80.

Wood SM, Wiesener MS, Yeates KM, Okada N, Pugh CW, Maxwell PH and Ratcliffe PJ (1998) Selection and analysis of a mutant cell line defective in the hypoxia-inducible factor-1 alpha-subunit (HIF-1alpha). Characterization of hif-1alpha-dependent and -independent hypoxia-inducible gene expression. *J Biol Chem* **273**:8360-8.

Wu X and Hasinoff BB (2005) The antitumor anthracyclines doxorubicin and daunorubicin do not inhibit cell growth through the formation of iron-mediated reactive oxygen species. *Anticancer Drugs* **16**:93-9.

Xu X, Persson HL and Richardson DR (2005) Molecular pharmacology of the interaction of anthracyclines with iron. *Mol Pharmacol* **68**:261-71.

Xu X, Sutak R and Richardson DR (2007) Iron Chelation by Clinically Relevant Anthracyclines: Alteration in Expression of Iron-Regulated Genes and Atypical Changes in Intracellular Iron Distribution and Trafficking. *Mol Pharmacol* **73**:1-12.

Yin Z, Purschke WG, Schafer G and Schmidt CL (1998) The glutamine synthetase from the hyperthermoacidophilic crenarcheon Sulfolobus acidocaldarius: isolation, characterization and sequencing of the gene. *Biol Chem* **379**:1349-54.

Yoshida M, Minamisawa S, Shimura M, Komazaki S, Kume H, Zhang M, Matsumura K, Nishi M, Saito M, Saeki Y, Ishikawa Y, Yanagisawa T and Takeshima H (2005) Impaired Ca2+ store functions in skeletal and cardiac muscle cells from sarcalumenin-deficient mice. *J Biol Chem* **280**:3500-6.

Yu Z, Persson HL, Eaton JW and Brunk UT (2003) Intralysosomal iron: a major determinant of oxidant-induced cell death. *Free Radic Biol Med* **34**:1243-52.

Zhang AS, Sheftel AD and Ponka P (2005) Intracellular kinetics of iron in reticulocytes: evidence for endosome involvement in iron targeting to mitochondria. *Blood* **105**:368-75.

Zweier JL, Gianni L, Muindi J and Myers CE (1986) Differences in O2 reduction by the iron complexes of adriamycin and daunomycin: the importance of the sidechain hydroxyl group. *Biochim Biophys Acta* **884**:326-36.